IL
NUOVO CIMENTO
ORGANO DELLA SOCIETÀ ITALIANA DI FISICA
SOTTO GLI AUSPICI DEL CONSIGLIO NAZIONALE DELLE RICERCHE

VOL. XI, N. 4 *Serie nona* 1° Aprile 1954

Pion Production by Polarized Beams of Nucleons.

R. E. MARSHAK

Faculté des Sciences, Sorbonne - Paris (*)

A. M. L. MESSIAH

C. E. N. Saclay - Gif sur Yvette, Seine et Oise, France

(ricevuto il 21 Gennaio 1954)

Summary. — Pion production by polarized beams of high energy nucleons can now be studied. It will be necessary to look for an azimuthal asymmetry in the angular distribution of the produced pions. As an illustration, the expected asymmetry of the π^+ mesons produced in the reaction $p + p \to \pi^+ + d$ is calculated assuming that the pion-nucleon interaction possesses both *s* and *p*-wave components. It is shown that a study of this reaction using polarized beams of protons may decide whether both the *s* and *p* interactions contribute to pion production by nucleons (say, at energies below 500 MeV).

Recent experiments by OXLEY *et al.* [1] have established the possibility of producing polarized beams of nucleons with energies in the neighborhood of 200 MeV. With targets such as carbon, the polarization of an emergent beam of 200 MeV protons has been measured to be as high as 50%. Pion production in complex nuclei by polarized beams of protons in this energy region could

(*) On sabbatical leave from the University of Rochester 1953-54.

(1) C. L. OXLEY, W. F. CARTWRIGTH, J. ROUVINA, E. BASKIR, D. KLEIN, J. RING and W. SKILLMAN: *Phys. Rev.*, **91**, 419 (1953).

be studied with some profit. However, if possible, it would be much more advantageous to investigate pion production in hydrogen by polarized beams of nucleons. This type of experiment would require an incident nucleon energy in excess of 300 MeV and it is not actually clear ([2]) that strongly polarized beams of nucleons can be produced at the higher energies. The remarks presented in this note presuppose that nucleon beams of sufficient polarization (the amount required will be discussed below) can be achieved in the energy region 300-500 MeV.

We examine the pion production reaction which has thus far been studied in greatest detail, namely the reaction: $p+p\rightarrow\pi^{+}+d$. The unpolarized cross-section for π^{+} production in this reaction has been measured at 340 MeV ([3]) (for the incident protons) and through measurements of the inverse reaction ($\pi^{+}+d\rightarrow p+p$) effectively up to 400 MeV ([4]). The angular distribution of the outgoing pions in the center of mass system has turned out to have essentially the form $a+\cos^{2}\theta$, with $a\cong 0.2$, and the integrated (total) cross-section has been found to vary by more than a factor two over the energy region 340-400 MeV. All attempts thus far ([5]) to understand the behaviour of the unpolarized cross-section have postulated that the only contribution to the cross-section comes from the pion-nucleon interaction in the p-state. The recently demonstrated importance of the s-wave in pion-nucleon scattering in the energy region in question ([6]) makes it interesting to decide whether the pion-nucleon interaction in the s-state plays any role in the nucleonic production of pions. We shall show that one possible method of deciding whether both the s- and p-state interactions contribute to pion production by nucleons is to look for an azimutal assymetry in the angular distribution of mesons from the reaction $p+p\rightarrow\pi^{+}+d$ using polarized beams of protons.

Let us write the amplitude of the wave scattered into the solid angle Ω in the form:

$$[A^{\mu}_{\mu_1\mu_2}(\Omega)+B^{\mu}_{\mu_1\mu_2}(\Omega)]\chi_{\mu}\,, \tag{1}$$

where $A^{\mu}_{\mu_1\mu_2}$ and $B^{\mu}_{\mu_1\mu_2}$ are the amplitudes of the s- and p-pion waves respectively, μ_1, μ_2, μ are the magnetic quantum numbers of the incident proton, target

([2]) J. MARSHALL, V. A. NEDZEL and L. MARSHALL: *Bull. of Am. Phys. Soc.*, **28**, no. 6 (1953).

([3]) W. WHITEHEAD and C. RICHMAN: *Phys. Rev.*, **83**, 855 (1951).

([4]) R. DURBIN, H. LOAR and J. M. STEINBERGER: *Phys. Rev.*, **84**, 581 (1951).

([5]) G. F. CHEW, N. L. GOLDBERGER, J. M. STEINBERGER and C. N. YANG: *Phys. Rev.*, **84**, 581 (1951); K. K. BRUECKNER and K. M. WATSON: *Phys. Rev.*, **86**, 923 (1952).

([6]) S. W. BARNES, C. E. ANGELL, J. P. PERRY, D. MILLER, J. RING and D. NELSON: *Phys. Rev.*, (in press); D. BODANSKY, A. M. SACHS and J. M. STEINBERGER: *Bull. Am. Phys. Soc.*, **28**, no. 6 (1953); H. L. ANDERSON, E. FERMI, R. MARTIN and D. E. NAGLE: *Phys. Rev.*, **91**, 155 (1953).

proton and deuteron respectively, and χ_μ is the deuteron amplitude. The polarized cross-section is obtained by summing the square of the scattered amplitude over μ and averaging over μ_2 and the unpolarized cross-section results from a further averaging over μ_1. Since the pion is a pseudoscalar particle, it can easily be shown that $A^\mu_{\mu_1\mu_2}$ can arise only from the $^3P_1$ state and $B^\mu_{\mu_1\mu_2}$ only from the $^1S_0$ and $^1D_2$ states of the two initial protons. Consequently, while the polarized cross-section will contain interference terms between the s- and p-waves, the unpolarized cross-section will depend only on $|A^\mu_{\mu_1\mu_2}|^2+|B^\mu_{\mu_1\mu_2}|^2$ (no interference). As a matter of fact, the polarized cross-section will only differ from the unpolarized cross-section when *both* s- and p-waves are present since a pure s-wave obviously cannot give rise to an azimuthal asymmetry nor can a pure p-wave in this case because the scattered amplitude then receives its contribution exclusively from the single states of the p-p system.

We can express the s and p scattered amplitudes in terms of spherical harmonic functions and Clebsch-Gordon coefficients (7) as follows:

$$A^\mu_{\mu_1\mu_2}(\Omega) = \alpha_1 \sum_{m\sigma} (11m\sigma\,|\,111\mu)\left(\frac{1}{2}\frac{1}{2}\mu_1\mu_2\,\middle|\,\frac{1}{2}\frac{1}{2}1\sigma\right) Y_1^m(\Omega)\,; \tag{2}$$

$$B^\mu_{\mu_1\mu_2}(\Omega) = [\alpha_0(110\mu\,|\,1100)\,Y_0^0(\Omega) + \alpha_2(110\mu\,|\,112\mu)\,Y_2^\mu(\Omega)]\left(\frac{1}{2}\frac{1}{2}\mu_1\mu_2\,\middle|\,\frac{1}{2}\frac{1}{2}00\right). \tag{3}$$

The α_J's ($J=0, 1, 2$) are the amplitudes arising from the $^1S_0$, $^3P_1$ and $^1D_2$ states of the p-p system respectively. We write the α_J's in the form:

$$\alpha_0 = \varrho_0 \exp[i\delta_0]\alpha\,, \qquad \alpha_1 = \varrho_1 \exp[i\delta_1]\alpha\,, \qquad \alpha_2 = \alpha \ \text{(real)}. \tag{4}$$

Using the notation of (4), the *unpolarized* cross-section becomes:

$$\frac{\mathrm{d}\sigma_{\text{unpol}}}{\mathrm{d}\Omega} \approx \alpha^2[(5 + 9\varrho_1^2 + \varrho_0^2) + (5 - 2\varrho_0 \cos\delta_0\sqrt{10})P_2(\cos\theta)] \approx a + \cos^2\theta, \tag{5}$$

where

$$a = \frac{2}{3}\,\frac{\varrho_0^2 + \varrho_0\sqrt{10}\cos\delta_0 + 5/2 + 9\varrho_1^2}{5 - 2\varrho_0\sqrt{10}\cos\delta_0}\,, \tag{6}$$

and the *polarized* cross-section:

$$\frac{\mathrm{d}\sigma_{\text{pol}}}{\mathrm{d}\Omega} = \frac{\mathrm{d}\sigma_{\text{unpol}}}{\mathrm{d}\Omega}\left\{1 - PQ\,\frac{a\sin\theta\cos\varphi}{a + \cos^2\theta}\right\}, \tag{7}$$

(7) E. U. Condon and G. H. Shortley: *Theory of Atomic Spectra*, Chap. III (Cambridge, 1951).

where:

$$Q = \frac{3\varrho_1[\varrho_0\sqrt{2}\sin(\delta_0 - \delta_1) - \sqrt{5}\sin\delta_1]}{\varrho_0^2 + \varrho_0\cos\delta_0\sqrt{10} + 5/2 + 9\varrho_1^2}$$

and $P = 2\langle S_y\rangle$ is the degree of polarization (taken to be in the y-direction; cf. ref. ([1])) of the incident proton beam. Therefore, the maximum fractionnal asymmetry $\Delta\sigma/\sigma$ in the azimuthal angular distribution of the π^+-mesons is given by:

$$\frac{\Delta\sigma}{\sigma} = PQ\,\frac{a\sin\theta}{a + \cos^2\theta}\,. \tag{9}$$

Several remarks should be made in connection with equ. (9). First, the asymmetry is proportional to the polarization of the incident proton beam, as might have been expected. Secondly, it reaches its maximum value at $\theta = \pi/2$, at which angle the unpolarized cross-section is a minimum. Finally, the magnitude of the effect depends through Q on the 4 parameters ϱ_0, δ_0, ϱ_1, δ_1 (cf. equ. (8)). It is readily verified, in particular, that it vanishes in the absence of s-waves ($\varrho_1 = 0$).

In fact, Q may be written:

$$Q = \frac{\sqrt{2}}{2}\,\frac{2b}{1 + b^2}\cos(\delta_1 - \varphi)\,, \tag{10}$$

with:

$$\varphi = \mathrm{tg}^{-1}\,\frac{\varrho_0\sqrt{2}\cos\delta_0 + \sqrt{5}}{\varrho_0\sqrt{2}\sin\delta_0}\,, \tag{11}$$

$$b = \frac{\sqrt{\varrho_0^2 + \varrho_0\cos\delta_0\sqrt{10} + 5/2}}{3\varrho_1}\,. \tag{12}$$

Therefore Q may take any value between -0.71 and $+0.71$; it attains its maximum absolute value for $\delta_1 = \varphi + n\pi$, $b = 1$. Such values of δ_1 and b are compatible with the observed angular distribution, so that a fractionnal asymmetry as high as $0.71P$ could be observed at $\theta = \pi/2$.

It is interesting to point out that the measurement of the unpolarized cross-section places an upper limit of $3a$ on the ratio of the s- to p-wave contributions (equal to $9\varrho_1^2/(5+\varrho_0^2)$). A measurement of the polarized cross-section would further bracket this ratio, the bracketing being sharper the larger the observed azimuthal asymmetry in the angular distribution.

The polarization discussed above differs from the polarization effect con-

sidered by WATSON and RICHMAN [8]. These authors examined the deuteron polarization resulting from the reaction $p + p \to \pi^+ + d$ initiated by an unpolarized proton beam, and expressed the polarization of the deuteron in terms of our parameters ϱ_0 and δ_0 characteristic of the p-wave pion-nucleon interaction exclusively. It is clear that, in the deuteron polarization problem, the s-wave does not contribute, either alone or in interference with the p-wave.

We are indebted to Dr. C. L. OXLEY for discussions leading to the calculation presented in this note. One of us (R.E.M.) whishes to acknowledge the hospitality of the Laboratoire de Physique of the École Normale Supérieure.

[8] K. M. WATSON and C. RICHMAN: *Phys. Rev.*, **83**, 1526 (1951).

RIASSUNTO (*)

Si può ora studiare la produzione di pioni da parte di fasci polarizzati di nucleoni di grande energia. È necessario ricercare un'asimmetria azimutale nella distribuzione angolare dei pioni prodotti. A titolo di esempio si calcola la prevedibile asimmetria dei mesoni π^+ prodotti nella reazione $p + p \to \pi^+ + d$ supponendo che l'interazione pione-nucleone possegga componenti sia delle onde s che delle onde p. Si dimostra che lo studio di questa reazione per mezzo di fasci polarizzati di protoni può dare elementi per decidere se sia le interazioni s che le interazioni p contribuiscono alla produzione di pioni da parte di nucleoni (per esempio, a energie inferiori a 500 MeV).

(*) *Traduzione a cura della Redazione.*

IL NUOVO CIMENTO Vol. XI, N. 4 1° Aprile 1954

Über Eigenschaften von Ausbreitungsfunktionen und Renormierungskonstanten quantisierter Felder.

H. Lehmann

Max-Planck-Institut für Physik - Göttingen, Deutschland

(ricevuto il 22 Gennaio 1954)

Summary. — It is attempted to derive some general properties of the propagation functions for coupled fields (Δ'_F, S'_F) without the use of power series expansions and to show their connection with the renormalization constants for field operators and masses. Assuming that the coupled functions exist, it appears possible to discuss their behavior near the light-cone (or for large momenta) and to obtain some information about the singularities of these functions when continued analytically. Attempts at the treatment of unrenormalizable theories are criticised on the basis of these results. Formulae are given for the mentioned renormalization constants which contain inequalities for the constants Z_2 and Z_3. Finally it is pointed out that the methods introduced are advantageous also for computations by means of power series expansion. As an example the lowest order correction to the S_F-function in pseudoscalar meson theory is calculated without the appearance of infinite terms during the calculation.

Einleitung.

In neueren Arbeiten zur Behandlung von Wechselwirkungsproblemen im Rahmen quantisierter Feldtheorien spielen die als Ausbreitungsfunktionen (oder als Greensche Funktionen) bezeichneten Größen Δ'_F und S'_F eine bedeutsame Rolle. Diese Größen sollten sich im Prinzip aus den Grundgleichungen der Theorien berechnen lassen; bislang sind jedoch nur störungstheoretische Näherungen bekannt, die vermutlich — mit Ausnahme der Quantenelektrodynamik — völlig unzureichend sind. Es erscheint deshalb der Versuch angebracht, Aussagen über diese Funktionen zu gewinnen, ohne dabei die Möglichkeit der Entwicklung nach einem Kopplungsparameter vorauszusetzen oder zu benutzen. Hiermit beschäftigt sich der erste Abschnitt

dieser Arbeit. Die hauptsächlichen Ergebnisse sind dabei: Die Ableitung von Formeln, die eine Darstellung der genannten Funktionen als Überlagerung von Ausbreitungsfunktionen freier Felder mit verschiedenen Massen ermöglichen und die sich hieraus ergebenden Folgerungen. Diese betreffen insbesondere das Verhalten der $\Delta_F'(x)$ und $S_F'(x)$ Funktionen für kleine Werte von x^2, bzw. das Verhalten ihrer Fouriertransformierten für große Impulse.

Im zweiten Teil wird gezeigt, daß sich die bei der Renormierung von Feldoperatoren und Massen auftretenden Konstanten in einfacher Weise durch die zur Darstellung der Ausbreitungsfunktionen eingeführten Größen ausdrücken lassen. Man erhält so Gleichungen, die unabhängig von der Störungsrechnung sind und zu einigen Aussagen über diese Konstanten führen. Im Gegensatz zu anderen Darstellungen wird dabei die Benutzung einlaufender Felder vermieden.

Abschließend wird zur Illustration der verwendeten Methoden eine störungstheoretische Berechnung der im 1. Abschnitt eingeführten Größen vorgenommen.

Es sei noch auf zwei Punkte hingewiesen:

Einmal ist bislang nicht bekannt, ob die Grundgleichungen irgendeiner quantisierten Feldtheorie (mit Ausnahme freier Felder) Lösungen besitzen. Wir gehen auf diese Frage nicht ein, sondern bemühen uns um Aussagen über die Ausbreitungsfunktionen unter der Annahme, daß diese existieren. Zum andern ist es zur Ableitung allgemeiner Resultate unerläßlich, mit Funktionen zu operieren, die nicht explizit bekannt sind. Manche der vorgenommenen mathematischen Umformungen (insbesondere Vertauschung von Integrationsreihenfolgen) haben deshalb formalen Charakter; ihre Berechtigung könnte wohl nur durch Ausführung detaillierter Rechnungen gezeigt werden.

1. – Eigenschaften der Ausbreitungsfunktionen.

a) Skalare Felder. – Um die Eigenschaften der Ausbreitungsfunktionen zu untersuchen, erweist es sich als zweckmäßig, neben Δ_F' weitere Funktionen einzuführen, die alle als Vakuumerwartungswerte von Heisenbergoperatoren definiert werden können. Die Situation ist hier ähnlich wie bei einem freien Feld, wo man üblicherweise von der Vertauschungsfunktion Δ sowie von $\Delta^{(1)}$ ausgeht und dann leicht zur Δ_F-Funktion übergehen kann.

Es soll zunächst ein hermitisches skalares Feld $A(x)$ betrachtet werden, das mit sich selbst in nichtlinearer Weise gekoppelt sein kann oder auch mit anderen (Bose- oder Fermi-) Feldern in Wechselwirkung stehen darf. Über die Art der Kopplung werden keine speziellen Voraussetzungen gemacht; sie kann lokal oder nichtlokal sein. Vorausgesetzt wird, daß die betrachtete Theorie lorentz-invariant ist. Demzufolge soll ein Energie-Impulsvierervektor P_μ exi-

stieren mit der Eigenschaft

$$\frac{\partial A(x)}{\partial x_\mu} = i\left[A(x), P_\mu\right]; \qquad \left[P_\mu, P_\nu\right] = 0. \tag{1}$$

Weiterhin wird angenommen, daß man einen Vakuumzustand definieren kann; d.h. der Energieoperator soll einen kleinsten Eigenwert besitzen, den wir auf Null normieren.

Die Kenntnis von Vertauschungsrelationen für die Feldoperatoren ist zunächst nicht erforderlich; es genügt die Beziehung (1).

Wir wollen jetzt die Vakuumerwartungswerte bilinearer Feldgrößen betrachten. Als Orthogonalsystem im Hilbertraum werden dabei die gemeinsamen Eigenvektoren der Operatoren P_μ benutzt, die ein vollständiges System bilden sollen. Es gilt also

$$P_\mu \Phi_k = k_\mu \Phi_k \qquad (k_0 \geqslant 0). \tag{2}$$

Die Eigenwerte k_μ können natürlich entartet sein.

In völliger Analogie zu einem freien Feld führen wir folgende Funktionen ein:

$$\left\{\begin{aligned}
&(\Phi_0, A(x)A(x')\Phi_0) = \langle A(x)A(x')\rangle_0 = i\Delta^{(+)\prime}(x-x') \\
&\langle A(x')A(x)\rangle_0 \quad\; = -i\Delta^{(-)\prime}(x-x') \\
&\langle [A(x), A(x')]\rangle_0 \;\; = i\Delta'(x-x') = -2i\varepsilon(x_0-x_0')\bar{\Delta}'(x-x') \\
&\langle \{A(x), A(x')\}\rangle_0 \;\; = \Delta^{(1)\prime}(x-x') \\
&\langle TA(x)A(x')\rangle_0 \;\; = \tfrac{1}{2}\Delta_F'(x-x')\,.
\end{aligned}\right. \tag{3}$$

Aus diesen Definitionsgleichungen der Vakuumfunktionen folgt, daß zwischen ihnen dieselben Zusammenhänge bestehen, wie bei einem freien Feld. Man kann z.B. alle Funktionen durch $\Delta^{(+)\prime}$ ausdrücken. Für die Ausbreitungsfunktion gilt: $\left[\theta(x_0) = \tfrac{1}{2}\,(1 + x_0/|x_0|)\right]$

$$\Delta_F'(x) = 2i\left[\theta(x_0)\Delta^{(+)\prime}(x) - \theta(-x_0)\Delta^{(-)\prime}(x)\right] = \Delta^{(1)\prime}(x) - 2i\bar{\Delta}'(x)\,. \tag{4}$$

Die Funktionen $\Delta^{(+)\prime}$ bzw. $\Delta^{(-)\prime}$ enthalten nur positive bzw. negative Frequenzen (sh. unten), so daß Δ_F' in derselben Weise wie bei einem freien Feld als eine kausale Funktion interpretiert werden kann. Um Aufschlüsse über die Struktur dieser Funktionen zu erhalten, betrachten wir die $\Delta^{(+)\prime}$-Funktion.

$$\begin{aligned}
\langle A(x)A(x')\rangle_0 &= \sum_k (\Phi_0, A(x)\Phi_k)(\Phi_k, A(x')\Phi_0) \\
&= \sum_k A_{0k}(x)A_{k0}(x) = \sum_k a_{0k}a_{0k}^* \exp\left[ik(x-x')\right].
\end{aligned} \tag{5}$$

Hierbei ist $(\Phi_0, A(x)\Phi_k) = A_{0k}(x) = a_{0k}\exp\left[ikx\right]$ gesetzt worden.

Die Möglichkeit dieser Umformung folgt in bekannter Weise aus

$$\frac{\partial A_{0k}(x)}{\partial x_\mu} = i(\Phi_0, [A(x), P_\mu]\Phi_k) = ik_\mu A_{0k}(x).$$

Die Summation in (5) ist über alle Zustände zu erstrecken.

Wir führen nun eine Funktion

$$\varrho(-k^2) = (2\pi)^3 \sum a_{0k} a_{0k}^* . \tag{6}$$

ein. Summiert wird hier über alle Zustände, die zum Eigenwert k_μ gehören.

Aus den Gleichungen (3), (5) und (6) folgt jetzt [1]:

$$\Delta^{(+)\prime}(x - x') = -\frac{i}{(2\pi)^3} \int \theta(k_0)\varrho(-k^2) \exp[ik(x - x')]\, \mathrm{d}^4k . \tag{7}$$

Dabei ist die Summation über die Eigenwerte durch eine Integration ersetzt worden, unter Beachtung des Umstandes, daß für alle Eigenwerte $k_0 \geqslant 0$ gilt.

Wir setzen in (7)

$$\varrho(-k^2) = \int_0^\infty \varrho(\varkappa^2)\, \delta(k^2 + \varkappa^2)\, \mathrm{d}(\varkappa^2) ,$$

und erhalten

$$\Delta^{(+)\prime}(x) = \int_0^\infty \Delta^{(+)}(x; \varkappa^2)\varrho(\varkappa^2)\, \mathrm{d}(\varkappa^2) . \tag{8}$$

Analoge Formeln gelten für alle Vakuumfunktionen (im folgenden mit $\Delta^{(\,)\prime}$ bezeichnet), da diese sich gemäß (3) in linearer Weise aus $\Delta^{(+)\prime}$ bilden lassen. Es ist also:

$$\Delta^{(\,)\prime}(x) = \int_0^\infty \Delta^{(\,)}(x; \varkappa^2)\varrho(\varkappa^2)\, \mathrm{d}(\varkappa^2) . \tag{9}$$

Die « gestrichenen » Funktionen lassen sich demnach durch lineare Überlagerung der entsprechenden freien Funktionen mit einer Massendichte $\varrho(\varkappa^2)$ darstellen [2].

Wir haben zur Ableitung der Formel (9) bereits benutzt, daß ϱ nur vom Argument k_μ^2 abhängt und für $k_\mu^2 > 0$ identisch Null ist. Beide Eigenschaften

---

[1] Darstellungen ähnlicher Art für Vakuumerwartungswerte von Feldoperatoren sind von G. KÄLLÉN: *Helv. Phys. Acta*, 25, 417 (1952) benutzt worden.

[2] Diese Darstellung hat eine formale Ähnlichkeit mit den Methoden der Regularisierung (W. PAULI und F. VILLARS: *Rev. Mod. Phys.*, 21, 434 (1949)). Jedoch ist hier $\varrho \geqslant 0$; d.h. die Regularisierungsbedingungen sind nicht erfüllt.

folgen aus der Lorentzinvarianz; andernfalls würden die Vakuumfunktionen (insbesondere die Vertauschungsfunktion Δ') keine invarianten Größen sein. Weiter folgt aus der Definitionsgleichung (6), daß ϱ eine positive Funktion ist. Es gilt

$$\varrho(\varkappa^2) \geqslant 0 \,. \tag{10}$$

Für den Spezialfall eines freien Feldes der Masse m ist natürlich $\varrho(\varkappa^2) = \delta(\varkappa^2 - m^2)$. Allgemein werden die diskreten Eigenwerte des Operators P_μ^2 zu δ-Funktionen in $\varrho(\varkappa^2)$ Anlaß geben, sofern nicht die Matrixelemente des Operators $A(x)$ zwischen dem Vakuum und den entsprechenden Zuständen (z. B. auf Grund von Auswahlregeln) verschwinden. Die diskreten Eigenwerte von P_μ^2 entsprechen den stabilen Teilchen, die von der Theorie geliefert werden. Von einer physikalisch sinnvollen Theorie wird man erwarten, daß sie mindestens ein stabiles Teilchen beschreibt, d.h. ϱ wird mindestens eine δ-Funktion enthalten. Falls sonst keine stabilen Teilchen auftreten, so gilt

$$\varrho(\varkappa^2) = \delta(\varkappa^2 - m^2) + \sigma(\varkappa^2); \qquad \sigma(\varkappa^2) = 0 \quad \text{für} \quad 0 \leqslant \varkappa^2 < (2m)^2,$$

wo $\sigma(\varkappa^2)$ frei von δ-Funktionen ist. Diese Struktur entspricht dem Umstand, daß in einem solchen Fall der Operator P_μ^2 einen diskreten Eigenwert besitzt, dem sich ein Kontinuum anschließt, wenn mindestens zwei Teilchen vorhanden sind [3].

Aus der Gleichung (9) und den eben angegebenen Eigenschaften der Funktion ϱ lassen sich verschiedene Folgerungen ziehen. Zunächst ist klar, daß (9) auch im Fourierraum gilt. ϱ ist also — bis auf einen Faktor — gleich der Transformierten der $\Delta^{(1)\prime}$- Funktion

$$\varrho(-k^2) = \frac{1}{2\pi} \Delta^{(1)\prime}(k^2) \,. \tag{11}$$

Weiter gilt z.B.

$$\Delta_F'(k^2) = -2i \int_0^\infty \frac{\varrho(\varkappa^2)\,\mathrm{d}(\varkappa^2)}{k^2 + \varkappa^2 - i\varepsilon} \qquad (\lim \varepsilon \to +0) \,. \tag{12}$$

Mit den angegebenen Beziehungen läßt sich jetzt das Verhalten der $\Delta^{(\prime)\prime}$- Funktionen in der Nähe des Lichtkegels, bzw. das ihrer Fouriertransformierten für große Werte von k^2 übersehen, da das Verhalten der «freien»

[3] Das ist natürlich auch bei einem freien Feld der Fall. Dann ist jedoch $\sigma(\varkappa^2)$ identisch Null, da die entsprechenden Matrixelemente des Operators $A(x)$ verschwinden.

Funktionen bekannt ist und nicht von der Masse abhängt. So erhält man z.B.

$$(13) \qquad \bar{\Delta}'(x) = \frac{1}{4\pi}\int_0^\infty \{\delta(x^2) + \ldots\}\varrho(\varkappa^2)\,\mathrm{d}(\varkappa^2) = \frac{1}{4\pi}\,\delta(x^2)\int_0^\infty \varrho(\varkappa^2)\,\mathrm{d}(\varkappa^2) + \ldots$$

und im Impulsraum

$$(14) \qquad \bar{\Delta}'(k^2) = P\int_0^\infty \frac{\varrho(\varkappa^2)\,\mathrm{d}(\varkappa^2)}{k^2+\varkappa^2} = \frac{1}{k^2}\int_0^\infty \varrho(\varkappa^2)\,\mathrm{d}(\varkappa^2) + \ldots$$

falls die dabei abgespaltenen Integrale konvergieren.

Die gestrichenen Funktionen haben also entweder das gleiche Verhalten wie die entsprechenden freien Funktionen, oder aber — falls $\int_0^\infty \varrho(\varkappa^2)\,\mathrm{d}(\varkappa^2)$ nicht konvergiert — sie sind am Lichtkegel stärker singulär (bzw. fallen für große Impulse schwächer ab) als die freien Funktionen. Hingegen ist es nicht möglich, daß die gestrichenen Funktionen weniger singulär sind als die freien Funktionen, da wegen Gl. (10) $\int_0^\infty \varrho\,\mathrm{d}(\varkappa^2) > 0$ ist. Es wird sich zeigen, dass die Frage nach der Konvergenz von $\int_0^\infty \varrho\,\mathrm{d}(\varkappa^2)$ für renormierbare Theorien gleichbedeutend ist mit der Frage, ob die Renormierungskonstanten für die Feldoperatoren endlich sind.

Damit die Funktion Δ_F' überhaupt existiert, ist gemäß (12) offenbar notwendig, daß das Integral

$$\int^\infty \frac{\varrho(\varkappa^2)}{\varkappa^2}\,\mathrm{d}(\varkappa^2)\,,$$

an der oberen Grenze konvergiert.

Eine weitere Folgerung betrifft die Eigenschaften der Funktion $\Delta_F'(k^2)$ bei analytischer Fortsetzung in der k_μ^2-Ebene. Es ist für reelle k^2

$$\Delta_F'(k^2) = \Delta^{(1)\prime}(k^2) - i2\bar{\Delta}'(k^2).$$

Weiter gilt:

$$(15) \qquad 2\bar{\Delta}'(k^2) = \frac{1}{\pi}\,P\int_0^\infty \frac{\Delta^{(1)\prime}(l^2)\,\mathrm{d}(-l^2)}{k^2-l^2}\,; \qquad \Delta^{(1)\prime}(k^2) = -\frac{1}{\pi}\,P\int_{-\infty}^\infty \frac{2\bar{\Delta}'(l^2)\,\mathrm{d}(-l^2)}{k^2-l^2}\,(4).$$

---

(4) Diese Gleichung folgt durch Umkehrung der vorangehenden Integralbeziehung oder aus den Definitionsgleichungen (3) der Vakuumfunktionen.

Die Funktionen $\Delta^{(1)\prime}(k^2)$ und $2\overline{\Delta}'(k^2)$ sind also konjugiert zueinander im Sinne der Hilbert-Transformation (5). Demzufolge läßt sich (unter einigen Voraussetzungen) die Funktion $\Delta_F'(k^2)$ analytisch fortsetzen und ist regulär in der unteren Halbebene (5). Dieses Resultat ist befriedigend, da das Auftreten von Polen in diesem Gebiet zu neuen (nichtrenormierbaren) Divergenzen (z. B. der S-Matrixelemente) führen könnte (6). Unsere Betrachtung zeigt jedoch, daß bei Benutzung der exakten Δ_F'-Funktion solche Schwierigkeiten nicht auftreten sollten. Dies gilt auch für die gleich zu besprechende S_F'-Funktion.

Wir wollen nun eine Folgerung für die gleichzeitigen Vertauschungsrelationen ziehen und benutzen dazu die Darstellung (9) für die Δ'-Funktion.

$$\Delta'(x) = \int_0^\infty \Delta(x; \varkappa^2)\varrho(\varkappa^2)\,\mathrm{d}(\varkappa^2)\,.$$

Es folgt unmittelbar:

$$(16)\qquad \begin{cases} \langle [A(\boldsymbol{x}, t), A(\boldsymbol{x}', t)] \rangle_0 = \langle [\dot{A}(\boldsymbol{x}, t), \dot{A}(\boldsymbol{x}', t)] \rangle_0 = 0\,, \\ \langle [\dot{A}(\boldsymbol{x}, t), A(\boldsymbol{x}', t)] \rangle_0 = -i\delta(\boldsymbol{x}-\boldsymbol{x}') \int_0^\infty \varrho(\varkappa^2)\,\mathrm{d}(\varkappa^2)\,. \end{cases}$$

Die gleichzeitigen V. R. zwischen den Operatoren A und $\dot{A}$ für den Vakuumzustand lassen sich demnach (bis auf einen Faktor) aus der Gleichung (1) ableiten. Die Operatoren sind für raumartige Punkte stets vertauschbar, und es tritt notwendig die Diracsche δ-Funktion auf. Dies gilt seiner Herleitung nach auch für Theorien mit nichtlokaler Wechselwirkung (7). Für Spinorfelder wird sich derselbe Sachverhalt ergeben.

Zur Gleichung (16) bemerken wir noch, daß danach bei Vorgabe der üblichen Vertauschungsrelation $[\dot{A}(\boldsymbol{x}), A(\boldsymbol{x}')] = -i\delta(\boldsymbol{x}-\boldsymbol{x}')$, $\int_0^\infty \varrho\,\mathrm{d}(\varkappa^2) = 1$ wäre. Die hier betrachteten Vakuumfunktionen sollen sich jedoch auf renormierte Operatoren beziehen, zu denen man bekanntlich übergehen muß. Wir gehen darauf im 2. Abschnitt genauer ein.

b) *Spinorfelder.* – Wir betrachten jetzt ein Spinorfeld unter denselben Voraussetzungen, wie sie für das schon behandelte skalare Feld gemacht

---

(5) Vgl. etwa E. C. Titchmarsh: *Theory of Fourier Integrals* (Oxford, 1937), Chap. V.

(6) In einer Arbeit von G. Feldman: *Modified propagators in field theory* – preprint-wird auf Grund von Näherungsformeln für die Ausbreitungsfunktionen die Existenz derartiger Pole vermutet und ihre Auswirkung diskutiert.

(7) Z.B. die Theorie von P. Kristensen und C. Møller: *Dan. Mat. Fys. Medd.*, **27**, no. 7 (1952).

wurden. Ausserdem fordern wir die Invarianz der Theorie gegen Teilchen-Antiteilchenkonjugation. Das Vorgehen und die Resultate sind naturgemäß ähnlich wie bei einem skalaren Feld.

Wir beginnen wieder mit der Definition von Vakuumfunktionen:

$$(17)\quad \begin{cases} \langle \psi_\alpha(x)\bar{\psi}_\beta(x')\rangle_0 = -iS^{(+)\prime}_{\alpha\beta}(x-x'); \qquad \langle \bar{\psi}_\beta(x')\psi_\alpha(x)\rangle_0 = -iS^{(-)\prime}_{\alpha\beta}(x-x') \\ \langle\{\psi_\alpha(x), \bar{\psi}_\beta(x')\}\rangle_0 = -iS'_{\alpha\beta}(x-x'); \quad \langle[\psi_\alpha(x), \bar{\psi}_\beta(x')]\rangle_0 = -S^{(1)\prime}_{\alpha\beta}(x-x') \\ \langle T\psi_\alpha(x)\bar{\psi}_\beta(x')\rangle_0 = -\tfrac{1}{2}S'_{F\alpha\beta}(x-x')\,. \end{cases}$$

Aus der Invarianz gegen Teilchen-Antiteilchenkonjugation folgt

$$\langle \bar{\psi}_\beta(x')\psi_\alpha(x)\rangle_0 = \langle \bar{\psi}'_\beta(x')\psi'_\alpha(x)\rangle_0 = -C^{-1}_{\beta\gamma}\langle \psi_\gamma(x')\bar{\psi}_\delta(x)\rangle_0 C_{\delta\alpha}\,.$$

Demnach:

$$(17a)\qquad S^{(-)\prime}_{\alpha\beta}(x-x') = -C^{-1}_{\beta\gamma}S^{(+)\prime}_{\gamma\delta}(x'-x)C_{\delta\alpha}\,.$$

Man kann also alle Funktionen durch $S^{(+)\prime}$ ausdrücken. Nun ist

$$(18)\qquad \langle \psi_\alpha(x)\bar{\psi}_\beta(x')\rangle_0 = \sum_k (\Phi_0, \psi_\alpha(x)\Phi_k)(\Phi_k, \bar{\psi}_\beta(x')\Phi_0) = \sum_k c^\alpha_{0k}\bar{c}^\beta_{0k}\exp[ik(x-x')].$$

Zunächst soll wieder die Summation über diejenigen Zustände ausgeführt werden, die zum Eigenwert k_μ gehören. Dementsprechend führen wir zwei Funktionen ϱ_1 und ϱ_2 ein:

$$(19)\qquad (i\gamma_{\alpha\beta}k - \sqrt{-k^2}\,\delta_{\alpha\beta})\varrho_1(-k^2) + \delta_{\alpha\beta}\varrho_2(-k^2) = -(2\pi)^3\sum c^\alpha_{0k}\bar{c}^\beta_{0k}\,.$$

Wegen der relativistischen Invarianz der Theorie kann der Ausdruck (19) nur in der angegebenen Weise von γ-Matrizen abhängen. Die Aufteilung der γ-freien Anteile auf ϱ_1 und ϱ_2 ist natürlich willkürlich.

Genau wie im skalaren Fall folgt jetzt

$$(20)\qquad S^{(+)\prime}(x) = -\frac{i}{(2\pi)^3}\int \theta(k_0)\{(i\gamma k - \sqrt{-k^2})\varrho_1(-k^2) + \varrho_2(-k^2)\}\exp[ikx]\,\mathrm{d}^4k = \\ = \int_0^\infty \{S^{(+)}(x;\varkappa)\varrho_1(\varkappa^2) + \Delta^{(+)}(x;\varkappa)\varrho_2(\varkappa^2)\}\,\mathrm{d}(\varkappa^2)\,.$$

Eine entsprechende Darstellung gilt gemäß (17) und (17a) für alle gestrichenen Funktionen:

$$(21)\qquad S^{(-)\prime}(x) = \int_0^\infty \{S^{(-)}(x;\varkappa)\varrho_1(\varkappa^2) + \Delta^{(-)}(x;\varkappa^2)\varrho_2(\varkappa^2)\}\,\mathrm{d}(\varkappa^2)\,.$$

Für ϱ_1 und ϱ_2 folgt aus (19) unmittelbar, daß beide Funktionen reell sind. Weiterhin wollen wir folgende Ungleichungen beweisen:

$$\varrho_1(\varkappa^2) \geqslant 0; \qquad 0 \leqslant \varrho_2(\varkappa^2) \leqslant 2\varkappa\varrho_1(\varkappa^2) . \tag{22}$$

Hierzu multiplizieren wir in (19) von links mit $i\gamma k + \alpha$ von rechts mit $(i\gamma k + \alpha)\gamma_4$ und erhalten $(f_{0k} = (i\gamma k + \alpha)c_{0k})$

$$\sum_\beta f_{0k}^\beta f_{0k}^{*\beta} = k_0\left[(\varkappa - \alpha)^2\varrho_1 + 2\alpha\varrho_2\right] \geqslant 0; \qquad (\varkappa^2 = -k^2) .$$

Diese Ungleichung gilt für beliebiges reelles α. Wegen $k_0 > 0$ ist

$$(\varkappa - \alpha)^2\varrho_1 + 2\alpha\varrho_2 \geqslant 0 . \tag{22a}$$

Für $\alpha = 0$ folgt

$$\varrho_1 \geqslant 0 .$$

Das Minimum von (22a) als Funktion von α wird für $\alpha = (\varkappa\varrho_1 - \varrho_2)/\varrho_1$ eingenommen. Einsetzen diese Wertes liefert

$$\varrho_2(2\varkappa\varrho_1 - \varrho_2) \geqslant 0 .$$

Dies führt direkt auf die angegebenen Ungleichungen für ϱ_2.

Für ein freies Spinorfeld ist $\varrho_1(\varkappa^2) = \delta(\varkappa^2 - M^2)$; $\varrho_2(\varkappa^2) \equiv 0$. Allgemein wird die Funktion ϱ_1 (da die Theorie mindestens ein stabiles Teilchen vom Spin $\frac{1}{2}$ beschreiben sollte) mindestens eine δ-Funktion enthalten.

Mit Hilfe der Gleichungen (21) und (22) kann man jetzt ähnliche Folgerungen ziehen wie im skalaren Fall. Im Impulsraum gilt z.B.

$$S_F'(k) = -2i\int_0^\infty \frac{(i\gamma k - \varkappa)\varrho_1(\varkappa^2) + \varrho_2(\varkappa^2)}{k^2 + \varkappa^2 - i\varepsilon}\,\mathrm{d}(\varkappa^2) . \tag{23}$$

Weiter kann man wieder auf das Verhalten der gestrichenen Funktionen in der Nähe des Lichtkegels, bzw. für große Impulse schließen. Da $\varrho_1 \geqslant 0$ ist, haben die gestrichenen Funktionen entweder das gleiche Verhalten wie die freien Funktionen, oder sie sind — falls $\int_0^\infty \varrho_1\,\mathrm{d}(\varkappa^2)$ nicht konvergiert — stärker singulär.

Die Schlüsse hinsichtlich des Verhaltens der Ausbreitungfunktion bei analytischer Fortsetzung lassen sich ebenfalls wie im skalaren Fall ziehen.

Wenn man S'_F in der Form $S'_F(k) = i\gamma k f_1(k^2) + f_2(k^2)$ schreibt, so sind Real- und Imaginärteil der Funktionen $f_i(k^2)$ zueinander konjugiert gemäß der Hilberttransformation. Bei Fortsetzung werden die Funktionen also in der unteren Halbebene regulär sein.

Schließlich erhält man für den gleichzeitigen Antikommutator aus der Formel (21) für die S'-Funktion:

$$\langle\{\psi_\alpha(\boldsymbol{x}, t), \bar{\psi}_\beta(\boldsymbol{x}', t)\}\rangle_0 = \gamma^4_{\alpha\beta}\delta(\boldsymbol{x} - \boldsymbol{x}') \int_0^\infty \varrho_1(\varkappa^2)\,\mathrm{d}(\varkappa^2)\,. \tag{24}$$

c) *Bemerkung zur Behandlung nichtrenormierbarer Theorien.* – Wir fügen hier eine Bemerkung ein hinsichtlich der Versuche [8], in nichtrenormierbaren Theorien konvergente Resultate zu erhalten. Bei diesen Methoden wird so vorgegangen, daß man zur Berechnung von S-Matrixelementen die Δ_F- bzw. S_F-Funktion durch die näherungsweise bestimmte Δ'_F-bzw. S'_F-Funktion ersetzt. Dem Verfahren liegt die Hoffnung zugrunde, daß infolge der Feldrückwirkung die gestrichenen Funktionen weniger singulär sind als die entsprechenden freien Funktionen. Tatsächlich erhält man mit dem üblichen Berechnungsschema (Berücksichtigung der irreduziblen Selbstenergiegraphen bis zu einer bestimmten Ordnung in der Kopplungskonstanten) Funktionen, die für große Impulse stark abfallen.

Unsere Ergebnisse zeigen jedoch, daß dies für die exakten Ausbreitungsfunktionen nicht der Fall ist; vielmehr ist das benutzte Näherungsverfahren ungeeignet zur Wiedergabe des asymptotischen Verhaltens der exakten Funktionen. Wir glauben deshalb nicht, daß die erwähnten Versuche sich zu einem konsequenten Verfahren ausbauen lassen.

2. – Renormierungskonstanten.

Der folgende Abschnitt soll dazu dienen, die im Zuge der Renormierung von Feldoperatoren und Massen auftretenden Konstanten durch die vorhin eingeführten Funktionen $\varrho(\varkappa^2)$ auszudrücken. Wir führen dies am Beispiel der pseudoskalaren Kopplung eines neutralen Mesonfeldes $A(x)$ an ein Spinorfeld $\psi(x)$ durch.

Aus der üblichen Lagrangefunktion, die unrenormierte Feldoperatoren

[8] N. Hu: *Phys. Rev.*, **80**, 1109 (1950); S. Kamefuchi und H. Umezawa: *Prog. Theor. Phys.*, **9**, 529 (1953).

$(A_u(x),\ \psi_u(x))$, Massen (M_0, m_0) und eine unrenormierte Kopplungskonstante (g_0) enthält, ergibt sich durch die Einführung renormierter Größen [9]

$$(25)\qquad \begin{cases} \psi(x) = Z_2^{-1/2}\cdot\psi_u(x); \qquad A(x) = Z_3^{-1/2}A_u(x) \\ M = M_0 + \delta M; \qquad m^2 = m_0^2 + \delta m^2; \qquad g = Z_1^{-1}Z_2 Z_3^{1/2} g_0\,, \end{cases}$$

$$(26)\qquad L = \begin{cases} -\tfrac{1}{4} Z_2\big\{[\bar\psi,(\gamma\partial + M)\psi] \quad [(\gamma^r\partial - M)\bar\psi, \psi]\big\} - \\ \qquad\qquad\qquad\qquad\qquad\qquad -\tfrac{1}{2} Z_3\big\{\partial_\nu A\partial_\nu A + m^2A^2\big\} \\ -i/2\, gZ_1[\bar\psi, \gamma_5\psi]A + \tfrac{1}{2} Z_2\,\delta M[\bar\psi, \psi] + \tfrac{1}{2}Z_3\delta m^2A^2\,. \end{cases}$$

Die renormierten Operatoren genügen demnach den Feldgleichungen

$$(27)\qquad \begin{cases} (\Box - m^2)A(x) = \dfrac{ig}{2} Z_1Z_3^{-1}[\bar\psi, \gamma_5\psi] - \delta m^2 A \\ \left(\gamma\dfrac{\partial}{\partial x} + M\right)\psi(x) = -igZ_1Z_2^{-1}\gamma_5 A\psi + \delta M\psi\,. \end{cases}$$

Die gleichzeitigen Vertauschungsrelationen lauten:

$$(28)\qquad \begin{cases} \big[A(x), \dot A(x')\big] = -i\delta(\boldsymbol{x} - \boldsymbol{x}')\cdot Z_3^{-1} \\ \big\{\psi_\alpha(x), \bar\psi_\beta(x')\big\} = \gamma^4_{\alpha\beta}\delta(\boldsymbol{x} - \boldsymbol{x}')\cdot Z_2^{-1}. \end{cases}$$

Alle übrigen Kommutatoren (bzw. Antikommutatoren) verschwinden für gleiche Zeiten.

Nach (25) und den früher gegebenen Definitionsgleichungen der Funktionen $\varrho(\varkappa^2)$ gehen die Konstanten Z_3 bew. Z_2 einfach als multiplikative Faktoren in die Funktionen ϱ (bzw. ϱ_1 und ϱ_2) ein. Wir müssen uns zunächst mit der Frage beschäftigen, wodurch die Konstanten Z_2 und Z_3 festgelegt sind. Hierzu beachten wir, daß die Theorie — falls sie physikalisch sinnvoll ist — mindestens zwei stabile Teilchen beschreiben muß; d.h. der Operator P_μ^2 muß einen diskreten Eigenwert zur Nukleonenzahl 0 mit der Masse m (exp. Masse des Mesons) und einen diskreten Eigenwert zur Nukleonenzahl 1 mit der Masse M (exp. Masse des Nukleons) haben. Zu den Funktionen ϱ geben natürlich nur Zustände mit der Nukleonenzahl 0 bzw. 1 einen Beitrag. Diese Funktionen enthalten demnach Terme der Form

$$\varrho(\varkappa^2) = c_3\delta(\varkappa^2 - m^2) + \ldots; \qquad \varrho_1 = c_2\delta(\varkappa^2 - M^2) + \ldots$$

---

[9] Um im Rahmen der Störungsrechnung stets konvergente Ausdrücke zu erhalten, muß man bekanntlich noch einen Term $\sim \lambda A^4$ einführen. Wir gehen darauf nicht ein, da dieser Term für die hier betrachteten Zusammenhänge ohne wesentliche Bedeutung ist.

Die Konstanten Z_3 und Z_2 werden nun dadurch festgelegt, daß man c_3 und c_2 auf Eins normiert ([10]). Dies entspricht dem Verfahren bei der störungstheoretischen Durchführung der Renormierung ([11]), bzw. den Renormierungsbedingungen von Källén ([1]).

Für die Konstanten Z_3 und Z_2 gilt nach (16), (24) und (28)

$$Z_3^{-1} = \int_0^\infty \varrho(\varkappa^2)\,\mathrm{d}(\varkappa^2); \qquad Z_2^{-1} = \int_0^\infty \varrho_1(\varkappa^2)\,\mathrm{d}(\varkappa^2)\,.$$

Da die Funktionen ϱ und ϱ_1 stets positiv sind und Summanden $\delta(\varkappa^2 - m^2)$ bzw. $\delta(\varkappa^2 - M^2)$ enthalten, gilt nach (29) für die Renormierungskonstanten:

(30) $$0 \leqslant Z_3 < 1; \qquad 0 \leqslant Z_2 < 1 \quad ([12])\,.$$

Wir wollen jetzt Formeln für die Massenkonstanten δm und δM gewinnen.

Betrachten wir zunächst die Mesonmasse:

Nach (9) und (27) ist

(31) $$(\Box - m_0^2)\,\langle[A(x), A(x')]\rangle_0 = \frac{ig}{2} Z_1 Z_3^{-1} \langle[[\bar\psi(x), \gamma_5\psi(x)], A(x')]\rangle_0 =$$

$$= i\int_0^\infty (\varkappa^2 - m_0^2) \Delta(x - x'; \varkappa^2)\,\varrho(\varkappa^2)\,\mathrm{d}(\varkappa^2)\,.$$

Wir differenzieren nach t' und setzen dann $t' = t$. Es ist

$$\langle[[\bar\psi(x), \gamma_5\psi(x)], \dot A(x')]\rangle_0 = 0 \qquad \text{für} \quad t' = t\,,$$

da für gleiche Zeiten

$$[\psi(x), \dot A(x')] = [\bar\psi(x), \dot A(x')] = 0\,.$$

Man erhält also

$$m_0^2 \int_0^\infty \varrho\,\mathrm{d}(\varkappa^2) = \int_0^\infty \varkappa^2 \varrho\,\mathrm{d}(\varkappa^2)\,,$$

([10]) Sollten die Funktionen ϱ noch weitere δ-Funktionen enthalten, so entsprechen diese ebenfalls stabilen Teilchen mit der Nukleonenzahl 0 bzw. 1. Von einer physikalisch brauchbaren Theorie der Wechselwirkung von π-Mesonen und Nukleonen sollten derartige Teilchen nicht geliefert werden, da sie experimentell nicht auftreten. Falls sie aus der Theorie folgen, so muß man (zur Festlegung von Z_2 und Z_3) genauer denjenigen diskreten Eigenwert charakterisieren, der zum experimentellen Meson bzw. Nukleon gehört.

([11]) Vgl. z.B. P. T. Matthews: *Phil. Mag.*, **41**, 185 (1950).

([12]) Diese Ungleichungen sind offenbar bisher nicht angegeben worden. Im Fall der Elektrodynamik gibt Z_3 gleichzeitig den Zusammenhang zwischen der nackten und der renormierten Ladung an. Die Ungleichung für Z_3 drückt dann den zuerst von Schwinger (vgl. W. Pauli: *Feldquantisierung* (Vorlesungen 1950-51)) bewiesenen Sachverhalt aus, daß die renormierte Ladung kleiner ist als die nackte Ladung.

oder

$$\delta m^2 = -\frac{\int_0^\infty (\varkappa^2 - m^2)\varrho\, \mathrm{d}(\varkappa^2)}{\int_0^\infty \varrho\, \mathrm{d}(\varkappa^2)} = -Z_3 \int_0^\infty (\varkappa^2 - m^2)\varrho\, \mathrm{d}(\varkappa^2) \leqslant 0\,. \tag{32}$$

Eine Formel für die Nukleonkonstante δM gewinnt man auf analoge Weise.

$$\left(\gamma\frac{\partial}{\partial x} + M_0\right) S'(x - x') = \tag{33}$$

$$= \int_0^\infty \left[(M_0 - \varkappa)\gamma\frac{\partial}{\partial x} + \varkappa(\varkappa - M_0)\right] \Delta(x - x';\varkappa^2)\varrho_1(\varkappa^2)\,\mathrm{d}(\varkappa^2) +$$

$$+ \int_0^\infty \left(\gamma\frac{\partial}{\partial x} + M_0\right) \Delta(x - x';\varkappa^2)\varrho_2(\varkappa^2)\,\mathrm{d}(\varkappa^2) =$$

$$= gZ_1Z_2^{-1}\gamma_5 \left\langle\{A(x)\psi x),\, \bar{\psi}(x')\}\right\rangle_0\,,$$

für $t' = t$ ist

$$\left\langle\{A(x)\psi(x),\, \bar{\psi}(x')\}\right\rangle_0 \sim \left\langle A(x)\right\rangle_0 = 0\,.$$

(Das Verschwinden von $\langle A(x)\rangle_0$ folgt dabei aus:

$$(\Box - m_0^2)\left\langle A(x)\right\rangle_0 = -m_0^2\left\langle A(x)\right\rangle_0 = \frac{ig}{2} Z_1Z_3^{-1} Sp\,\{\gamma_5 S^{(1)\prime}(0)\} = 0\,.$$

Nach (32) ist $m_0^2 \neq 0$; also $\langle A(x)\rangle_0 = 0$).

Demnach gilt

$$M_0 \int_0^\infty \varrho_1\,\mathrm{d}(\varkappa^2) = \int_0^\infty (\varkappa\varrho_1 - \varrho_2)\,\mathrm{d}(\varkappa^2)$$

oder

$$\delta M = \frac{\int_0^\infty [(M - \varkappa)\varrho_1 + \varrho_2]\,\mathrm{d}(\varkappa^2)}{\int_0^\infty \varrho_1\,\mathrm{d}(\varkappa^2)} = Z_2 \int_0^\infty [(M - \varkappa)\varrho_1 + \varrho_2]\,\mathrm{d}(\varkappa^2)\,. \tag{34}$$

Die Formeln (29), (32) und (34) drücken die Konstanten Z_2, Z_3, δm^2, δM durch die Funktionen $\varrho(\varkappa^2)$ aus. Auf die Konstante Z_1 wollen wir in dieser Arbeit nicht eingehen.

Es dürfte klar sein, daß die abgeleiteten Zusammenhänge nicht auf das spezielle Beispiel der Kopplung pseudoskalarer Mesonen mit Nukleonen beschränkt sind, sondern sich leicht auf andere Fälle übertragen lassen. Für eine Anwendung auf die Quantenelektrodynamik sind naturgemäß — wegen der Lorentzbedingung — einige zusätzliche Überlegungen erforderlich.

Die in diesem Abschnitt erhaltenen Resultate berühren sich eng mit der von Källén durchgeführten Definition der Renormierungskonstanten für die Quantenelektrodynamik.

Methodisch unterscheiden sich die beiden Darstellungen darin, daß hier die Benutzung einlaufender Felder und die damit verknüpfte Problematik des adiabatischen Einschaltens vermieden wird; zum andern legen wir Wert auf den Zusammenhang zwischen den Renormierungskonstanten und den Eigenschaften der Ausbreitungsfunktionen.

3. – Bestimmung der Vakuumfunktionen in g^2 Näherung.

Obwohl es unser eigentliches Anliegen ist, Aussagen über die Ausbreitungsfunktionen zu gewinnen, die unabhängig von der Störungsrechnung sind, wollen wir darauf hinweisen, daß die hier benutzten Methoden auch für die störungsmäßige Berechnung dieser Funktionen von Vorteil sind. Wir illustrieren diese Methoden indem wir die Funktionen ϱ_1, ϱ_2 und S'_F in der g^2-Näherung für das vorhin betrachtete Beispiel der pseudoskalaren Kopplung von Mesonen und Nukleonen bestimmen. Im Gegensatz zu anderen Darstellungen treten dabei in diesem Schema keine divergenten Bestandteile auf, deren Elimination bei der sonst üblichen Methode zu relativ umständlichen Umformungen Anlaß gibt ([13]).

Wir setzen also

$$\varrho_1(\varkappa^2) = \varrho_{10}(\varkappa^2) + g^2\varrho_{11}(\varkappa^2) + \ldots$$
$$\varrho_2(\varkappa^2) = \varrho_{20}(\varkappa^2) + g^2\varrho_{21}(\varkappa^2) + \ldots$$

und bestimmen diese Größen, indem wir z.B. die $S^{(+)\prime}(x)$-Funktion nach Potenzen von g^2-entwickeln.

$$S^{(+)\prime}(x - x') = i\,\langle\psi(x)\bar{\psi}(x')\rangle_0 = S^{(+)}(x - x';\, M) + 0(g^2)\,. \tag{35}$$

In nullter Näherung tritt natürlich die ungestrichene $S^{(+)}$-Funktion auf und demnach ist:

$$\varrho_{10} = \delta(\varkappa^2 - M^2)\,; \qquad \varrho_{20} = 0\,; \qquad \delta M_0 = 0\,; \qquad Z_{20} = 1\,.$$

([13]) W. Zimmermann (*Nuovo Cimento*, im Erscheinen) hat ein allgemeines Verfahren entwickelt, um die Ausbreitungsfunktionen in beliebiger Ordnung zu berechnen, ohne daß dabei divergente Terme auftreten.

Um den g^2-Term der Gleichung (35) zu finden, bilden wir

$$(36)\qquad \left(\gamma\frac{\partial}{\partial x}+M\right)\left(\gamma^x\frac{\partial}{\partial x'}-M\right)S^{(+)\prime}(x-x')=i\,\langle f(x)\bar{f}(x')\rangle_0=$$

$$=ig^2\gamma_5\,\langle A(x)\psi(x)A(x')\bar{\psi}(x')\rangle_0+\ldots=ig^2\Delta^{(+)}(x-x';\,m)\gamma_5 S^{(+)}(x-x';\,M)\gamma_5+\ldots.$$

In (36) ist $f(x)=-igZ_1Z_2^{-1}\gamma_5 A(x)\psi(x)+\delta M\psi(x)$.
Bei der weiteren Umformung sind nur Terme $\sim g^2$ ausgeschrieben worden. Durch Übergang zum Fourierraum ergibt sich ($\varkappa^2=-k^2$)

$$(37)\qquad \theta(k_0)(i\gamma k+M)\left[(i\gamma k-\varkappa)\varrho_{11}+\varrho_{21}\right](i\gamma k+M)=$$

$$=-\frac{1}{(2\pi)^3}\int\theta(k_0-q_0)\theta(q_0)\gamma_5(i\gamma q-M)\gamma_5\,\delta[q^2+M^2]\,\delta\left[(k-q)^2+m^2\right]\mathrm{d}^4q\,.$$

Zur Elimination der γ-Matrizen wird einmal die Spur von (37), zum andern die Spur der mit $i\gamma k$ multiplizierten Gleichung gebildet. Man erhält

$$(38)\qquad\begin{cases}\theta(k_0)\left[-\varkappa(\varkappa-M)^2\varrho_{11}+(\varkappa^2+M^2)\varrho_{21}\right]=\\ \qquad=\dfrac{M}{(2\pi)^3}\displaystyle\int\theta(k_0-q_0)\theta(q_0)\,\delta[q^2+M^2]\,\delta\left[(k-q)^2+m^2\right]\mathrm{d}^4q\\ \theta(k_0)\varkappa^2\left[(\varkappa-M)^2\varrho_{11}+2M\varrho_{21}\right]=\\ \qquad=-\dfrac{1}{(2\pi)^3}\displaystyle\int\theta(k_0-q_0)\theta(q_0)(kq)\,\delta[q^2+M^2]\,\delta\left[(k-q)^2+m^2\right]\mathrm{d}^4q.\end{cases}$$

Die hier auftretenden Integrale sind elementar ausführbar und konvergent. Man findet für ϱ_{11} und ϱ_{21}:

$$(39)\qquad\begin{cases}\varrho_{11}=\dfrac{1}{32\pi^2}\,\theta\left[\varkappa^2-(M+m)^2\right]\cdot\\ \qquad\cdot\dfrac{\sqrt{(\varkappa^2-M^2-m^2)^2-4m^2M^2}}{\varkappa^4}\left\{1-\dfrac{m^2(\varkappa^2+M^2)}{(\varkappa^2-M^2)^2}\right\}\\ \varrho_{21}=\dfrac{1}{32\pi^2}\,\theta\left[\varkappa^2-(M+m)^2\right]\cdot\\ \qquad\cdot\dfrac{\sqrt{(\varkappa^2-M^2-m^2)^2-4m^2M^2}}{\varkappa^3}\left\{1-\dfrac{m^2}{(\varkappa+M)^2}\right\}.\end{cases}$$

Für $S_F'=S_F+g^2S_{F1}'+\ldots$ gilt demnach

$$S_{F1}'(k)=-2i\int_0^\infty\frac{\left[(i\gamma k-\varkappa)\varrho_{11}+\varrho_{21}\right]\mathrm{d}(\varkappa^2)}{k^2+\varkappa^2-i\varepsilon}\,.$$

Zur expliziten Angabe von $S'_{F1}(k)$ ist also noch ein konvergentes Integral über $\varkappa^2$ auszuführen. Die Integration läßt sich elementar durchführen und ist im Spezialfall $m = 0$ trivial. Wir geben für diesen Fall das Resultat an ([14]):

$$S'_{F1}(k) = \frac{i}{16\pi^2}\frac{i\gamma k}{k^2}\left\{1-\left(1+\frac{M^2}{k^2}\right)\ln\left(1+\frac{k^2}{M^2}-i\varepsilon\right)\right\}. \tag{40}$$

Daß während der Rechnung keine divergenten Glieder auftraten, ist in der vorgenommenen Aufspaltung der S'_F-Funktion begründet. Man kann die hier nicht in Erscheinung getretenen Renormierungskonstanten natürlich aus ϱ_{11} und ϱ_{21} mit Hilfe der Formeln (29) und (34) bestimmen.

Abschließend möchte ich Herrn Prof. W. Heisenberg für viele Anregungen und den Herren K. Symanzik und W. Zimmermann für zahlreiche Diskussionen danken.

([14]) Dies stimmt mit dem Resultat überein, das man bei Benutzung der üblichen Methode von Dyson erhält. Vgl. R. Karplus *et al.*: *Phys. Rev.*, **90**, 1073 (1953).

RIASSUNTO (*)

Il presente lavoro espone un tentativo di dedurre alcune proprietà generali delle funzioni di propagazione per campi accoppiati (Δ'_F, S'_F) senza l'impiego di sviluppi in serie di potenze e di dimostrare la loro connessione con le costanti di rinormalizzazione degli operatori di campo e delle masse. Assumendo come esistenti le funzioni accoppiate, diventa possibile discuterne il comportamento in prossimità del cono di luce (o per momenti elevati) e ottenere informazioni sulle singolarità di queste funzioni analiticamente estrapolate. Basandosi su questi risultati si fa la critica dei tentativi fatti per trattare le teorie non rinormalizzabili. Si danno formule per le suddette costanti di rinormalizzazione che comprendono disequazioni per le costanti Z_2 e Z_3. Finalmente si osserva che i metodi esposti sono utili anche per calcoli di sviluppo in serie di potenze. Come esempio si espone il calcolo della correzione del minimo ordine della funzione S nella teoria mesonica pseudoscalare, senza che nello sviluppo del calcolo compaiano termini infiniti.

(*) *Traduzione a cura della Redazione.*

IL NUOVO CIMENTO Vol. XI, N. 4 1° Aprile 1954

On the Relation between Fundamental Tensor and Affinity in Unified Field Theory.

B. Bertotti (*)

Dublin Institute for Advanced Studies

(ricevuto il 1° Febbraio 1954)

Summary. — With the aim of generalizing the relation between the fundamental tensor and the affine connexion of the real and the hermitian case of the unified field theory, a relation with eight arbitrary constants is contemplated; conditions for its general invariance and transposition invariance are imposed, and a relation with only two arbitrary coefficients is obtained; which, however, except in three particular cases, is substantially nothing else but the real or hermitian relation. One of the particular cases is noteworthy, as it imposes the first quadruplet of Maxwell's equations on the skew part of the fundamental tensor [relation (19) in the text].

1. – In the two formulations of the unified field theory, the real and the hermitian, the field equations are, as is well known (1), formally identical; the only difference is that, while in the first the field variables are real, in the second their skew parts are purely imaginary. In particular the relation between the fundamental tensor and the affinity—a relation which, for short-

(*) On leave of absence from the Istituto Nazionale di Fisica Nucleare - Sezione di Milano.

(1) For the hermitian formulation—the first in time order—see: A. Einstein: *Ann. of Math.*, **46**, 578 (1945); A. Einstein and E. G. Straus: *Ann. of Math.*, **47**, 731 (1946). For the real one, see e.g. the three papers by E. Schrödinger which appeared in the *Proceedings of the Royal Irish Academy*: I, A **51**, 163 (1947); II, A **51**, 205 (1948); III, A 52, 1 (1948); and, mainly for what concerns the inadmissability of the « strong » form of the field equations: A. Einstein and B. Kaufman: *Sur l'état actuel de la théorie générale de la gravitation*, published in the volume *Louis de Broglie, physicien et penseur* (Paris, 1953), page 321.

ness and remembering the Riemannian case, I will call the Christoffel relation—reads:

$$(1) \qquad \underset{+-}{g_{i\,j\,;\,l}} = 0\,.$$

Actually, however—as V. HLAVATÝ (2) has recently pointed out—(1) for the real case differs substantially from (1) for the hermitian case, put in a real form.

In the real case, in fact, we have

$$(*) \qquad \begin{cases} g_{ij} = \underset{-}{g_{ij}} + \underset{\vee}{g_{ij}} \\ \Gamma^r_{\ st} = \underset{-}{\Gamma^r_{\ st}} + \underset{\vee}{\Gamma^r_{\ st}}\,, \end{cases}$$

and (1) may be written:

$$(2) \qquad g_{ij,l} - (g_{sj}\Gamma^s_{\ il} + g_{is}\Gamma^s_{\ lj}) = 0.$$

With the same real quantities of (*) we form the hermitian quantities

$$g'_{ij} = \underset{-}{g_{ij}} + i\underset{\vee}{g_{ij}}\,,$$

$$\Gamma'^r_{\ st} = \underset{-}{\Gamma^r_{\ st}} + i\underset{\vee}{\Gamma^r_{\ st}}\,;$$

then (1) for the primed field variables may be put in the following real form:

$$(3) \qquad \begin{aligned} &g_{ij,l} - \tfrac{1}{2}(g_{sj}\Gamma^s_{\ il} + g_{is}\Gamma^s_{\ lj}) - \tfrac{1}{2}(g_{sj}\Gamma^s_{\ li} + g_{is}\Gamma^s_{\ jl}) - \\ &- \tfrac{1}{2}(g_{js}\Gamma^s_{\ il} + g_{si}\Gamma^s_{\ lj}) + \tfrac{1}{2}(g_{js}\Gamma^s_{\ li} + g_{si}\Gamma^s_{\ jl}) = 0\,. \end{aligned}$$

This suggests the consideration of other possible types of Christoffel relations. In this paper we start from a generalized one, containing eight (real) coefficients:

$$(4) \qquad \begin{aligned} &g_{ij,l} + a_1 g_{sj}\Gamma^s_{\ il} + a_2 g_{is}\Gamma^s_{\ lj} + a_3 g_{sj}\Gamma^s_{\ li} + a_4 g_{is}\Gamma^s_{\ jl} + \\ &+ b_1 g_{js}\Gamma^s_{\ il} + b_2 g_{si}\Gamma^s_{\ lj} + b_3 g_{js}\Gamma^s_{\ li} + b_4 g_{si}\Gamma^s_{\ jl} = 0. \end{aligned}$$

2. – At first, we must impose on the coefficients of (4) the condition for general invariance. If from the first member of (4) we subtract the two

(2) V. HLAVATÝ: *Proc. of the Nat. Acad. of Sciences*, **39**, 507 (1953).

tensors

$$(^{+}_{+}) \qquad g_{ij/l} \equiv g_{ij,l} - g_{sj}\Gamma^{s}_{\underline{il}} - g_{is}\Gamma^{s}_{\underline{lj}} ,$$

$$(^{++}_{++}) \qquad (a_1 - a_3)g_{sj}\overset{\vee}{\Gamma}{}^{s}_{il} + (a_2 - a_4)g_{is}\overset{\vee}{\Gamma}{}^{s}_{lj} + (b_1 - b_3)g_{js}\overset{\vee}{\Gamma}{}^{s}_{il} + (b_2 - b_4)g_{si}\overset{\vee}{\Gamma}{}^{s}_{lj} ,$$

the remaining expression is the following:

$$(a_1 + a_3 + 1)g_{sj}\Gamma^{s}_{\underline{il}} + (a_2 + a_4 + 1)g_{is}\Gamma^{s}_{\underline{lj}} + (b_1 + b_3)g_{js}\Gamma^{s}_{\underline{il}} + (b_2 + b_4)g_{si}\Gamma^{s}_{\underline{lj}} ,$$

or, with other constants:

$$(5) \qquad (a\underline{g_{sj}} + b\overset{\vee}{g}_{sj})\Gamma^{s}_{\underline{il}} + (c\underline{g_{is}} + d\overset{\vee}{g}_{is})\Gamma^{s}_{\underline{jl}} .$$

We must therefore (and this is sufficient) impose the tensorial property on this last expression (5).

We may contemplate the case $\overset{\vee}{g}_{ij} = 0$; then the following expression must be distinctively a tensor:

$$(6) \qquad a\underline{g_{sj}}\Gamma^{s}_{\underline{il}} + c\underline{g_{is}}\Gamma^{s}_{\underline{jl}} ;$$

and also its symmetric and skew parts with respect to the indices i and j:

$$\frac{a + c}{2}(\underline{g_{sj}}\Gamma^{s}_{\underline{il}} + \underline{g_{is}}\Gamma^{s}_{\underline{jl}})$$

$$\frac{a - c}{2}(\underline{g_{sj}}\Gamma^{s}_{\underline{il}} - \underline{g_{is}}\Gamma^{s}_{\underline{jl}})$$

must be tensors. The symmetric part, equal to

$$\frac{a + c}{2}(\underline{g_{ij/l}} - \underline{g_{ij,l}}) ,$$

not being a tensor, demands

$$a + c = 0 .$$

Also the skew part imposes

$$a - c = 0 ;$$

this may be seen, for example, by observing that it is equal to

$$\frac{a - c}{2}(\underline{g_{il/j}} - \underline{g_{jl/i}} - \underline{g_{il,j}} + \underline{g_{jl,i}}) ,$$

and that while the first two terms are tensors, this is not so for the group of the latter two.

Equation (5) therefore reduces to

$$b\underset{\vee}{g_{sj}}\Gamma^{s}_{\underline{il}} + d\underset{\vee}{g_{is}}\Gamma^{s}_{\underline{jl}} .$$

The skew part of this expression, analogously to the symmetric part of (6), demands

$$b + d = 0 .$$

Let us now multiply the symmetric part

$$\frac{b-d}{2}(\underset{\vee}{g_{sj}}\Gamma^{s}_{\underline{il}} - \underset{\vee}{g_{is}}\Gamma^{s}_{\underline{jl}})$$

by h^{ij}, the normalized minor of $g_{\underline{ij}}$, defined by

$$h^{ij}g_{\underline{ir}} = \delta^{j}_{r} .$$

Inside the brackets the non-tensorial expression

$$2h^{ij}\underset{\vee}{g_{sj}}\Gamma^{s}_{\underline{il}}$$

comes out; hence

$$b - d = 0.$$

We conclude that the four constants a, b, c and d vanish, and on the left hand side of (4) we are left with only the terms contained in the expressions labelled $(^{+}_{+})$ and $(^{++}_{++})$; with a further new choice of constants, we get the tensorial relation:

$$g_{ij/l} - (Ag_{sj} + Bg_{js})\underset{\vee}{\Gamma^{s}_{il}} - (Cg_{is} + Dg_{si})\underset{\vee}{\Gamma^{s}_{lj}} = 0 , \tag{7}$$

with only four arbitrary coefficients.

Let us now demand that (5) be invariant if we replace g_{ij} and Γ^{r}_{st} by their transposed

$$\tilde{g}_{ij} = g_{ji} ; \qquad \tilde{\Gamma}^{r}_{st} = \Gamma^{r}_{ts} .$$

This condition is usually imposed in unified field theory, and amounts to demanding invariance with respect to a change of sign of the electromagnetic field.

It can easily be checked that this implies

$$A = C \quad \text{and} \quad B = D\ ;$$

and we get the final form:

$$g_{ij/l} - (Ag_{sj} + Bg_{js})\Gamma^s_{\underset{\vee}{il}} - (Ag_{is} + Bg_{si})\Gamma^s_{\underset{\vee}{lj}} = 0 \tag{8}$$

with only two arbitrary coefficients.

3. – By splitting (8) into symmetric and skew parts, we can write

$$g_{\underline{ij}/l} - (A - B)g_{\underset{\vee}{sj}}\Gamma^s_{\underset{\vee}{il}} - (A - B)g_{\underset{\vee}{is}}\Gamma^s_{\underset{\vee}{lj}} = 0\ , \tag{9a}$$

$$g_{\underset{\vee}{ij}/l} - (A + B)g_{\underline{sj}}\Gamma^s_{\underset{\vee}{il}} - (A + B)g_{\underline{is}}\Gamma^s_{\underset{\vee}{lj}} = 0\ . \tag{9b}$$

Adding together (9*a*) and the other two equations obtained from it by cyclic permutation (*ijl*), we get

$$g_{\underline{ij}/l} + g_{\underline{li}/j} + g_{\underline{jl}/i} = 0\ . \tag{10}$$

This verifies that in every case the necessary and sufficient condition for the metric

$$\mathrm{d}s^2 = g_{\underline{ij}}\,\mathrm{d}x^i\,\mathrm{d}x^j$$

to be the same as the «rudimentary» one defined on every geodesic, is satisfied [3].

Excluding for the moment the cases in which $|A| = |B|$, we put

$$\alpha = \pm\sqrt{\frac{A - B}{A + B}}\ ; \qquad \beta = \pm\sqrt{A^2 - B^2}$$

(where the signs are such that $\alpha\beta = A - B$), and multiply (9*b*) by α. With the simple changes in the skew parts of the field variables

$$\begin{cases} \alpha\, g_{\underset{\vee}{ij}} \to g_{\underset{\vee}{ij}}\ , \\ \beta\Gamma^r_{\underset{\vee}{st}} \to \Gamma^r_{\underset{\vee}{st}}\ , \end{cases} \tag{12}$$

---

[3] See, e.g., L. P. EISENHART: *Non-riemannian geometry* (New York, 1927), p. 83 and following.

and adding together (9*a*) and (9*b*), we get the canonical relation (1) again. We see that (8) always gives just the real or the hermitian case according as the two constants α and β are both real or both imaginary (and a « mixed » case is not possible); i.e., according as $|A|$ is greater or smaller than $|B|$.

4. – The particular cases.

I. If $A = B \neq 0$, (9*a*) is the Riemannian Christoffel relation and leads to

13*a*) $$\Gamma^r_{st} = \left\{ \begin{matrix} r \\ st \end{matrix} \right\},$$

where $$\left[\left\{ \begin{matrix} r \\ st \end{matrix} \right\} = \frac{1}{2} h^{rk}(g_{\underline{kt},s} + g_{\underline{sk},t} - g_{\underline{ts},k}) \right];$$

then (9*b*) can easily be solved with respect to $\underset{\vee}{\Gamma}{}^r_{st}$:

(13*b*) $$\underset{\vee}{\Gamma}{}^r_{st} = \frac{1}{4A} h^{rl}(\underset{\vee}{g}_{lt/s} + \underset{\vee}{g}_{sl/t} - \underset{\vee}{g}_{ts/l}) .$$

II. The case $A = -B \neq 0$ is interesting. Changing the notation, and substituting $\underset{\vee}{\Gamma}{}^r_{st}$ for $2A\underset{\vee}{\Gamma}{}^r_{st}$, equations (9) read now:

(14*a*) $$g_{\underline{ij}/l} - \underset{\vee}{g}_{sj}\underset{\vee}{\Gamma}{}^s_{il} - \underset{\vee}{g}_{is}\underset{\vee}{\Gamma}{}^s_{lj} = 0 ,$$

(14*b*) $$\underset{\vee}{g}_{ij/l} = 0 ,$$

[where the bar / indicates the derivative with respect to the affinity $\Gamma^r_{\underline{st}}$].

We can solve (14*a*) in the usual way with respect to $\Gamma^r_{\underline{lj}}$:

(15) $$\Gamma^r_{\underline{lj}} = \left\{ \begin{matrix} r \\ lj \end{matrix} \right\} + h^{ri}(\underset{\vee}{g}_{sj}\underset{\vee}{\Gamma}{}^s_{li} + \underset{\vee}{g}_{sl}\underset{\vee}{\Gamma}{}^s_{ji}) .$$

This relation may be written

(15′) $$\Gamma^r_{\underline{lj}} = \left\{ \begin{matrix} r \\ lj \end{matrix} \right\} + h^{ri}T_{jli} ,$$

where

(16) $$T_{jli} = \underset{\vee}{g}_{sj}\underset{\vee}{\Gamma}{}^s_{li} + \underset{\vee}{g}_{sl}\underset{\vee}{\Gamma}{}^s_{ji}$$

is a tensor which is symmetric in the first two subscripts, and satisfies

(17) $$T_{jli} + T_{lij} + T_{ijl} = 0 ;$$

this reduces the number of its independent components to twenty. (15′), with an arbitrary T_{jli}, is the most general symmetric affinity compatible with the condition (10) (4). We may express $g_{\underset{\vee}{sl}}\Gamma^{s}_{\underset{\vee}{ij}}$ (with 24 components) as a function of T_{jli} in the following way, as can be verified:

$$g_{\underset{\vee}{sl}}\Gamma^{s}_{\underset{\vee}{ij}} = \tfrac{1}{3}A_{lij} + \tfrac{1}{3}(T_{lij} - T_{lji}), \tag{18}$$

where

$$A_{lij} \equiv g_{\underset{\vee}{sj}}\Gamma^{s}_{\underset{\vee}{li}} + g_{\underset{\vee}{sl}}\Gamma^{s}_{\underset{\vee}{ij}} + g_{\underset{\vee}{si}}\Gamma^{s}_{\underset{\vee}{jl}}$$

is an arbitrary totally skew tensor.

But the novelty comes from (14*b*). Owing to the identity

$$g_{\underset{\vee}{ij}|l} + g_{\underset{\vee}{jl}|i} + g_{\underset{\vee}{li}|j} \equiv g_{\underset{\vee}{ij},l} + g_{\underset{\vee}{jl},i} + g_{\underset{\vee}{li},j},$$

it demands for the fundamental tensor the condition:

$$g_{\underset{\vee}{ij},l} + g_{\underset{\vee}{jl},i} + g_{\underset{\vee}{li},j} = 0, \tag{19}$$

which is of the same type as the first quadruplet of Maxwell's equations. The number of independent equations of the system (14*b*) is therefore reduced by four.

The relation (14*b*), for (15′), reads

$$g_{\underset{\vee}{ij}//l} = g_{\underset{\vee}{sj}}h^{st}T_{ilt} - g_{\underset{\vee}{si}}h^{st}T_{jlt}, \tag{20}$$

where the double bar // indicates the derivative with respect to the « curly brackets » $\left\{ \begin{matrix} r \\ sl \end{matrix} \right\}$.

When the determinant $|g_{\underset{\vee}{ij}}|$ is not zero, the system (20), together with the condition (17), may be put in a more convenient form in the following manner. Contemplate the totally symmetric tensor (with twenty components):

$$U_{ilj} \equiv g_{\underset{\vee}{sj}}h^{st}T_{ilt} + g_{\underset{\vee}{si}}h^{st}T_{ljt} + g_{\underset{\vee}{sl}}h^{st}T_{jit}; \tag{21}$$

---

(4) See E. Schrödinger: *Space-Time Structure* (Cambridge, 1950), p. 64 and following.

we get then from (20):

$$g_{si}\underset{\vee}{h^{st}}T_{ilt} = \tfrac{1}{3}U_{ilj} + \tfrac{1}{3}(\underset{\vee}{g_{li//j}} + \underset{\vee}{g_{ji//l}}) , \tag{22}$$

as can be verified. The tensor U_{ilj} may be calculated, obtaining T_{ilt} from (22), and demanding for it the twenty linear conditions (17).

III. Finally, if $A = B = 0$, equations (9) read:

$$\underline{g_{ij\,l}} = 0 , \tag{23a}$$

$$\underset{\vee}{g_{ij/l}} = 0 . \tag{23b}$$

From the first of these it follows that

$$\underline{\Gamma^{r}_{st}} = \left\{ \begin{matrix} r \\ st \end{matrix} \right\} ;$$

the second then becomes a condition on the fundamental tensor:

$$\underset{\vee}{g_{ij//l}} = 0 . \tag{25}$$

This case is physically inadmissible: it leads, for instance, to the two electro magnetic field invariants $\sqrt{|\underset{\vee}{g_{ij}}|}/\sqrt{-|g_{ij}|}$ and $\underset{\vee}{g_{ik}}\underset{\vee}{g_{rs}}h^{ir}h^{ks}$ being constants.

I wish to thank Professor E. Schrödinger for valuable discussions and suggestions.

RIASSUNTO

Nell'intento di generalizzare le relazioni tra il tensore fondamentale e la connessione del caso reale e del caso hermitiano della teoria unitaria, si considera una relazione contenente otto costanti arbitrarie; imponendo ad essa le condizioni di invarianza tensoriale e di invarianza per trasposizione, il numero dei coefficienti arbitrari viene ridotto a due. Tuttavia, fatta eccezione per tre casi particolari, tale nuova relazione si riduce ancora, sostanzialmente, al caso reale o al caso hermitiano. Uno dei casi particolari è notevole, in quanto impone alla parte emisimmetrica del tensore fondamentale il primo quadrupletto delle equazioni di Maxwell.

IL NUOVO CIMENTO Vol. XI, N. 4 1° Aprile 1954

The S-Wave in Pion-Nucleon Scattering. (*)

M. M. LÉVY

École Normale Supérieure - Paris, France

R. E. MARSHAK

University of Rochester - Rochester, N.Y., U.S.A.

(ricevuto il 3 Febbraio 1954)

Summary. — A calculation is made of the two S-phase shifts of pion-nucleon scattering corresponding to isotopic spin states $T=1/2$ and $T=3/2$, using the Tamm-Dancoff method and an extended source model for the nucleon. The magnitude and energy variation of the α_3 phase-shift agree reasonably well with experiment. The sign of the α_1 phase-shift is correct, but its magnitude is completely wrong. It is likely, however, that α_1 is the S-phase shift which will be seriously altered by taking account of renormalization effects in a more rigorous treatment of the problem.

Recent experiments on pion-nucleon scattering, particularly at Rochester [1] and Columbia [2] in the 35-65 MeV region, have fixed [3] the absolute signs as well as the magnitudes of α_3 and α_1, the S-phase shifts corresponding to the isotopic spin $T=3/2$ and $T=1/2$ states respectively. It turns out that α_3 is negative and changes by a factor of 3 (from -2° at 35 MeV to -6° at 65 MeV), whereas α_1 is positive and remains essentially constant (at about 10°). When these results are considered in conjunction with the results of the

(*) These calculations were started during the authors' visit to the Tata Institute of Fundamental Research (Bombay) in August 1953.

(1) S. W. BARNES, C. E. ANGELL, J. P. PERRY, D. MILLER, J. RING and D. NELSON: *Phys. Rev.* **92**, 1327 (1953).

(2) D. BODANSKY, A. M. SACHS and J. STEINBERGER: *Bull. Amer. Phys. Soc.*, **28** (n. 6), 14 (1953).

(3) The Fermi-Yang duality still remains, of course; however, the S-phase shifts are chosen so that the α_{33} phase shift is positive and the largest of the P-phase shifts (cf. *Proc. Rochester Conference on High Energy Physics*, Interscience Publishers, 1953).

Chicago experiments at higher energies ([3a]), it becomes clear that α_3 is a rapidly varying negative, and α_1 a slowly varying positive function of the energy from 35 to at least 150 MeV. The opposite signs of the two phase shifts and their completely different energy dependence can easily be explained by a phenomenological theory ([4]) which postulates an attractive potential with a a repulsive core for the α_3 phase shift and a pure attractive potential for α_1. However, in this note, we report on an attempt to determine whether the renormalizable PS(PS) theory (pseudoscalar theory with pseudoscalar coupling) can explain even qualitatively the signs and energy dependence of the S-phase shifts.

At first sight, the PS(PS) theory does not offer a promising explanation of the S-phase shifts. Since we are interested in pion-nucleon scattering at non-relativistic energies (for the nucleon), we can examine the two leading terms in the canonically transformed Hamiltonian which are usually considered ([5]), namely:

$$\frac{G\mu\psi^*}{2M}\boldsymbol{\tau}\sigma\cdot\nabla\boldsymbol{\varphi}\psi+\frac{G^2\mu}{2M}\psi^*\boldsymbol{\varphi}^2\psi\,, \tag{1}$$

where ψ is the nucleon wave function, $\boldsymbol{\varphi}$ the pion wavefunction, M and μ are the respective masses, G is the coupling constant and σ and $\boldsymbol{\tau}$ are the spin and isotopic spin operators of the nucleon. The first term in (1) gives the P wave scattering and the second term (core term) gives S scattering: however, it is clear that the repulsive core term yields the same negative sign and magnitude for α_3 and α_1 in all approximations — in contradiction to experiment. The next term in the canonically transformed PS(PS) Hamiltonian is ([6])

$$\left(\frac{G\mu}{2M}\right)^2\psi^*\boldsymbol{\tau}\cdot\boldsymbol{\varphi}\wedge\boldsymbol{\pi}\psi\,, \tag{2}$$

where $\boldsymbol{\pi}$ is the canonically conjugate momentum to $\boldsymbol{\varphi}$; (2) represents a coupling between the isotopic spins of the nucleon and the pion ($\int d\boldsymbol{r}\boldsymbol{\varphi}\cdot\boldsymbol{\pi}$ is equal to $\boldsymbol{\theta}$, the isotopic spin of the pion) and leads immediately, in Born approximation, to a negative α_3 but to an $\alpha_1=-2\alpha_3$. If one now recalls that an improved Tamm-Dancoff calculation ([7]) of the P-phase shifts changes the Born approximation results in the direction of enhancing the attractive α_{33}

([3a]) H. L. Anderson, E. Fermi, R. Martin and D. E. Nagle: *Phys. Rev.*, **91**, 155 (1953).

([4]) R. E. Marshak: *Phys. Rev.*, **88**, 1208 (1952); A. E. Woodruff: *Bull. Amer. Phys. Soc.*, **28** (n. 4), 19 (1953).

([5]) Cfr. F. J. Dyson: *Phys. Rev.*, **73**, 929 (1948).

([6]) Cf. S. Drell and E. Henley: *Phys. Rev.*, **88**, 1053 (1952).

([7]) G. F. Chew: *Phys. Rev.*, **89**, 591 (1953).

($T=3/2$, $J=3/2$) phase shift and decreasing the repulsive $\alpha_{31}(T=3/2,\ J=1/2)$, α_{13} ($T=1/2$, $J=3/2$), α_{11} ($T=1/2$, $J=1/2$) phase shifts—in agreement with experiment—one may entertain the hope that an improved Tamm-Dancoff calculation of the S-phase shifts, taking into account the contribution of (2) in addition to the core term, would at least lead to opposite signs for α_3 and α_1.

We have performed a lowest order Tamm-Dancoff calculation of the S-phase shifts using an extended source for the nucleon which is essentially analogous to Chew's methods [7] of calculation for the P-phase shifts. In writing down the Tamm-Dancoff equation for the problem, we have utilized the original PS(PS) Hamiltonian (and not the canonically transformed Hamiltonian given by (1) and (2)) for the sake of consistency in going to the non-relativistic approximation for the nucleon. The fundamental equation is:

$$a(\boldsymbol{p}) = \delta(\boldsymbol{p}-\boldsymbol{k}) + \frac{1}{2(\varepsilon-\omega_p)}\left[3E_{1/2}A + (2E_{3/2}-E_{1/2})B\right], \tag{3}$$

where

$$A = -\frac{G^2}{(2\pi)^3}\int \frac{a(\boldsymbol{p}')\,\mathrm{d}\boldsymbol{p}'\,S(p)S(p')}{2\sqrt{\omega_p\omega_{p'}}(\varepsilon-2M-\omega_p-\omega_{p'})},$$

and

$$B = -\frac{G^2}{(2\pi)^3}\int \frac{a(\boldsymbol{p}')\,\mathrm{d}\boldsymbol{p}'\,S(p)\,S(p')}{2\sqrt{\omega_p\omega_{p'}}(\varepsilon-2M)}.$$

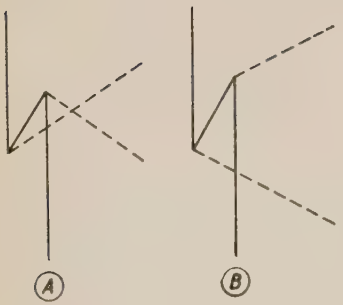

Fig. 1.

In Eq. (3), $a(\boldsymbol{p})$ is the S wave amplitude corresponding to the pion momentum p with an associated energy ω_p, k and ε are the momentum and energy of the incident pion, $E_{\frac{3}{2}}$ and $E_{\frac{1}{2}}$ are the projection operators corresponding to the $T=3/2$ and $T=1/2$ states respectively, and $S(p)$ is the source function for the nucleon. The integrals A and B represent the contributions of the two nucleon pair diagrams (shown in Fig. 1) with their sum *roughly* equivalent to the contribution of the core term in Eq. (1) and their difference to the isotopic spin-dependent term (2). Eq. (3) leads to an equation for the $T=3/2$ amplitude which can be solved rigorously for the phase shift α_3 with the result:

$$\operatorname{tg}\alpha_3 = -\frac{G^2kQ(k)}{4\pi(2M-\varepsilon)}\cdot\frac{1}{1+\dfrac{G^2\mu}{8\pi(2M-\varepsilon)}\Delta_0}, \tag{4}$$

where

$$Q(k) = S^2(k) \quad \text{and} \quad \Delta_0 = \frac{2}{\pi\mu} P \int_0^\infty \frac{Q(p)p^2\,\mathrm{d}p}{\omega_p(\omega_p - \varepsilon)} \qquad (P \text{ denotes principal part}).$$

The integral equation for the $T = 1/2$ amplitude is more complicated and does not yield an analytic expression for α_1; the equation for $\alpha_{\frac{1}{2}}(p)$ is:

$$(5) \qquad \alpha_{\frac{1}{2}}(p) = \delta(p-k) + \\ + \frac{G^2}{4\pi^2(\varepsilon - \omega_p)(2M - \varepsilon)} \int_0^\infty \frac{a(p')p'^2\,\mathrm{d}p'\,S(p)S(p')}{\sqrt{\omega_p\omega_{p'}}} \left[1 - \frac{3}{2}\frac{\omega_p + \omega_{p'}}{2M + \omega_p + \omega_{p'} - \varepsilon}\right].$$

To solve Eq. (5) approximatively we replace p by k in the bracket of the integrand on the R.H.S.; this approximation yields the correct Born approximation ratio ([8]) of α_1 to α_3 and also the correct asymptotic behaviour of the wave function in configuration space. The expression derived for α_1 in the above approximation is:

$$(6) \qquad \operatorname{tg}\alpha_1 = -\frac{G^2 k Q(k)}{4\pi(2M - \varepsilon)} \cdot \frac{\left(1 - \dfrac{3\varepsilon}{2M + \varepsilon}\right)}{1 + \dfrac{G^2\mu}{8\pi(2M - \varepsilon)}\left(\Delta_0 - \dfrac{3}{2}\Delta_1\right)},$$

where

$$\Delta_1 = \frac{2}{\pi\mu} P \int_0^\infty \frac{Q(p)p^2\,\mathrm{d}p\,(\omega_p + \varepsilon)}{\omega_p(\omega_p - \varepsilon)(\omega_p + 2M)}.$$

We have checked the validity of approximation (6) for α_1 and found the convergence to be very rapid.

Numerical computations of α_3 and α_1 have been performed at several incident meson energies corresponding to the source function $Q(k) = \beta^2/(k^2 + \beta^2)$ where two values of β have been chosen, M and $2M$; two choices of the coupling $G^2/4\pi$, namely 10 and 15, were also tried. Table I contains the results for α_3/k and α_1/k (k in units of μ) at zero incident kinetic energy for the four combinations of constants. Table II lists the predicted values of α_3 and α_1 at the Rochester, Columbia, and Chicago energies for two choices of constants, namely $G^2/4\pi = 10$, $\beta = M$ and $G^2/4\pi = 15$, $\beta = 2M$.

([8]) J. Ashkin, A. Simon and R. E. Marshak: *Prog. Theor. Phys.*, 5, 634 (1950); there is a misprint in formula (19) for σ_1(N.R.) which should read

$$\pi\left(\frac{g^2}{M}\right)^2\left(1 + \frac{\mu}{2M}\right)^{-2}\left(1 + \frac{\mu}{M}\right)^{-2}.$$

TABLE I.

β \ $G^2/4\pi$		10	15
M	α_3/k	— 0.182	— 0.197
	α_1/k	— 0.265	— 0.308
$2M$	α_3/k	— 0.110	— 0.110
	α_1/k	— 0.256	— 0.295

TABLE II.

$(\varepsilon-\mu)$(MeV) \ $G^2/4\pi$, β		10, M	15, $2M$
32	α_3	— 11.1°	— 8.2°
	α_1	— 19.0°	+ 86.3°
62	α_3	— 14.6°	— 11.1°
	α_1	— 24.2°	+ 77.7°
135	α_3	— 21.0°	— 16.7°
	α_1	— 31.3°	+ 78.5°

It is seen from Table I that (α_3/k) is rather insensitive to the coupling constant (because of the importance of the second term in the denominator of (4)); (α_1/k) seems to be insensitive to both the coupling constant and the cutoff momentum. Although comparison with experiment is a dubious procedure at this stage, it is worth noting that $\frac{\alpha_3}{k}-\frac{\alpha_1}{k}$ is in better accord with the value deduced from the zero energy charge-exchange scattering cross-section [9] when the higher cutoff momentum is used. Moreover, the higher cutoff momentum [10] ($\beta = 2M$) leads (cfr. Table II) to values of α_3 in closer agreement with experiment and interestingly enough to *positive* values of α_1 (although its magnitude is completely wrong). The large positive values of α_1 result from the reversal of sign of the denominator in Eq. (6) as the meson energy is increased, giving rise to a « resonance » at some intermediate energy between 0 and 37 MeV.

Our calculation, despite its primitive character, possesses several points

[9] The value $8^0/100$ MeV/c is deduced for $\left|\frac{\alpha_3}{k}-\frac{\alpha_1}{k_1}\right|$ from recent photomesic measurements near threshold at M.I.T. and Cornell (B. T. FELD and R. R. WILSON, private communications).

[10] There seems to be some reason for requiring a higher cutoff momentum in the meson theory of nuclear forces (cf. M. M. LÉVY: *Proc. Japanese Conf. on Theor. Phys.*, September 1953).

of interest ([11]). The sign of the α_3 phase shift is correct and its magnitude reasonable in the measured range of energies; this is encouraging since the effects of renormalization on α_3 should be relatively unimportant ([12]). On the other hand, renormalization effects play a very important role ([12]) in the case of the α_1 phase shift so that the numerical values of α_1 can certainly not be trusted. It is even difficult to say wehther the resonance at a finite kinetic energy will persist in a more correct calculation. However, the possibility of reversing the sign of α_1 is a promising feature of our admittedly crude calculation and demonstrates the fact that, for sufficiently large values of the cutoff momentum, the contribution of the isotopic spin-dependent term (2) to the α_1 phase shift, may exceed the contribution of the core term in (1). It should be remarked that the behaviour of the α_3 and α_1 phase shifts in the neighborhood of zero energy predicted by our version of the PS(PS) theory differs from that postulated in the usual phenomenological theory ([4]): the α_1 rather than the α_3 phase shift reverses sign. Both possibilities are equally compatible with the charge-exchange scattering cross-section at zero energy and it will be necessary to perform differential scattering experiments in the very low energy region in order to decide which S-phase shift, if any, reverses sign.

We are indebted to Mr. E. C. George of the Tata Institute and Mademoiselle C. Jauzein of the École Normale Supérieure for assistance with the numerical computations. The hospitality of Dr. H. J. Bhabha, Director of the Tata Institute of Fundamental Research, and of Professor Y. Rocard, Directeur du Laboratoire de Physique de l'École Normale Supérieure, is gratefully acknowledged.

([11]) A similar independent calculation has been performed by N. Fukuda: *Proc. Japanese Conf. on Theor. Phys.*, September 1953.

([12]) M. M. Lévy: *Phys. Rev.* (in press).

RIASSUNTO (*)

Si calcolano i due spostamenti della fase S dello scattering pione-nucleone corrispondenti agli stati di spin isotopico $T=1/2$ e $T=3/2$ per mezzo del metodo di Tamm-Dancoff e di un modello a sorgente estesa pel nucleone. La grandezza e la variazione d'energia dello spostamento di fase α_3 si accordano soddisfacentemente coll'esperienza. Il segno dello spostamento di fase α_1 è il giusto, ma la sua grandezza risulta totalmente diversa dal risultato sperimentale. È, tuttavia, probabile che lo spostamento α_1 della fase S risulti profondamente modificato, se in una trattazione più rigorosa del problema si tien conto degli effetti della rinormalizzazione.

(*) *Traduzione a cura della Redazione.*

Distribuzioni e correlazioni angolari e distribuzioni energetiche dei rami in stelle di disintegrazione nucleare prodotte dalla radiazione cosmica.

G. Belliboni e B. Vitale

Istituto di Fisica dell'Università - Padova
Istituto Nazionale di Fisica Nucleare - Sezione di Padova

(ricevuto il 4 Febbraio 1954)

Riassunto. — Sono state studiate le distribuzioni e le correlazioni angolari dei rami di bassa, media ed alta energia, in stelle di disintegrazione nucleare. Le stelle studiate sono state divise in cinque categorie, corrispondenti a differenti energie medie dei primari, variabili tra 100 MeV e 10 GeV circa; per ciascuna categoria è stata analizzata la distribuzione degli angoli nello spazio ζ con la verticale o il primario e la distribuzione degli angoli nello spazio ψ tra i rami. Per le stelle di più alta energia è stato determinato anche lo spettro energetico dei rami. L'insieme dei fenomeni osservati permette di raccogliere, in un unico quadro fenomenologico, le informazioni sull'andamento delle disintegrazioni nucleari, ottenibili da analisi angolari ed energetiche dei rami.

L'analisi sistematica delle distribuzioni e correlazioni angolari e delle distribuzioni energetiche dei rami di bassa, media ed alta energia in stelle di disintegrazione nucleare, della quale abbiamo già pubblicato alcuni risultati preliminari [1], è stata estesa ad una statistica più ampia, comprendente anche stelle a pochi rami di bassa energia.

Abbiamo suddiviso la discussione dei risultati ottenuti in tre parti, ciascuna delle quali è preceduta da una breve sintesi dei risultati già ottenuti da altri autori:

1) Distribuzioni angolari dei rami.
2) Correlazioni angolari tra i rami.
3) Distribuzioni energetiche dei rami.

[1] G. Belliboni e B. Vitale: *Nuovo Cimento*, **10**, 72 (1953).

1. – Distribuzioni angolari dei rami.

Le distribuzioni angolari dei prodotti di una disintegrazione nucleare sono direttamente determinate dai processi che danno luogo ad essa o vi intervengono; il loro studio può quindi fornire dei dati sperimentali utili nell'analisi della validità dei meccanismi proposti per le disintegrazioni nucleari e per la critica dei modelli che li giustificano.

Le distribuzioni angolari sperimentalmente osservabili risultano dalla sovrapposizione di distribuzioni diverse, ciascuna corrispondente ad uno degli stadi della disintegrazione; è quindi interessante seguire le loro variazioni al variare dell'energia del primario o, in mancanza di questo dato, al variare della « grandezza » della stella.

Il legame tra distribuzioni angolari e meccanismi di disintegrazione è di immediata interpretazione fisica solo per le distribuzioni in ζ_p (angolo nello spazio tra il ramo considerato e la direzione del primario); esso si attenua quando si considerano le distribuzioni, più rapidamente raccolte sperimentalmente, in ϑ_p (angolo nel piano dell'emulsione tra le proiezioni del ramo e del primario). Inoltre, la difficoltà di identificare il primario e l'alta frequenza di primari neutri nelle stelle prodotte dalla radiazione cosmica costringe spesso a limitarsi alle distribuzioni in ζ_v e ϑ_v (angoli, rispettivamente, nello spazio tra il ramo e la verticale, e nel piano dell'emulsione tra le proiezioni del ramo e della verticale).

Per analizzare l'influenza che i diversi stadi della disintegrazione hanno sulle distribuzioni angolari, definiamo, qui e nel seguito:

« anisotropie intrinseche » le deviazioni da una distribuzione isotropa che si conservano inalterate in un sistema nel quale il nucleo è fermo;

« anisotropie estrinseche » le deviazioni da una distribuzione isotropa che scompaiono in tale sistema;

un rapporto $B(\zeta_p)$ dato dalla relazione:

$$B(\zeta_p) = \frac{0^\circ \leqslant \zeta_p < 90^\circ}{90^\circ \leqslant \zeta_p \leqslant 180^\circ}, \tag{1}$$

ed analoghi rapporti $B(\vartheta_p)$; $B(\zeta_v)$; $B(\vartheta_v)$. Nelle relazioni del tipo (1) gli angoli sono misurati a partire dalla direzione in avanti del primario o dalla direzione della verticale verso il basso.

1·1. *Distribuzioni angolari dei rami evaporativi.* – Gli stati attraverso i quali passa il nucleo composto, durante la sua diseccitazione, e quindi le distribuzioni angolari ed energetiche delle particelle emesse, sono legati alla condizione che, in ogni stato, il momento angolare totale, la sua componente nella direzione di moto del primario e la parità siano gli stessi presenti nello stato iniziale.

La conservazione della prima e della terza di queste grandezze determina particolari regole di selezione (BETHE [2]); la conservazione della seconda determina le distribuzioni angolari delle particelle emesse (WOLFENSTEIN [3]).

Le anisotropie che verrebbero così a determinarsi nelle distribuzioni in ζ_p sono però estremamente deboli e praticamente inapprezzabili; si può concludere che, se tutti i rami delle stelle di disintegrazione fossero emessi in una fase evaporativa, conseguenza della formazione di un nucleo composto, le distribuzioni in ζ_p non dovrebbero mostrare anisotropie intrinseche.

I dati sperimentali mettono in luce notevoli anisotropie: ecco, ad esempio, i valori di $B(\vartheta_p)$ calcolati dai dati di GARDNER *et al.* [4]:

TABELLA I. – *Valori di* $B(\vartheta_p)$ *per stelle generate da deutoni.*

	35 MeV	90 MeV	130 MeV	190 MeV
$B(\vartheta_p) =$	$4{,}2 \pm 0{,}5$	$3{,}2 \pm 0{,}3$	$2{,}6 \pm 0{,}3$	$2{,}6 \pm 0{,}3$

Analizzando i dati finora pubblicati da vari autori, si osserva:

a) l'anisotropia cresce al crescere dell'energia dei rami;

b) l'anisotropia decresce, per rami di eguale energia, al crescere dell'energia del primario e della grandezza della stella (GARDNER *et al.* [4]; MANFREDINI [5]; BELLIBONI *et al.* [6]; WANIEK *et al.* [7]);

c) l'anisotropia tende a scomparire, per i rami di più bassa energia, quando si considerano le sole stelle con rinculo visibile (MANFREDINI [5]; BELLIBONI *et al.* [6]; GRILLI *et al.* [7]).

I risultati di GARDNER e l'osservazione *c*) possono venir spiegati ammettendo che, all'aumentare dell'energia del primario o considerando le sole stelle con rinculo visibile, la percentuale di stelle in nuclei pesanti diviene molto alta; si ammette quindi che le anisotropie osservate siano puramente estrinseche. Ma non tutti i dati sperimentali possono venire inquadrati in uno schema così semplice: il crescere dell'anisotropia al crescere della energia dei rami mette in luce il suo legame diretto con un primo stadio della disintegrazione, quello cioè che porta alla emissione di particelle di alta energia, per le quali il modello del nucleo composto cade in difetto. Inoltre il moto del

(2) H. A. BETHE: *Rev. Mod. Phys.*, **9**, 108 (1937).
(3) L. WOLFENSTEIN: *Phys. Rev.*, **82**, 690 (1951).
(4) E. GARDNER e V. PETERSON: *Phys. Rev.*, **75**, 364 (1949).
(5) A. MANFREDINI: *Nuovo Cimento*, **8**, 195 (1951).
(6) R. W. WANIEK e T. OHTSUKA: *Phys. Rev.*, **89**, 1307 (1953).
(7) M. GRILLI e B. VITALE: *Nuovo Cimento*, **10**, 1047 (1953).

nucleo non potrebbe spiegare la residua, se pur debole, anisotropia osservata, anche per i rami di più bassa energia, in stelle con molti rami ionizzanti, generate certamente in nuclei pesanti.

1·2. *Distribuzioni angolari dei rami di emissione diretta.* – Le anisotropie osservate vanno quindi considerate come intrinseche, legate ad uno degli stadi della disintegrazione. Un tale stadio è predetto dal modello proposto da SERBER ([8]), che descrive la prima fase dell'interazione del primario con il nucleo con lo sviluppo di una cascata nucleonica i cui termini in parte escono dal nucleo (e costituiscono i rami di emissione diretta), in parte vengono assorbiti e determinano l'eccitazione del nucleo residuo, la cui diseccitazione può ancora essere descritta come una fase puramente evaporativa.

Le distribuzioni angolari dei rami di e.d. di varia energia sono state analizzate con metodi statistici (Montecarlo) (GOLDBERGER ([9]); BERNARDINI *et al.* ([10]); MEADOWS ([11]); MUIRHEAD ([12])). Le anisotropie trovate ($B > 1$; aumento di B al crescere dell'energia dei rami) sono in buon accordo con i dati sperimentali: si può quindi concludere che la maggior parte delle anisotropie sperimentali in stelle generate in nuclei pesanti, è da attribuire alla presenza di rami di e.d., anche alle più basse energie.

Il modello di Serber prevede un minimo marcato nelle distribuzioni angolari dei rami di alta energia per angoli molto piccoli con il primario, conseguenza della selezione tra le collisioni possibili, imposta dal principio di esclusione. Questo minimo non è stato osservato sperimentalmente, malgrado l'alta risoluzione angolare con la quale sono state condotte le ultime analisi (HADLEY *et al.* ([13]); HOFMANN *et al.* ([14])): forse fenomeni di rifrazione sulla superficie del nucleo deformano la distribuzione angolare interna dell'e.d. e mascherano eventuali deboli anisotropie (ipotesi avanzata da SERBER, citata in ([13])).

1·3. *Influenza di eventuale riassorbimento di mesoni.* – Quando l'energia del primario è al di sopra della soglia per produzione di mesoni, alcuni dei mesoni prodotti possono essere riassorbiti da una coppia di nucleoni: due piccole cascate nucleoniche partono allora dal punto del nucleo in cui ha luogo l'assorbimento, danno luogo a rami di e.d. e lasciano al nucleo una certa eccitazione residua (PUPPI *et al.* ([15])). Questo fenomeno potrebbe sovrapporsi all'anda-

([8]) R. SERBER: *Phys. Rev.*, **72**, 1114 (1947).
([9]) M. L. GOLDBERGER: *Phys. Rev.*, **74**, 1269 (48).
([10]) G. BERNARDINI, E. T. BOOTH e S. J. LINDENBAUM: *Phys. Rev.*, **88**, 105 (1952).
([11]) J. W. MEADOWS: *Phys. Rev.*, **88**, 143 (1952).
([12]) H. MUIRHEAD: comunicazione privata.
([13]) J. HADLEY e H. YORK: *Phys. Rev.*, **80**, 345 (1950).
([14]) A. HOFMAN, K. STRAUCH: *Phys. Rev.*, **90**, 449 (1953).
([15]) G. PUPPI, V. DE SABBATA e E. MANARESI: *Nuovo Cimento*, **9**, 726 (1952).

mento della normale cascata nucleonica, spiegando così le alte energie di eccitazione osservate nelle stelle molto grandi, eccitazioni difficilmente compatibili con le ipotesi necessarie per giustificare la formazione del nucleo composto.

Le due piccole cascate nucleoniche non avranno alcun legame angolare con la direzione del primario; i termini di e.d. ai quali esse danno luogo risulteranno isotropi rispetto al primario, anche se collimati rispetto ad un loro asse di simmetria. L'intervento di riassorbimento di mesoni può quindi giustificare l'osservata diminuzione dell'anisotropia dei rami di bassa e media energia, all'aumentare dell'energia del primario.

1·4. *Influenza di eventuale evaporazione locale.* – La fase evaporativa dà luogo a rami isotropi solo se interessa tutto il nucleo, uniformemente riscaldato; se invece si creano sulla superficie del nucleo delle zone a più alta temperatura, dalle quali le particelle cominciano ad evaporare prima che si stabilisca l'equilibrio termico con tutto il nucleo, le distribuzioni angolari risentiranno della distribuzione di tali zone rispetto alla direzione del primario.

Zone di alta eccitazione potrebbero formarsi in corrispondenza della parte del nucleo in avanti rispetto al primario, sulla cui superficie urta, in parte riflettendosi, la parte più densa della cascata nucleonica: l'intervento di fenomeni di evaporazione locale tenderebbe quindi ad aumentare l'anisotropia rispetto al primario, accrescendo il valore di B (KIND ([16])).

1·5. *Dati sperimentali.* – Sono state analizzate 585 stelle di bassa e media energia, generate dalla radiazione cosmica in lastre nucleari Ilford G5, spesse 1200 μ, esposte verticali, circondate da 5 cm di Pb, a 4 550 m s.l.m. (Monte Rosa); 95 stelle di alta energia, generate dalla radiazione cosmica in lastre nucleari Ilford G5, spesse 400 e 600 μ, esposte verticali a circa 30 000 m s.l.m. (Minneapolis (U.S.A.) e Cagliari, 1952).

I rami delle stelle sono stati divisi in quattro categorie, in base alla loro ionizzazione specifica I/I^0:

Neri	N	$(I/I^0 > 6{,}5$	corrispondenti a protoni di $E < 30$ MeV)
Nero-grigi	NG	$(6{,}5 \geqslant I/I^0 > 4{,}0$	» » $30 \leqslant E < 100$ MeV)
Grigi	G	$(4{,}0 \geqslant I/I^0 > 2{,}0$	» » $100 \leqslant E < 300$ MeV)
Al minimo	s	$(I/I^0 \leqslant 2{,}0$	» » $E \geqslant 300$ MeV).

Sono stati considerati « rinculi » i rami grossi con $R \leqslant 6$ μ.

a) *Stelle di bassa e media energia.* – Sono state studiate solo le stelle che presentavano non più di un ramo s nel semipiano in avanti rispetto alla verti-

([16]) A. KIND: *Nuovo Cimento*, **10**, 176 (1953).

cale; ogni eventuale s nel semipiano opposto è stato considerato come primario della stella.

Le stelle sono state poi suddivise in tre categorie (indicate qui e nel seguito come I, II e III categoria), per cercare di raggruppare quelle generate da primari di E_p compresa in un intervallo non troppo largo; per ottenere questa suddivisione, ci siamo basati sul numero di rami N, NG, G ed s che esse presentavano, utilizzando per paragone dati ottenuti da altri autori con stelle generate da primari di energia nota (vedi, per una discussione più dettagliata del metodo seguito, GRILLI *et al.* [7]). Le stelle studiate sono state così suddivise:

TABELLA II. - *Stelle di bassa e media energia.*

Categoria	Probabile energia dei primari	N. stelle con rinculo	N. stelle senza rinculo
I	0 – 300 MeV	98	67 (*)
II	300 – 500 MeV	49	93
III	500 – 1000 MeV	98	179
	TOTALE . .	245	339

(*) Sono state escluse le stelle a 2 rami senza rinculo.

Per ogni ramo N, NG, G ed s sono stati misurati: la ionizzazione specifica I/I^0, l'angolo ϑ_v, l'angolo φ di inclinazione della traccia rispetto al piano dell'emulsione. Le due ultime misure ci hanno permesso di calcolare l'angolo ζ_v di ogni ramo.

b) *Stelle di alta energia.* – Sono state studiate solo le stelle che presentavano almeno 8 rami N, con primario visibile ed al minimo di ionizzazione.

Le stelle sono state poi suddivise in due categorie (indicate qui e nel seguito come IV e V categoria), ponendo nella IV le stelle per le quali la somma delle energie di tutti i rami N, NG e G (tenendo conto anche dei neutroni), E_T, cadeva tra 700 e 1500 MeV; nella V le stelle con E_T compresa tra 2500 e e 4000 MeV. Le stelle con E_T intermedia, compresa quindi tra 1500 e 2500 MeV, sono state poste nella IV categoria se presentavano non più di 2 rami s, nella V nel caso contrario. Questa suddivisione è sembrata opportuna perchè le stelle di vario tipo che compongono ciascuna delle due ultime categorie mostrano distribuzioni angolari ed energetiche analoghe.

Il calcolo di E_T è stato fatto, per i NG ed i G, partendo dalla I/I^0 ed associando, allo spettro di protoni, un analogo spettro per i neutroni. L'energia media associata ad ogni N è stata invece calcolata utilizzando i rapporti tra emissione diretta ed evaporazione ed i rapporti n/p ed α/p dati da PUPPI

et al. ([17,18]) per stelle di σ: l'energia media associata ad ogni N è di circa 70 MeV.

La identificazione dei rinculi è resa difficile e dubbia dall'elevato numero di rami, e non è stato tenuto conto della presenza o meno del rinculo nelle seguenti analisi delle distribuzioni e correlazioni angolari e delle distribuzioni energetiche.

Le stelle studiate sono state così suddivise:

TABELLA III. – *Stelle di alta energia.*

Categoria	E_T (MeV)	N. stelle
IV	$700-1\,500$; $1\,500-2\,500$ ($N_s \leqslant 2$)	66
V	$1\,500-2\,500$ ($N_s > 2$); $2\,500-4\,000$	29
	TOTALE	95

Per ogni rami N, NG, G ed s è stata misurata la ionizzazione specifica I/I^0, e calcolato l'angolo ζ_v.

La tabella seguente dà i valori di $B(\zeta_v)$ per le prime tre categorie e di $B(\zeta_p)$ per le ultime due.

TABELLA IV. – *Distribuzioni angolari dei rami N, NG e G, per le stelle delle cinque categorie, con rinculo (c.r.) e senza rinculo (s.r.) visibile.*

	Neri		Nero-grigi		Grigi	
	c.r.	s.r.	c.r.	s.r.	c.r.	s.r.
A) Distribuzioni degli angoli nello spazio con la verticale. Valori di $B(\zeta_v)$:						
I	$0{,}94 \pm 0{,}17$	$1{,}42 \pm 0{,}27$	$1{,}43 \pm 0{,}99$	$2{,}20 \pm 1{,}65$	—	—
II	$0{,}95 \pm 0{,}21$	$1{,}25 \pm 0{,}20$	$0{,}64 \pm 0{,}31$	$1{,}41 \pm 0{,}49$	$0{,}58 \pm 0{,}39$	$2{,}60 \pm 1{,}33$
III	$1{,}24 \pm 0{,}18$	$1{,}26 \pm 0{,}12$	$1{,}12 \pm 0{,}33$	$1{,}38 \pm 0{,}32$	$2{,}12 \pm 0{,}62$	$2{,}28 \pm 0{,}50$

B) Distribuzione degli angoli nello spazio con il primario. Valori di $B(\zeta_p)$:

	Neri	Nero-grigi	Grigi
IV	$1{,}20 \pm 0{,}13$	$2{,}39 \pm 0{,}59$	$2{,}81 \pm 0{,}57$
V	$1{,}28 \pm 0{,}19$	$1{,}70 \pm 0{,}46$	$2{,}29 \pm 0{,}68$

([17]) G. PUPPI: comunicazione privata.

([18]) M. CECCARELLI e G. ZORN: *Nuovo Cimento*, **10**, 540 (1953).

Le fig. 1, 2 e 3 danno le distribuzioni angolari $P(\zeta_r)\,d\zeta_r$, per unità di angolo solido, dei rami N delle stelle delle prime tre categorie; le fig. 4, 5 e 6 danno le distribuzioni angolari $P(\zeta_p)\,d\zeta_p$, per unità di angolo solido, dei rami N, NG e G, rispettivamente, per le stelle della IV categoria.

1·6. *Discussione.* – I dati ottenuti ci permettono di analizzare l'andamento delle distribuzioni angolari al variare dell'energia dei rami e del primario. Le distribuzioni raccolte, relative agli angoli nello spazio, sono indipendenti dalle deformazioni introdotte da una loro proiezione sul piano dell'emulsione; tuttavia, le distribuzioni relative alle stelle di bassa e media energia risentono in modo sfavorevole dello sparpagliamento dei primari rispetto alla verticale. È quindi difficile discutere l'andamento di B al passaggio dal primo gruppo di stelle (I, II e III categoria) al secondo, in quanto le discontinuità presenti possono essere attribuite sia a modificazioni introdotte nel meccanismo di disintegrazione dalla produzione ed eventuale assorbimento di mesoni, sia dal passaggio dalle distribuzioni in ζ_r a quelle in ζ_p. Discuteremo quindi i dati sperimentali indipendentemente per i due gruppi di stelle.

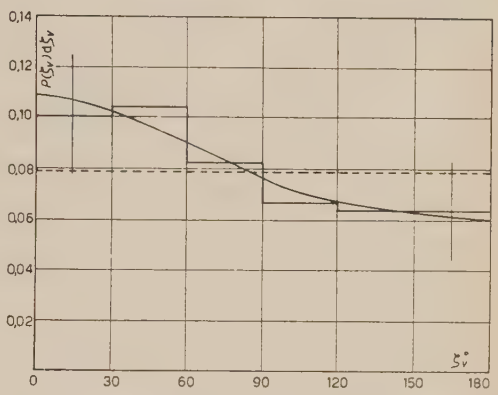

Fig. 1. – Stelle di I categoria s.r. – Rami N – (223 angoli).

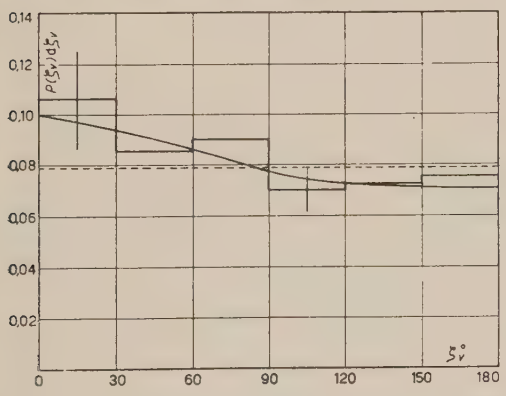

Fig. 2. – Stelle di II categoria s.r. – Rami N – (307 angoli).

a) *Rami di bassa energia in stelle del primo gruppo* (I, II e III categoria) *s.r.* (fig. 1, 2 e 3). – L'anisotropia maggiore è presentata dalle stelle molto piccole (I categoria), tra le quali la percentuale di disintegrazioni in nucleo leggero è certamente alta. È difficile stimare l'influenza del moto del nucleo sulla distribuzione angolare; si può però senz'altro affermare che, se il primario venisse assorbito dal nucleo, dando luogo a nucleo composto, le stelle in soli nuclei leggeri darebbero luogo ad una anisotropia molto maggiore di quella osservata in distribuzioni angolari ri-

spetto al primario. Ne concludiamo che non occorre, per giustificare le distribuzioni angolari anisotrope dei rami neri in stelle piccole, introdurre meccanismi di disintegrazione diversi dalla pura evaporazione isotropa.

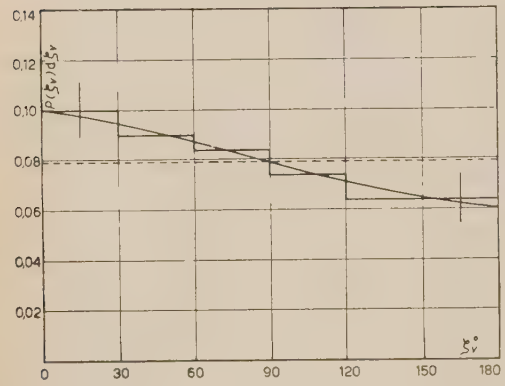

Fig. 3. – Stelle di III categoria s.r. – Rami N – (836 angoli).

Al crescere dell'energia del primario, in stelle (II e III categoria) tra le quali il contributo dei nuclei leggeri è praticamente nullo, l'anisotropia raggiunge un valore costante, che è spiegabile solo con l'introduzione di termini di bassa energia tra i rami di emissione diretta o, eventualmente, con fenomeni di evaporazione locale.

b) *Rami di bassa energia in stelle del secondo gruppo* [IV categoria (fig. 4) e V]. – Il valore dell'anisotropia raggiunta dai rami N nelle stelle della III categoria si mantiene praticamente inalterato all'aumentare dell'energia del primario. Questo fenomeno può essere attribuito ad un riassorbimento dei mesoni prodotti, che tende a riportare la distribuzione angolare dei rami verso l'isotropia e che avrebbe sempre più peso, all'aumentare dell'energia del primario; o a una diminuzione (dovuta alle caratteristiche che determinano l'andamento della cascata, quali la diminuzione della sezione d'urto nucleone-nucleone libero e la minore influenza del principio di esclusione, all'aumentare della energia dei rami della cascata) della percentuale di rami di bassa energia tra i rami di e.d.

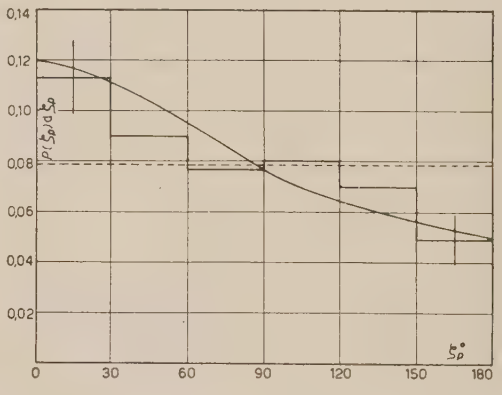

Fig. 4. – Stelle di IV categoria – Rami N – (637 angoli).

c) *Rami di media ed alta energia in stelle del primo e secondo gruppo* (fig. 5, 6 per la IV categoria). – L'anisotropia tende progressivamente a diminuire in tutte le stelle del primo gruppo s.r. ed in quelle del secondo gruppo, man mano che aumenta l'energia del primario. Questo può essere attribuito al particolare andamento assunto a queste energie dalla cascata nucleonica

(nella quale hanno luogo anche urti con produzione di mesoni). C'è infatti da tener presente che, poichè i nostri rami G hanno energie inferiori a 300 MeV, essi possono essere considerati sempre più, all'aumentare dell'energia del primario, come rami di bassa energia, e quindi c'è da attendersi che ne assu-

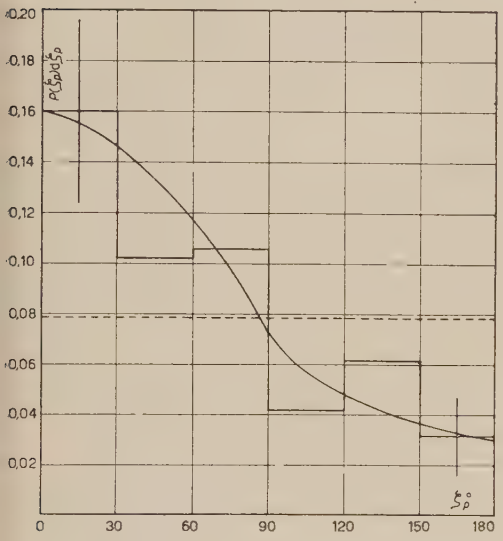

Fig. 5. – Stelle di IV categoria – Rami NG – (149 angoli).

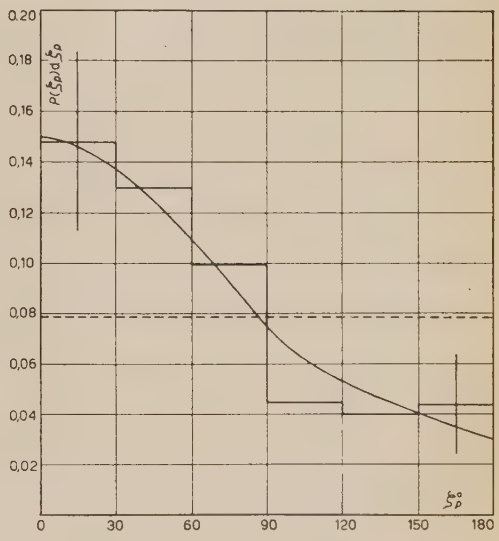

Fig. 6. – Stelle di IV categoria Rami G – (137 angoli).

mano la distribuzione angolare corrispondente. Potrebbe anche intervenire in queste stelle un processo di riassorbimento dei mesoni prodotti.

d) *Rami di bassa, media ed alta energia in stelle del primo gruppo c.r.* – I rami di bassa energia risultano, nelle stelle con rinculo visibile, praticamente isotropi; i rami di media ed alta energia notevolmente meno anisotropi dei corrispondenti rami in stelle s.r.. Nella I categoria questo effetto è probabilmente dovuto in gran parte alla maggiore frequenza di disintegrazioni in nucleo leggero, presenti tra le stelle s.r. rispetto a quelle c.r.; nelle altre, invece, esso rispecchia le caratteristiche fluttuazioni dei vari stadi della disintegrazione, che determinano, nello stesso tempo, la formazione di un rinculo visibile (Grilli *et al.* (7)).

2. – Correlazioni angolari tra i rami.

L'analisi delle distribuzioni angolari dei rami rispetto alla verticale o al primario non esaurisce le possibili indagini sulle caratteristiche angolari che sono connesse ad una disintegrazione nucleare.

Se la distribuzione angolare rispetto a una qualsiasi direzione nello spazio è isotropa, se cioè la $P(\zeta)\,\mathrm{d}\zeta$ è data da:

$$P(\zeta)\,\mathrm{d}\zeta = \frac{1}{4\pi}\,\mathrm{d}\zeta\,, \tag{2}$$

la distribuzione degli angoli ψ nello spazio tra i rami sarà anch'essa data da:

$$P(\psi)\,\mathrm{d}\Omega = \frac{1}{4\pi}\,\mathrm{d}\Omega\,. \tag{3}$$

Definiremo come « correlazione » tra i rami delle stelle ogni fenomeno che discosti la $P(\psi)\,\mathrm{d}\Omega$ dalla distribuzione (3).

Se la distribuzione angolare rispetto a una qualsiasi direzione nello spazio, che sia però il suo asse di simmetria, è, più generalmente, data da una particolare $P(\zeta)\,\mathrm{d}\zeta$, la distribuzione in ψ sarà:

$$P(\psi)\,\mathrm{d}\Omega = \frac{\mathrm{d}\Omega}{4\pi}\int_0^{\pi}\sin\zeta\,P(\zeta)\,\mathrm{d}\zeta\int_0^{2\pi}P(\cos\zeta\cos\psi+\sin\zeta\cos\psi'\sin\psi)\,\mathrm{d}\psi'\,. \tag{4}$$

Essa è quindi direttamente sensibile ad ogni anisotropia presente nelle $P(\zeta)\,\mathrm{d}\zeta$; definiremo, qui e nel seguito:

« correlazioni intrinseche » le deviazioni della $P(\psi)\,\mathrm{d}\Omega$ da una distribuzione (4);

« correlazioni estrinseche » le deviazioni della $P(\psi)\mathrm{d}\Omega$ da una distribuzione (3), quando però la $P(\psi)\,\mathrm{d}\Omega$ sia in accordo con una distribuzione (4).

Le correlazioni estrinseche, quindi, dipendono solo dalla distribuzione angolare dei rami rispetto ad una direzione nello spazio; quelle intrinseche ne sono del tutto indipendenti.

Lo studio delle correlazioni intrinseche mediante l'analisi delle $P(\psi)\,\mathrm{d}\Omega$ è il metodo più diretto e di immediata interpretazione fisica per mettere in luce caratteristici comportamenti angolari delle disintegrazioni nucleari (Belliboni *et al.* [6]; Ceccarelli *et al.* [18]). La necessità di calcolare gli angoli nello spazio tra i rami ha però indotto finora la maggior parte degli autori a limitare le misure a grandezze più facilmente determinabili sperimentalmente: angoli in proiezione sul piano dell'emulsione (Lovera [19]); minimo tra gli angoli proiettati in una stella (Hodgson [20]); « apertura » (angolo minimo comprendente le tre proiezioni) di stelle a tre rami (Della Corte *et al.* [21]);

[19] G. Lovera: *Nuovo Cimento*, **6**, 233 (1949); **9**, 134, 857 (1952).
[20] P. E. Hodgson: *Phil. Mag.*, **43**, 190 (1952).
[21] M. Della Corte e M. Giovannozzi: *Nuovo Cimento*, **8**, 741 (1951).

risultante ottenuta associando un vettore unitario, o proporzionale alla energia, ad ogni ramo (PERKINS [22]; HARDING *et al.* [23]; DELLA CORTE *et al.* [21]).

Questi metodi, pur permettendo la rapida raccolta di ampie ed utili statistiche, portano a correlazioni deformate in modo non precisabile rispetto a quelle degli angoli ψ; non permettono una sicura discriminazione tra correlazioni intrinseche ed estrinseche; ed, infine, i risultati ottenuti non sono suscettibili di diretta e sicura interpretazione fisica. I risultati ottenuti possono invece, come mostreremo più avanti, essere ricondotti alle correlazioni presentate dalle $P(\psi)\,\mathrm{d}\Omega$.

Un metodo che è, invece, indipendente dallo studio delle $P(\psi)\,\mathrm{d}\Omega$, e i cui risultati non possono essere direttamente ricondotti ad esso, è l'analisi del « volume » delle stelle (DELLA CORTE *et al.* [21]) per stelle a tre rami). Quando si studino però stelle a più di tre rami il calcolo del volume del solido, costruito con i rami della stella, diviene eccessivamente laborioso, e non è possibile raccogliere le ampie statistiche necessarie; inoltre questo metodo è, ancora più degli altri metodi, influenzato dalla presenza di rami neutri nelle stelle di disintegrazione studiate.

2·1. *Correlazioni intrinseche tra i rami evaporativi.* – Nel modello classico della fase evaporativa non sembrano prevedibili correlazioni intrinseche tra le particelle evaporate.

2·2. *Correlazioni intrinseche tra i rami di emissione diretta.* – Durante lo sviluppo della cascata nucleonica nel nucleo la distribuzione degli angoli tra i rami della cascata sarà funzione della distribuzione degli impulsi dei nucleoni nel nucleo freddo, della energia del primario e delle sezioni d'urto differenziali nucleone-nucleone libero. Essa presenterà però un netto massimo intorno ai 90°, angolo con il quale due nucleoni escono da un urto, nel sistema in cui uno dei due è inizialmente fermo. Se quindi la cascata nucleonica è descrivibile mediante interazioni nucleone-nucleone libero fino alla superficie del nucleo, è prevedibile che i rami di e.d. mostrino una correlazione intrinseca a circa 90°.

Un fenomeno di questo tipo è già stato osservato (CHAMBERLAIN *et al.* [24]; BELLIBONI *et al.* [6]); esso è confermato dagli attuali dati sperimentali.

2·3. *Correlazioni intrinseche dovute al riassorbimento di mesoni.* – Il meccanismo di riassorbimento di mesoni (§ 1·3), dando luogo a due cascate nucleoniche opposte, potrebbe portare a una correlazione tra i rami di emissione diretta, nel senso di rendere per essi più probabili angoli piccoli e grandi a

---

(22) D. H. PERKINS: *Nature*, **160**, 299 (1947); **161**, 486 (1948).

(23) B. HARDING, S. LATTIMORE e D. H. PERKINS: *Proc. Roy. Soc.*, **196**, 325 (1949).

(24) O. CHAMBERLAIN e E. SEGRÈ: *Phys. Rev.*, **87**, 81 (1952).

scapito di quelli intermedi. Questa correlazione è essenzialmente estrinseca (legata come è alla distribuzione angolare dell'emissione diretta), ma è da considerarsi intrinseca dal punto di vista sperimentale, non esistendo alcun legame tra la direzione del primario o della verticale e l'asse delle cascate generate dal riassorbimento.

Un effetto di questo tipo è già stato osservato per categorie di stelle particolarmente selezionate (CECCARELLI *et al.* ([18])); esso è stato interpretato come risultato dell'assorbimento di circa 3 mesoni per stella.

2·4. *Correlazioni intrinseche dovute alla evaporazione locale.* – Un eventuale fenomeno di evaporazione locale, se la zona del nucleo che evapora emette, prima che si raggiunga l'equilibrio termico, più di un ramo ionizzante, dovrebbe favorire gli angoli piccoli tra i rami. La distribuzione delle risultanti, ottenute associando ad ogni ramo un vettore unitario o proporzionale alla sua energia, dovrebbe in tal caso presentare un eccesso di valori alti, rispetto a quelli prevedibili per eventi non correlati.

Un effetto di questo tipo è stato ritrovato da PERKINS ([22]) e da HARDING *et al.* ([23]), in stelle molto grandi e limitatamente alle sole particelle α, da DELLA CORTE *et al.* ([21]) in stelle a soli tre rami con rinculo visibile.

2·5. *Dati sperimentali.* – Le fig. 7-11 danno le distribuzioni $P(\psi)\,\mathrm{d}\Omega$ per gli angoli ψ nello spazio tra i rami N, in stelle delle cinque categorie e, per il primo gruppo, senza rinculo visibile.

La curva a tratto pieno indica la distribuzione calcolata per ogni categoria utilizzando la (4). In questo calcolo, le distribuzioni angolari rispetto alla verticale o al primario, $P(\zeta)\,\mathrm{d}\zeta$ sono state approssimate con una espressione, del tipo:

$$P(\zeta)\,\mathrm{d}\zeta = (A + B\cos\zeta + C\cos^2\zeta)\,\mathrm{d}\zeta\,, \tag{5}$$

con i coefficienti A, B e C opportunamente normalizzati (curva a tratto pieno nelle fig. 1-6); in questo caso, la (4) diviene:

$$P(\psi)\,\mathrm{d}\Omega = (A' + B'\cos\psi + C'\cos^2\psi)\,\mathrm{d}\Omega\,, \tag{6}$$

con A', B' e C' coefficienti dipendenti da A, B e C.

Gli errori indicati nelle figure sono i soli errori statistici.

2·6. *Discussione.* – Nella discussione dei dati sperimentali, è da tener presente che le $P(\zeta)\,\mathrm{d}\zeta$ per le prime tre categorie, essendo relative alla verticale, risultano indubbiamente meno anisotrope delle effettive distribuzioni rispetto al primario. Le deformazioni introdotte nelle $P(\psi)\,\mathrm{d}\Omega$ dalle anisotropie ango-

lari dovrebbero quindi essere più marcate di quelle indicate dalle curve a tratto pieno, nelle figg. 7-9, e portare ad una maggiore preferenza per gli angoli piccoli. (Inoltre, la (4) non è, in questo caso, a rigore, applicabile, non essendo la verticale asse di simmetria per le stelle).

a) *Rami di bassa energia in stelle della I categoria s.r.* (fig. 7). – Gli angoli ψ risultano correlati, con preferenza per gli angoli grandi (120°-160°).

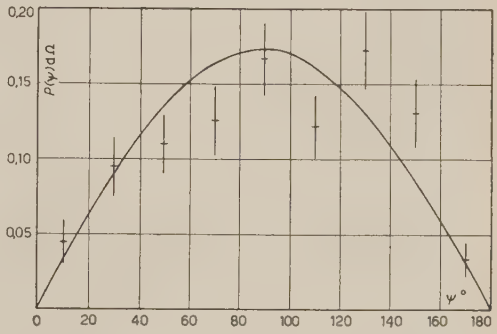

Fig. 7. – Stelle di I categoria s.r. – Correlazioni N-N – (239 angoli).

Questo fenomeno può essere dovuto alla necessità che i rami, prodotti nella disintegrazione totale di un nucleo leggero, conservino l'impulso del nucleo composto.

Per analizzare l'influenza che la presenza dei nuclei leggeri può avere sulle correlazioni angolari delle stelle piccole, abbiamo raccolto, dalla I categoria, i dati relativi alle stelle con solo tre rami neri, s.r.; la fig. 12 indica i punti sperimentali ottenuti, e la distribuzione prevista in base alla distribuzione angolare rispetto alla verticale. È evidente un massimo marcato per angoli intorno ai 120°; tutti gli altri angoli sembrano, nei limiti degli errori, quasi equiprobabili, cosa che sarebbe da attendersi se i rami fossero complanari ed isotropi.

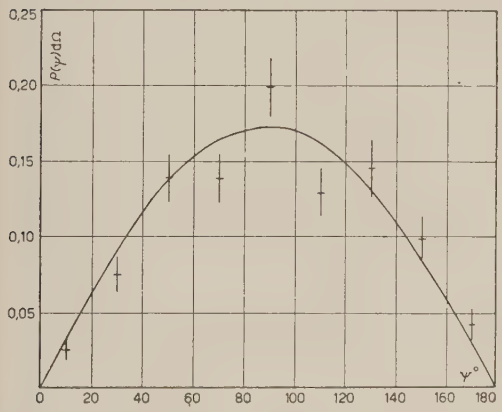

Fig. 8. – Stelle di II categoria s.r. – Correlazioni N-N – (491 angoli).

Questo andamento denota evidentemente la presenza, tra le stelle a tre rami N, di un'alta percentuale di nuclei leggeri, che disintegrano completamente dando luogo in molti casi a soli tre rami, tutti ionizzanti (ad esempio, tre particelle α) o a tre rami ionizzanti ed a qualche neutrone di bassa energia. Abbiamo cercato di analizzare in modo più quantitativo il contributo che tali disintegrazioni possono portare alle correlazioni angolari, nelle ipotesi semplificatrici che:

la stella sia a soli tre rami, tutti ionizzanti e di eguale massa;
l'impulso ceduto dal primario al nucleo sia trascurabile;
i rami abbiano uno spettro energetico di tipo evaporativo.

Imponendo allora la condizione che l'impulso totale dei rami sia nullo, si ottiene:

$$(7) \qquad P(\psi)\,\mathrm{d}\Omega = \frac{\sin\psi\,\mathrm{d}\Omega}{(p''-p')^2}\cdot\int_{p'}^{p''} p_2 \exp\left[-Kp_2^2\sin^2\psi\right]\cdot\left[\exp\left[-y'^2\right]-\exp\left[-y''^2\right]+\right.$$

$$\left.+\,p_2\cos\psi\cdot\sqrt{\pi}\cdot\sqrt{K}(\Phi(y')-\Phi(y''))\right]\mathrm{d}p_2\,,$$

dove:

gli spettri in impulso di due dei rami sono stati schematizzati da una funzione rettangolare, del tipo $\mathrm{d}p/(p''-p')$ tra p'' e p', e nulla fuori di questo intervallo;

lo spettro in impulso del terzo ramo è stato semplificato in una funzione del tipo: $2Kp_3\cdot\exp-(Kp_3^2)$;

$$y' = K(p_3 + p'\cos\psi); \qquad y'' = K(p_3 + p''\cos\psi);$$

la $\Phi(y)$ rappresenta l'integrale degli errori.

Abbiamo tabulato la (7), per $E' = 10$ MeV; $E'' = 20$ MeV; $K = 0{,}33$; la $P(\psi)\,\mathrm{d}\Omega$ risultante è data dalla curva tratteggiata in fig. 12: si ritrova in tal modo il massimo a 120°, che risulterà tanto più marcato quanto più stretti si prenderanno gli spettri delle particelle emesse.

Questo calcolo non permette però conclusioni quantitative sulla percentuale di nuclei leggeri nelle disintegrazioni studiate, a causa della arbitrarietà delle ipotesi fatte; esso giustifica solo, in modo qualitativo, il comportamento osservato, ed è in accordo con una attribuzione di esso alle disintegrazioni in nucleo leggero.

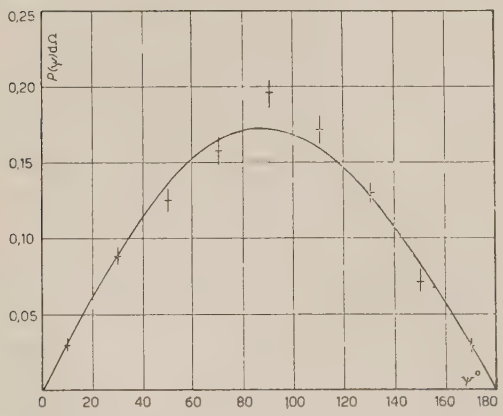

Fig. 9. – Stelle di III categoria s.r. – Correlazioni N-N – (2034 angoli).

b) *Rami di bassa energia in stelle della II e III categoria s.r.* (figg. 8, 9). – Nelle stelle della II categoria s.r., già praticamente tutte in nucleo pesante, i punti sperimentali sono in completo accordo con la $P(\psi)\,\mathrm{d}\Omega$ prevista, tranne che per un lieve massimo a 90°, che potrebbe essere ancora incluso nelle fluttuazioni statistiche. Questo massimo diviene notevolmente più pronunciato, e chiaramente fuori degli errori, nelle stelle della III categoria.

Come abbiamo già detto, riteniamo che questo massimo sia una correlazione intrinseca introdotta dai rami di bassa energia di e.d. (§ 2·2). Il fenomeno ora accertato mette in luce che, anche alle medie energie (fino a quasi 1000 MeV) il meccanismo della cascata può essere semplificato in un succedersi di collisioni nucleone-nucleone libero.

c) *Rami di bassa energia in stelle della IV e V categoria* (figg. 10, 11). – Non esiste alcuna correlazione sensibile, nei limiti degli errori statistici.

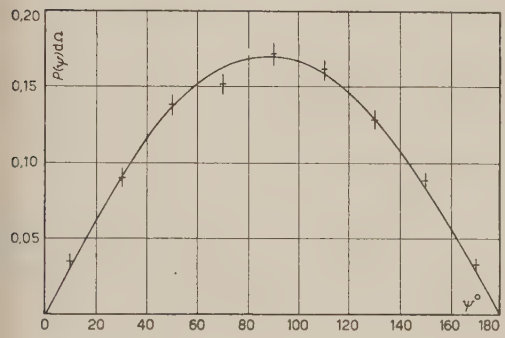

Fig. 10. – Stelle di IV categoria – Correlazioni N-N – (2 936 angoli).

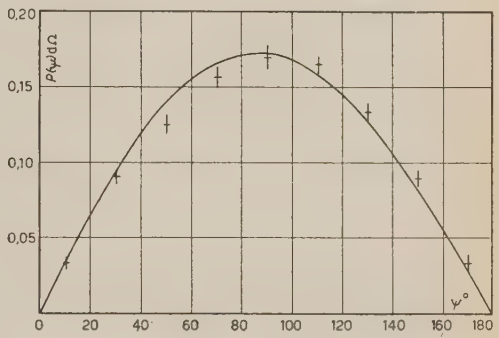

Fig. 11. – Stelle di V categoria – Correlazioni N-N – (2 337 angoli).

Se l'interpretazione data in *b*) del massimo a 90° nelle stelle della III categoria è corretta, l'assenza di una analoga correlazione nelle stelle di più grande energia porta alla conclusione che i termini di bassa energia tra i rami di e.d. divengono sempre meno importanti (v. anche § 1·6-b).

d) *Rami di bassa energia in stelle del primo gruppo, c.r.* – In nessuna delle tre categorie esiste alcuna correlazione apprezzabile, nei limiti degli errori statistici.

L'ipotesi di un meccanismo simile alla fissione, avanzata nel nostro precedente articolo ([6]), non ci sembra giustificabile in base agli attuali dati sperimentali, anche se non può essere esclusa per una piccola percentuale delle stelle c.r. studiate.

e) *Rami di media ed alta energia in stelle del primo e secondo gruppo.* – Si nota un lieve eccesso di angoli piccoli (0°-20°); questo dato è in accordo qualitativo con le osservazioni di CECCARELLI *et al.* ([18]), ma la scarsezza della statistica raccolta ci impedisce di considerarlo come una conferma del fenomeno.

3. – Distribuzioni energetiche dei rami.

L'analisi statistica fatta da GOLDBERGER ([9]), con un « Montecarlo », sull'andamento della cascata nucleonica mise in luce una debole irregolarità nello spettro di energia dei rami di e.d., che presentava un leggero massimo secondario ad energie vicine a quelle del primario (neutrone da 90 MeV); questa irregolarità non è stata in seguito ritrovata nè in altri Montecarlo ([10-12]) nè sperimentalmente ([14]).

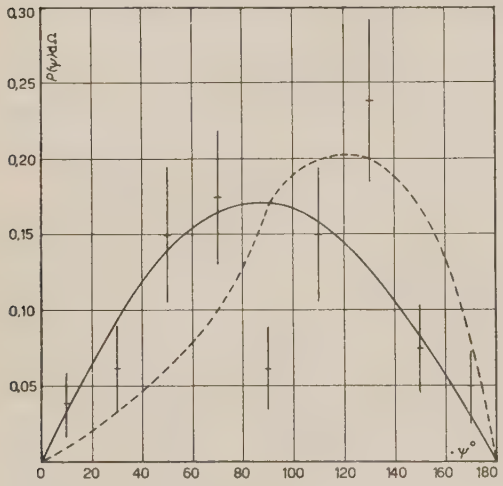

Fig. 12. – Stelle di I categoria s.r. a tre rami N soltanto – Correlazioni N-N – (80 angoli).

Abbiamo analizzato gli spettri energetici dei rami NG e G della IV e V categoria (figg. 13, 14). Si nota un andamento diverso degli spettri nelle due categorie: nella V la frequenza dei rami con $40 \leqslant E < 80$ MeV è inferiore a quella dei rami con $80 \leqslant E < 120$ MeV.

Per ogni traccia, si è contato un totale di 400 grani, ottenendo così un errore statistico medio del 5% sull'energia corrispondente. Escludiamo inoltre che si sia compiuto un errore sistematico sulle tracce di maggiore ionizzazione ($I/I^0 \sim 5{,}0$) aventi un grande angolo φ di inclinazione sul piano dell'emulsione (verrebbero così sistematicamente eliminate dalla zona di minore energia delle NG delle tracce, per essere trasportate tra le N); e, anche se questo errore è presente, esso non dovrebbe poter determinare un andamento come quello discusso. Infatti, anche se tutti i rami NG con $\varphi \geqslant 50^0$ venissero considerati rami N, la percentuale di NG che scompare non potrebbe superare, per ragioni geometriche, il 25% (nella ipotesi più sfavorevole di distribuzione isotropa dei NG).

Escluso che si tratti di errori sistematici di misura, l'andamento osservato può essere interpretato come un eccesso di particelle con energia sui 100 MeV, o come una lacuna nello spettro intorno ai 60 MeV.

La prima interpretazione confermerebbe il risultato di GOLDBERGER; le irregolarità osservate sarebbero allora peculiari di particolari andamenti della cascata nucleonica, nella quale, al variare dell'energia del primario, intervengono fenomeni nuovi che ne modificano lo svolgimento (quali la produzione di mesoni e la variazione delle sezioni d'urto). Inoltre il massimo osservato

potrebbe anche essere dovuto a fenomeni di riassorbimento di mesoni, se questo processo portasse ad una emissione preferenziale di protoni di energia intorno ai 100 MeV, e fosse molto più notevole in stelle grandi con molti rami di sciame.

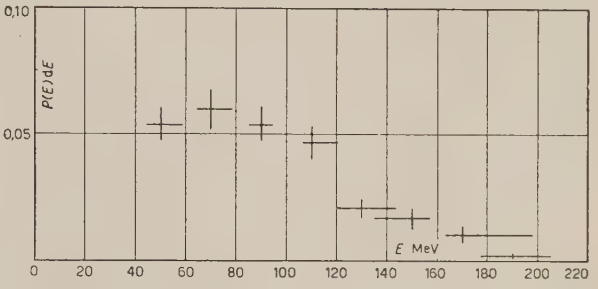

Fig. 13. – Stelle di IV categoria – Spettro energetico – (1 010 rami).

Gli spettri dei rami di e.d. in stelle generate dall'assorbimento di un π^- (Puppi [16]) non mostrano però alcun andamento analogo. Inoltre i rami *NG* e *G* che compongono il massimo, studiati separatamente dagli altri, non hanno mostrato alcuna correlazione angolare nè con i rami *N*, nè tra di loro, almeno nei limiti della debole statistica possibile; se essi fossero stati dovuti almeno in parte a riassorbimento di mesoni, le correlazioni alle quali questo fenomeno porta (§§ **2-3**) avrebbero dovuto risultarne esaltate.

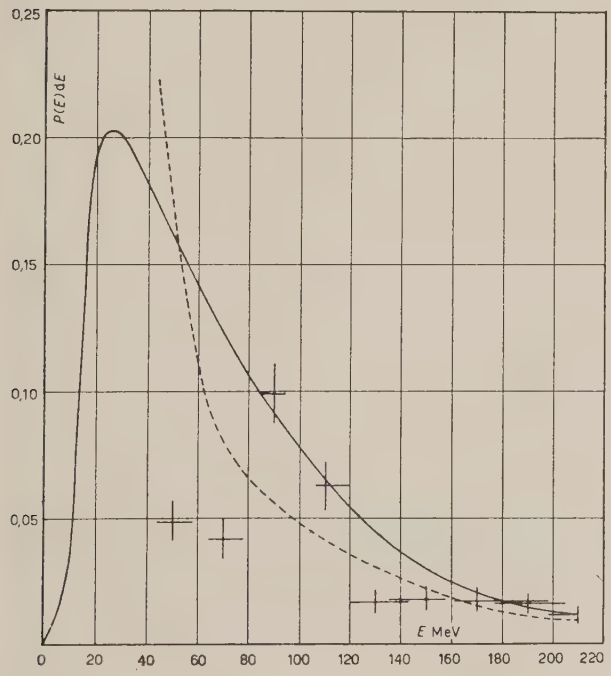

Fig. 14. – Stelle di V categoria – Spettro energetico – (671 rami).

Escluso quindi l'intervento del riassorbimento di mesoni, abbiamo cercato di discutere la seconda interpretazione proposta, di chiarire cioè per quali ragioni potrebbe formarsi nello spettro energetico una lacuna intorno ai 60 MeV. L'interpretazione più semplice suggerisce di ricorrere a fenomeni di pick-up (Chew *et al.* [25]): una parte dei protoni della cascata, intorno ai 100 MeV (energia alla quale

([25]) G. F. Chew e M. L. Goldberger: *Phys. Rev.*, **77**, 470 (1950).

la sezione d'urto per pick-up sembra raggiungere il suo valore massimo), scompare dallo spettro per formare deutoni, che sono in parte riassorbiti dal nucleo ed in parte emessi e, stimati protoni, trasportati in un intervallo di energia molto più basso.

Si è tentata una correzione dello spettro sperimentale in base alle percentuali date da Bristol per i deutoni in stelle di media ed alta energia (Fowler [26]); la correzione risulta però inadeguata, forse perchè ottenuta in base ai soli deutoni uscenti dalle stelle, senza tener conto dell'assorbimento (vedi, ad esempio, Hadley *et al.* [13]).

Si è calcolata allora analiticamente la deformazione dello spettro iniziale di e.d. $P_i(E)\,\mathrm{d}E$ quando intervengono fenomeni di pick-up. Sono state inoltre utilizzate le sezioni d'urto per pick-up $\sigma(E)$ date da Heidemann [27], estrapolandole alle basse energie.

In fig. 14, la linea a tratto continuo dà la $P_i(E)\,\mathrm{d}E$; la linea tratteggiata lo spettro corretto $P(E)\,\mathrm{d}E$. La correzione tentata non giustifica l'andamento osservato, il quale deve quindi essere attribuito, con molta probabilità, a caratteristiche variazioni nello sviluppo della cascata; ogni tentativo di interpretazione di queste caratteristiche è però connesso ad uno studio dettagliato dell'andamento della cascata nucleonica ad alta energia.

Un massimo analogo, anche se per energie più alte, è stato osservato anche da Ceccarelli *et al.* [18].

Conclusioni.

L'insieme dei fenomeni ora discussi ci permette di raccogliere, in un unico quadro fenomenologico, le informazioni sull'andamento delle disintegrazioni nucleari, ottenibili da analisi angolari ed energetiche dei rami.

In stelle molto piccole, senza rinculo visibile, la forte anisotropia e l'eccesso di angoli grandi tra i rami può essere attribuito all'alta percentuale di stelle in nucleo leggero: il moto del nucleo nella direzione del primario determina l'anisotropia, la necessità di conservare l'impulso totale in disintegrazioni complete del nucleo determina l'eccesso di angoli grandi. La correlazione intrinseca osservata dà luogo ad eccesso di grandi « aperture », di grandi angoli tra i rami in proiezione, di grandi angoli nella distribuzione del minimo angolo proiettato [19-21]; la presenza di disintegrazioni complete con soli rami ionizzanti o con pochi neutroni di bassa energia dà luogo all'eccesso di piccoli « volumi » [21].

---

[26] P. H. Fowler: *Phil. Mag.*, **41**, 169 (1950).
[27] J. Heidmann: *Phys. Rev.*, **80**, 171 (1950).

In stelle di media energia, senza rinculo visibile, l'anisotropia è spiegabile con l'intervento dei termini di bassa, media ed alta energia della cascata nucleonica; le osservate correlazioni a 90° rappresentano una diretta evidenza del contributo dei rami di e.d.

In stelle di bassa e media energia, con rinculo visibile, tutte le distribuzioni angolari risultano più isotrope delle analoghe distribuzioni in stelle s.r.; esse possono essere attribuite per la maggior parte a disintegrazioni in nucleo pesante, anche per le stelle a pochi rami, disintegrazioni durante le quali la maggiore isotropia dei rami emessi è direttamente legata alla formazione del rinculo visibile ([7]).

In stelle di alta energia, l'anisotropia dei rami neri si conserva praticamente costante al variare dell'energia del primario; inoltre l'assenza di correlazioni sensibili a 90°, denunziando un debole contributo di rami neri di e.d., porta ad attribuire la debole anisotropia residua a fenomeni nuovi, che entrano in gioco ad alte energie: tra di essi, il più probabile è quello di evaporazione locale. I rami di media ed alta energia divengono sempre più isotropi all'aumentare dell'energia del primario: questo è probabilmente dovuto ad uno slittamento di tutti i termini della cascata verso energie maggiori, così che, come si ritrova sperimentalmente, i rami grigi, ad esempio, della V categoria si comportano come i rami nero-grigi della IV categoria; si spiega così anche il debole contributo di rami neri di e.d., ad alte energie del primario.

La maggiore isotropia dei rami di media ed alta energia può essere anche attribuita all'intervento di riassorbimento di mesoni, prodotti nei primi stadi della cascata; la mancanza di sensibili correlazioni angolari tra questi rami ci impedisce di decidere a favore di questa ipotesi.

Nello spettro energetico dei rami, in stelle molto grandi, è presente una anomalia, notandosi un massimo secondario sui 100 MeV; esclusa l'attribuzione di questo massimo a riassorbimento di mesoni o a fenomeni di pick-up, crediamo che questo andamento dello spettro sia peculiare della cascata nucleonica ad alte energie, nella quale si sovrappongono, alle interazioni nucleone-nucleone libero, fenomeni nuovi, quali la produzione di mesoni.

Siamo lieti di ringraziare il prof. N. Dallaporta per l'interesse e l'aiuto continuo con cui ha seguito il nostro lavoro; gli osservatori M. Greco e G. Marinolli per l'intelligente impegno con cui hanno esplorato le lastre e calcolato gli angoli nello spazio tra i rami.

SUMMARY

The angular distributions and angular correlations of the low, average and high energy prongs in nuclear disintegration stars produced by the cosmic radiation in nuclear plates are analysed for 585 low and average energy stars and 95 high energy stars. For each group of stars, the distribution in space of the angles ζ, between the prong and the vertical or the primary, and ψ, between two prongs, are given. For the high energy stars the energy spectrum is also given. The whole of the observed phenomena allow us to collect, in a phenomenological picture, the information about the nuclear disintegrations, obtainable from angular and energetic analyses of the prongs. In little stars, without visible recoil tracks, the large anisotropy and the excess of large angles between prongs may be ascribed to the disintegrations of light nuclei; in average energy, without visible recoils, the anisotropy and the excess of correlations at 90° between the prongs are due to the knock-on prongs. On the other hand, the low and average energy stars, with visible recoils, show angular distributions nearly isotropic. In high energy stars, the anisotropy of the « black » prongs becomes practically constant when the energy of the primary increases, while that of one of the « sparse-black » and « grey » prongs becomes more isotropic. We ascribe these features of the high energy disintegrations to a shift of all the prongs of the nucleonic cascade toward larger energies; the residual anisotropy of the black prongs being due to some new phenomena, such as local evaporation of the nuclear surface. The energy spectrum of the highest energy stars shows a secondary maximum for $E \sim 100$ MeV; we exclude any interpretation of it in terms of meson reabsorption or pick-up process.

IL NUOVO CIMENTO Vol. XI, N. 4 1° Aprile 1954

Air-Shower Transition in Water; Interpretation of Under-Water Decoherence Curves.

W. E. Hazen (*)

Laboratoire de l'École Polytechnique - Paris

(ricevuto il 13 Febbraio 1954)

Summary. — Under-water decoherence curves taken with ionization chambers by El-Mofti are reinterpreted by means of a more detailed calculation. The observations require no core multiplicity for interpretation but are consistent with the occasional occurrence of multiple-cored showers with core separations $\lesssim$ one meter. The rate versus depth in water indicates a rather soft energy spectrum in air.

In a recent report (1), data for air showers obtained from under-water measurements have been interpreted in terms of core multiplicity with a rather broad lateral distribution, half-breadth of about 2 or 3 meters. Since this result disagrees with some other recent experiments (2,3), the under-water measurements will be reinterpreted by means of a more detailed analysis.

1. – The lateral density distribution in water.

As the first step in interpreting a decoherence curve (counting rate versus separation of the detectors), it is necessary to know or to assume a density distribution function (density of rays as a function of distance from the

(*) Fulbright Research Scholar, on leave from the University of Michigan, Ann Arbor, Michigan.

(1) O. El-Mofti: *Phys. Rev.*, **92**, 461 (1953).

(2) W. E. Hazen, C. A. Randall and R. W. Williams: *Phys. Rev., Feb.* (1954).

(3) W. P. Davis: *Ph. D. thesis, Univ. of Michigan* (1954).

shower axis). In view of previous experiments which have indicated the utility of the Molière distribution for distances from 1 or 2 meters out to 200 meters ([2-5]), we are led to the use of a monotonically decreasing (that is single-core) distribution function, in general, and the Molière distribution, in particular, as the first model in attempting a description of an under-water measurement.

Only incident rays of energy $E/\varepsilon_0 \gtrsim 5$ (where E is the energy of the ray and ε_0 is the critical energy in air) contribute appreciably to the electron density at $t > 5$ shower units depth in water and at $r < 10$ meters distance from the shower axis. Therefore, we can use approximation A of shower theory for the energy distribution among the electrons and among the photons in air. In the customary notation, we have $\pi(E_0, E, t')\,\mathrm{d}E$ and $\gamma(E_0, W, t')\,\mathrm{d}W$ for the differential electron and photon spectra, respectively, where E_0 is the energy of the shower initiator and t' the height of the effective production layer above the level of observation.

Again because we are concerned only with $E/\varepsilon_0 \gtrsim 5$, we can use the lateral distribution functions of Eyges and Fernbach for air ([6]). The electron distribution was used for both electrons and photons, i.e., the stronger central peaking of photons was ignored. On the other hand, the distribution at the shower maximum was used and thus the electron distribution is probably too peaked. The two errors are not large and are in opposite directions. The distribution will be designated by $P(E, r)$ and is expressed in terms of probability per m² for a ray of energy E to be at a distance r from the axis. It is normalized by $\int_0^\infty 2\pi r P(E, r)\,\mathrm{d}r = 1$.

Finally, the number of electrons of energy > 0 due to one electron or photon (the distinction is not important at $t > 5$) incident on the water was obtained from standard results of approximation B of shower theory ([7]). This quantity will be designated by $\Pi(E, 0, t)$.

The lateral distribution under water, $D(E_0, r, t)$, where D is the number of electrons per m² at depth t and distance r is

$$(1) \qquad D(E_0, r, t) = \int_{5\varepsilon_0}^{\infty} P(E, r)[\pi(E_0, E, t') + \gamma(E_0, E, t')]\,\Pi(E, 0, t)\,\mathrm{d}E\,.$$

Even in air, the shape of the distribution near the core is largely determined

([4]) G. Cocconi, V. Cocconi Tongiorgi and K. Greisen: *Phys. Rev.*, **76**, 1020 (1949).

([5]) R. W. Williams: *Phys. Rev.*, **74**, 1689 (1948).

([6]) L. Eyges and S. Fernbach: *Phys. Rev.*, **82**, 23 (1951).

([7]) B. Rossi: *High-Energy Particles* (Prentice-Hall, 1952).

by the rays with $E \gg \varepsilon_0$ and the above integral without the last factor fairly well represents the density distribution near the axis in air. Therefore, the chief difference between the distribution in air and that under several radiation units of water is the factor $\Pi(E, 0, t)$ for $E \gg \varepsilon_0$, which is roughly proportional to E. Finally, since the lateral distribution function nearly depends only on the product Er for the energies in question ([6]), one finds the density proportional to $1/r^{2-s}$ in air ([8]) and, similarly, one can show that the density is proportional to $1/r^{3-s}$ in water at depths where $\Pi(E, 0, t)$ is proportional to E. Near the shower maximum ($s=1$), we have the $1/r$ density variation in air changing to $1/r^2$ under water. This rough estimate checks the numerical integration discussed in the next paragraph.

The integral (1) was evaluated numerically for the two dephts $t=5$ and $t=7\frac{1}{2}$ and for two values of E_0 that were representative of the shower sizes that contributed to the counting rates of El-Mofti's experiment (local density at both detectors > 230 electrons per m^2). Since $\pi(E_0, E, t')$ is roughly linear in E_0, it was possible to interpolate or extrapolate from the two calculated examples with sufficient accuracy. A value of 16 was used for t'.

The density is about proportional to $1/r^2$ as predicted by the analytical method. AMALDI *et al.* ([9]) have made a similar calculation for the transition of air showers in lead. They also find roughly a $1/r^2$ distribution for similar depths and air-shower sizes; also, the absolute values are comparable when one takes the difference in critical energy between water and lead into account.

2. – Decoherence curves in water.

The counting rate for two ionization chambers separated by $2a$ meters and requiring an average density $\geqq \varrho$ at both chambers is obtained from ([10])

$$W(a, \varrho) = \int_a^\infty S(\varrho, R)\, \mathrm{d}A(R)\,, \tag{2}$$

where $S(\varrho, R)$ is the absolute frequency ($m^{-2}h^{-1}$) of showers that will give a density $\geqq \varrho$ at distance R from the farther chamber. The function $S(\varrho, R)$ is determined from a) the frequency of occurence $S(N)$ of showers with more

---

([8]) A. MIGDAL: *J. Phys. USSR*, **9**, 183 (1945).

([9]) E. AMALDI, C. CASTAGNOLI, A. GIGLI and S. SCIUTI: *Nuovo Cimento*, **7**, 401 (1950).

([10]) J. M. BLATT: *Phys. Rev.*, **75**, 1584 (1948).

than N electrons, for which we use Williams' rate ([5]) at 3 050 meters (the altitude correction is small and will be made later), and *b*) the density distribution $D(E_0, r, t)$ discussed in section 1. E_0 and N are related implicitly from the earlier assumption of an energy spectrum in air characteristic of a single cascade, which gives us $N = \Pi(E_0, 0, t)$. The resulting decoherence curves are compared with the data of El-Mofti in Fig. 1. The calculated curves have been lowered by a factor 3.5 at $t=5$ and a factor 1.5 at $t = 7.5$ in order to compare with the data as far as shape of the curves is concerned. It is seen that the curves adequately describe the data for the dependence of counting rate on chamber separation. Thus, there is no need to hypothesize a multiplicity of shower cores in order to understand the dependence of counting rate on separation.

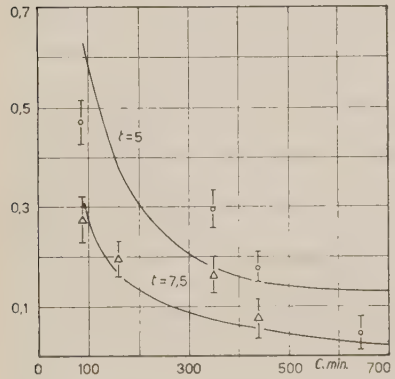

Fig. 1. – Calculated decoherence curves under water compared with the data obtained by El-Mofti. The abscissae are distances between ionisation chambers and the ordinates are counting rates. The curves have been adjusted in height.

3. – Absolute rates and variation with depth in water.

The coincidence rate of ionization chambers in air was measured in air by Williams at 3 050 meters ([5]) and also at 4 300 meters. It is necessary to extrapolate from $\varrho=300$ to $\varrho = 230$ in minimum particle density and from 3 050 to 2 765 meters in altitude in order to compare with the data of El-Mofti, but *a*) the extrapolations are small and *b*) counter measurements, which do not involve extrapolation, give about the same result. From Williams we find 2.9 h^{-1} for separations less than one meter and $\varrho \geqq 230$ m^{-2} and an altitude effect 0.75 as we go from 3 050 m to 2 765 m. The expected rate at 2 765 m from Williams' data is 2.2 h^{-1} which we compare with 0.87 h^{-1} of El-Mofti. It is very unlikely that the altitude variation is larger than 0.75 because this factor is already the largest of any of the measured values. The difference may be due to the difference in method of recording which was from measurements of oscilloscope pulses in one case and from discriminator coincidences in the other.

The calculated variation with depth in water is compared with the experiment in Fig. 2, where the curve has been fitted to the data at $t=0$, i.e., to the counting rate in air. The differences are more or less as expected as we shall see below.

4. – Discussion.

The most serious errors in the calculations of the decoherence curves stem from the assumption of a single cascade. This approximation was deliberate in the sense that one expects the resulting decoherence curve to give an upper limit for the rapidity of the decrease in frequency with separation (unless the relative intensity of the N-component is unexpectedly large very near the shower axis). We know *a*) that the spectrum of electrons and photons is softer than that given by the above model ([2]), and *b*) that some of the showers of the sizes in question have multiple peaks in their density distributions with separations $\lesssim 1$ m ([3]). Thus the « calculated » decoherence curve should certainly be rather flatter and there is no need to hypothesize multiple shower cores spread over an area of several square meters.

The calculated depth variation is too slow because of the fact, noted above, that the actual air showers have a smaller proportion of energetic rays than we have assumed. Therefore, the sharp drop in the observed intensity between $t=0$ and $t=5$ is understandable. However, we might expect a continued rapid decrease between $t=5$ and $t=7.5$ on the basis of the above argument. In the case of water, the penetration of low energy photons is not nearly so marked as in lead and is probably not sufficient to explain the observation. But there probably is no evidence for any new phenomenon, since the penetrating component will make a contribution whose importance increases with depth and the experimental uncertainty may be underestimated.

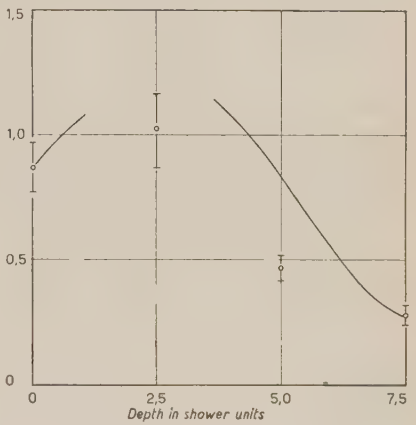

Fig. 2. – Calculated variation of counting rate with depth in water for two ionisation chambers separated by 87 cm compared with the data of El-Mofti. The depth is expressed in radiation units. The curve was adjusted in height in order to pass through the experimental point at $t=0$.

We have not considered the effect of fluctuations. Williams has found that the effect is not negligible ([11]), since we are demanding two independent samples larger than a certain value for each event. In air, where one is justified in assuming a Poissonian distribution, the correction is an increase

([11]) R. W. Williams: private communication.

by 22 %. Under water, the radius of the « shower » from each incident on the water ray is smaller than the detector and the fluctuations will therefore be greater than Poissonian. *a*) The effect on a decoherence curve depends on two factors: as the separation of the chambers is increased, the counts are due to showers that strike at increasing average distance from the chambers with a consequent expectation of lower-energy rays and smaller fluctuations under water; on the other hand, the average shower size also increases with detector separation, hence the showers are younger on the average and contain a higher proportion of energetic rays. The net effect is probably only a small change in the average energy of the rays striking above the chambers as their separation is increased. Therefore the interpretation of the decoherence curves would probably not be altered. *b*) The effect of fluctuations increases with depth, since, the greater the depth, the greater the average energy possessed by the contributing rays in air. The result would be a less rapid decrease of the observed rates when one made the correction. Again, the conclusions are probably not greatly affected by neglecting the fluctuations.

This analysis was made while the author enjoyed the hospitality of the cosmic-ray laboratory under the direction of Professor Le Prince-Ringuet at the École Polytechnique.

RIASSUNTO (*)

Le curve di transizione per sciami d'aria ottenute con camere di ionizzazione da El-Mofti sono state nuovamente interpretate per mezzo di calcoli più particolareggiati. Le osservazioni sperimentali non richiedono l'ipotesi che i « cores » siano sempre multipli, ma occasionalmente. Nel qual caso, la separazione è $\lesssim 1$ m. La frequenza in funzione della profondità in acqua indica uno spettro di bassa energia.

(*) *A cura della Redazione.*

IL NUOVO CIMENTO Vol. X, N. 4 1° Aprile 1954

Self-Diffusion in Liquid Indium.

G. Careri, A. Paoletti

Istituto di Fisica dell'Università - Roma

F. L. Salvetti

Istituto di Chimica Generale ed Inorganica dell'Università - Roma

(ricevuto il 18 Febbraio 1954)

Summary — The self-diffusion coefficient of liquid indium has been measured in the range from 160 to 480 °C with results which are very close to the ones for liquid mercury. Near the melting point some complication occur, which are discussed in terms of crystallite formation.

At the present day there is still no liquid state theory capable of describing a phenomenon as common as melting. This being the case, the measurement of a physical property which has a simple microscopic significance can help us to form a picture of these phenomena and later to test the theories which may be formulated.

For this reason it seemed interesting to study systematically a quantity which can change considerably about the melting point, the coefficient of self-diffusion D. A measurement of this quantity for the liquid state which can be compared with the analogous one for the solid state, has existed for some time and is due to Van Hevesy in 1920 [1]. It refers to a single temperature for lead, and shows that D varies by a factor 40 000 in passing through the melting point. A similar variation at the melting point has been noted recently for indium [2]. In neither case was the dependence on temperature studied for the liquid state.

(1) J. Groh and G. Hevesy: *Ann. Phys.*, **63**, 85 (1920).

(2) R. E. Eckert and H. G. Drickamer: *Journ. Chem. Phys.*, **20**, 13 (1952).

At the present time, the coefficient of self-diffusion has been measured in many associated liquids, or liquids of complex structure, with results which will be difficult to interpret. The only simple case is that of mercury which has been examined recently ([3]) in the temperature range 0–90 °C with results which will be discussed later. It has not, however, been examined the solid state, where, on the other hand, a large number of other metals have been fully investigated.

It therefore seemed reasonable to determine D for the liquid state for those metals which have been studied in the solid state, and which can be considered as sufficiently simple liquids. Among these indium has several practical advantages, and so it was chosen as the first.

Experimental Technique.

Several methods exist for measuring the diffusion coefficient between two liquids. After examining the various alternatives a scheme was chosen which is substantially as follows. A porcelain capillary is filled half with activated metal and half with non-activated metal, both solid. The two metals are then melted and the system is brought rapidly to a controlled temperature where they diffuse into each other for a certain time. The whole is then cooled rapidly and a thin rod of solid metal extracted. From the activity at the various points of the rod D is deduced.

The capillary was chosen of diameter 1.6 mm and length 160 mm so as to have a substantially one-dimensional phenomenon for which the solution of the diffusion equation is known under our initial conditions. Keeping the time of diffusion sufficiently short, it can be ensured that the activated metal does not reach the end of the non-activated metal, so that the system is effectively infinite and one-dimensional. The diameter of the rod was increased to 2 mm in several cases without appreciably influencing the results. The rods of activated and non-activated metal were prepared by extrusion of very pure indium, and de-oxydized by us with borax, and fused under vacuum. The indium was supplied by the firm of W. Franke of Frankfurt, and had a purity of 99.99. A spectroscopic analysis revealed only traces of silver.

The capillary was held in a vertical position, with the non-activated metal placed in its lower half, and the activated metal in its upper half. To prevent the activated part descending during melting into the gaps between the non-activated metal and the walls of the capillar, it was necessary to melt the non-activated metal first so that is adhered well to the walls, then to solidify

([3]) R. R. HOFFMAN: *Journ. Chem. Phys.*, **20**, 1567 (1952).

it and add the solid rod of activated metal, and finally to start again the melting of the whole. In the first measurements particular care was taken at the moments of melting and solification to keep the strata parallel in the solid and liquid phases. To do this, during the change of state the upper part of the rod was kept a few degrees hotter than the lower part, and the change of state was made to take place slowly in about twenty minutes. It was realized later that these precautions were excessive. The fact that the value of the coefficient of self-diffusion measured was independent on the duration of the experiment is the best proof of the non-existence of convection and other perturbative phenomena.

During all the diffusion experiment and in the operations of melting of the metal in the capillary, a vacuum was maintained with a rotary pump, to prevent oxidation of the metal and formation of gas bubbles inside the rod. The temperature during the experiments was always controlled by three chromel-alumel thermocouples placed externally at the centre and at the two extremities of the capillary. A tubular furnace was adopted so that the temperature gradient would be very low in the central 16 cm occupied by the capillary. Temperature variations due to drift in the thermal regulation, and variations of temperature at the ends of the capillary were both usually within ± 1 °C.

While the capillary was being brought from the melting point to the experimental temperature a partial diffusion took place, and again while it was being cooled to solidification at the end of the experiment. For this reason some uncertainty arises about the duration of the process of diffusion itself. It was decided then, to attribute the value of D found, not to the thermostated temperature which is the maximum reached in the thermal cycle, but to a slightly lower mean temperature, evaluated in the following manner. A first examination of the results showed that even without adopting this correction, the coefficient of diffusion varies according to an exponential law of the type

$$D = D_0 \exp[-E/RT], \tag{1}$$

where T is the absolute temperature.

Now the experimental value D_e, which is a mean value for the time Δt of the experiment, can be made to correspond to an ideal isothermal experiment at the mean temperature T_m, with

$$D_e = \frac{D_0}{\Delta t}\int_0^{\Delta t} \exp[-E/RT(t)]\,\mathrm{d}t = D_0 \exp[-E/RT_m], \tag{2}$$

from which

$$\exp\left[-E/RT_m\right] = \frac{D_0}{\Delta t}\int_0^{\Delta t} \exp\left[-E/RT(t)\right]. \tag{3}$$

Naturally, care was taken to maintain a constant thermostated temperature for long enough to ensure that the correction applied to the temperature was only a small percentage of the absolute value. The corrected data gave a second approximation value of E which was very near the value previously assumed for carrying out the correction. For reasons which will become clear later, the time zero was taken as the instant in which the temperature was 159 °C and not 156 °C (melting point of indium).

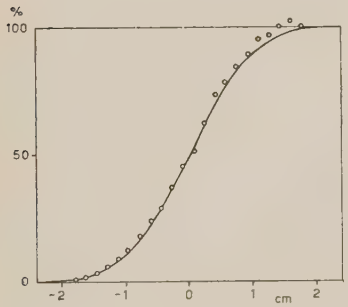

Fig. 1. – The penetration curve obtained in a typical experiment of autodiffusion of In^{114} into non-activated indium. The ordinates represent the activity and the abscissae the position of the centres of gravity of the sections of rod. Note that the diffusion has affected only the central part of the rod, which can therefore be considered infinite in both directions. The circles, represent the experimental points, and the curve the equation (4) with $D = 2.99.10^{-5}$.

Once the diffusion was completed, the rod was cut into 2 mm lengths, and the activity of these determined, reducing them with a press, to the form of discs of diameter 7 mm and weigth $20 \div 40$ mg/cm², and placing them under a mica window counter. A correction had to be applied for the activity absorbed in the sample itself, reducing the measurements to the activity at infinite thickness. The coefficient of absorption of the γ-rays produced by In^{114} (4) was found to be $\mu = 0.0085$ cm² mg^{-1}. The soft γ-component emitted by the surface layer was eliminated with an indium foil of 20 mg/cm². 10 000 disintegrations were counted for the more active specimens, so that the measurements were affected by an error of $\pm 2\%$, comprising the statistical error of the counting and the error in the determination of the weight and area. For the less active specimens at least 3 000 disintegrations were counted.

Plotting the activity $C(x)$ of the sections of rod as a function of the distance x, a curve of penetration is obtained as shown in Fig. 1. Now with our

(4) Obtained from « The Radiochemical Centre » Amersham, Bucks, England.

initial conditions, the diffusion equation gives (5)

$$(4) \qquad \begin{cases} C(x) = \dfrac{C_0}{2}\left(1 - 2\pi^{-\frac{1}{2}}\displaystyle\int_0^y \exp\left[-y^2\right] dy\right) \\ \\ y = x/2\sqrt{Dt}\,, \end{cases}$$

where t is the period of time in which diffusion takes place. Using tabulated values of the probability integral, a value of D can be determined for each

TABLE I.

Run	T °C	$10^2 \frac{1}{T\,°\mathrm{K}}$	Duration	$D \cdot 10^5$
20	159.5	0.2315	6h 15 min	2.86 ± 0.20
21	160	0.2310	9h 25 min	2.48 ± 0.14
19	160	0.2310	3h 10 min	2.94 ± 0.05
14	165	0.2280	7h 45 min	2.79 ± 0.20
24	167	0.2270	7h 50 min	2.17 ± 0.16
25*a*	168	0.2265	3h	3.19 ± 0.06
25*b*	168	0.2265	3h	2.75 ± 0.10
18*a*	172	0.2250	8h 15 min	2.35 ± 0.20
18*b*	172	0.2250	8h 15 min	2.68 ± 0.12
12	184	0.2190	8h 30 min	3.68 ± 0.21
11	229	0.1990	6h 45 min	4.51 ± 0.22
8	250	0.1910	9h 30 min	4.62 ± 0.16
23	281	0.1800	8h	5.25 ± 0.24
9	480	0.1330	9h 30 min	6.8 ± 0.26

(5) See for example: W. JOST: *Diffusion in solids, liquids, gases* (New York, 1952), p. 20.

experimental point, and thus the mean can be taken. The readings in the neighbourhood of $G(x) = 0$; 0.50 and 1.00 were systematically rejected because all the curves of the family are crowded together near these points and therefore the errors are appreciably increased (Fig. 1).

Naturally the distance x computed in equation (4) is not that measured in the solid rod, but that corresponding to the liquid rod at the experimental temperature. The correction was made using the recent data on the density of liquid indium (6), and increases by about 10% at 250 °C and about 20% at 500 °C, the value of D which would be determined using simply the distance measured in the solid rod.

Results and discussion.

The results of our measurements are shown in Table I and in Fig. 2 and 3. As can be seen, the values of D at temperatures greater than 175 °C shown on a semi-logarithmic scale, lie well on a straight line, while those in the neighbourhood f the meloting point fall away from it and are not even reproducible. It is therefore convenient to discuss the two regions, which we will simply call the high and low temperature regions, separately.

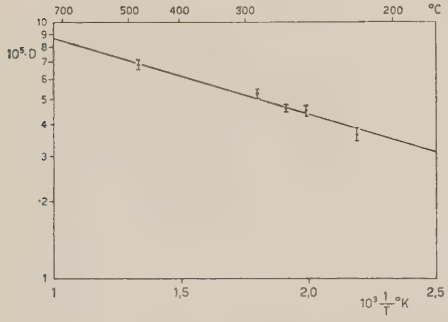

Fig. 2. – The self-diffusion coefficient of liquid mercury plotted against $1/T$. The straight line is the equation (5).

a) The high temperature results can be expressed by an exponential relation

$$(5) \qquad D = 1.76 \cdot 10^{-4} \exp[-1 \cdot 350/RT].$$

For solid indium self-diffusion, ECKERT and DRICKAMER found

$$D = 1.02 \exp[-17 \cdot 900/RT].$$

This is the first case in which a comparison is possible between the energy of activation in the liquid and in the solid state for a non-associated molecular system. Since both the exponential and the pre-exponential terms of (5) are widely different from the corresponding quantities which have been found in the solid state, this comparison shows that the fundamental mechanism responsible for the process of diffusion must be very different.

Another element for which the coefficient of diffusion is known in the liquid state is mercury, for which is found $D = 1.16 \cdot 10^{-4} \exp[-1 \cdot 160/RT]$. Both the energies of activation and the pre-exponential factor for liquid indium

(6) D. D. WILLIAMS and R. R. MILLER: *J.A.C.S.*, **72**, 3821 (1950).

and mercury are extremely close, hardly outside the limits of experimental error. The well known Johnson rule, correlating the self diffusion activation energies of solids with melting temperature and vaporization energy, do not seem to apply to the liquid data. This suggests that the mechanism of diffusion in the liquid state, unlike that in the solid state, does not depend on the structure of the state itself; because it is known that mercury and indium, in addition to crystallizing in different systems in the solid state, in the liquid state present a different coordination number (7).

Further experiments will be carried out in this laboratory to test these conclusions on other liquid metals.

b) In the low temperature region the experimental values of D turn out to be systematically below the values extrapolated from equation (5), and also not reproducible as shown in Fig. 3. Naturally all the precautions were taken to avoid oxidation and contamination of the specimen, and the diameter was changed as well as the nature of the capillary, without conclusive results. It must be remembered that ECKERT and DRICKAMER also found an inexplicable effect in the measurements carried out in the liquid-solid transition zone, and in the liquid at a few degrees from the melting point. In contrast to the measurements in the solid state where diffusion was uniform throughout the specimen, as soon as liquid appeared the diffusion at the surface for a thickness of several tenths of a millimetre was perceptibly lower than at the central part of the specimen. Without offering an explanation of this, they considered as more characteristic of the material the coefficient of

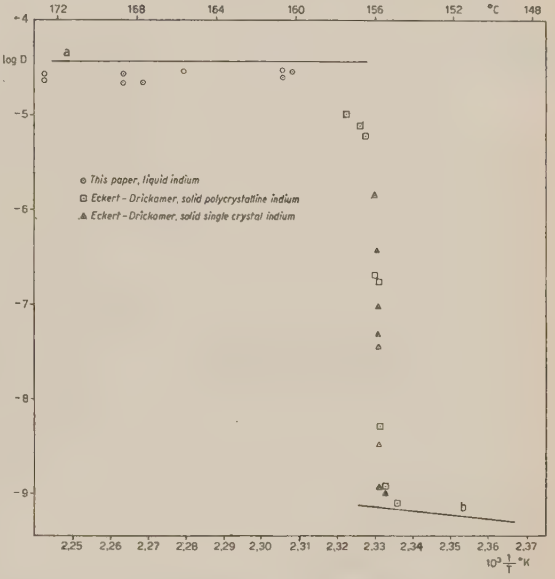

Fig. 3. – The self-diffusion coefficient of indium near the melting point. The line *a* is the equation (5) valid as higher temperature for liquid indium; the line *b* is extrapolated from ECKERT and DRICKAMER's data for solid indium. The indium melting point was 156.3 °C for our samples and 156.51 °C for the samples of ECKERT and DRICKAMER.

(7) H. HENDUS: *Zeits. f. Naturforsch.*, **2***a*, 505 (1947); R. N. BOYD and R. R. WAKERHAM: *Journ. Chem. Phys.*, **7**, 958 (1939).

diffusion obtained from the penetration curve for the internal strata, rejecting the surface stratum. A simple explanation of this strange phenomenon observed by ECKERT and DRICKAMER, together with the poor reproducibility and low value of our measurements, seems to us to be as follows. It is known that crystallites form in a liquid near the melting point, which act as crystallising centres for the solid phase, and which have substantially the properties of the solid. It is also known that in general these crystallites are formed on impurities at the surface of the liquid, or inside the liquid at the surface of colloidal suspensions. Some recent work by TURNBULL ([8]) has given complete evidence that in the case of supercooled mercury, the surface oxide is a catalyst for these nucleation processes. Therefore, it seems to us that faint traces of oxide may have produced the surface layer with the low coefficient of diffusion in the case of ECKERT and DRICKAMER, and may have distorted our results near the melting point in an erratic manner.

This interpretation is substantially similar to the explanation given by WANG ([9]) of the low coefficient of diffusion in the system H_2O—D_2O near the freezing point of water. According to WANG this drop is due to the beginning of the formation of «icebergs», and he finds a confirmation of this in the abnormal density of water near the freezing point.

The density measurements for liquid indium are not accurate enough to permit a similar verification. In connection with this, it must be remembered that the density varies by only a few per cent in the melting while the coefficient of autodiffusion varies by a factor 10^4. Therefore, although melting is considered to be discontinuous for many physical properties, it must be regarded as continuous for self-diffusion where the change is much more marked. Thus, while the effect of the crystallites is not appreciable for the other physical properties, as much as the variations of these properties are small in the neighbourhood of the melting point, in the case of the coefficient of self-diffusion, which undergoes a large increase at the melting point, such effect is easily observed.

([8]) D. TURNBULL: *Journ. Chem. Phys.*, **18**, 198 (1950); **19**, 411 (1952).
([9]) J. WANG: *J.A.C.S.*, **73**, 510 (1951).

RIASSUNTO

Il coefficiente di autodiffusione in indio liquido è stato misurato da 160 a 480 °C, con risultati molto vicini a quelli del mercurio liquido. Vicino alla temperatura di fusione si sono notate delle misure poco riproducibili, che sono state attribuite alla formazione di cristalliti.

IL NUOVO CIMENTO Vol. X, N. 4 1° Aprile 1954

Polarization of High Energy Protons Scattered by Nuclei.

E. Fermi

University of Chicago - Institute for Nuclear Studies - Chicago

(ricevuto il 22 Febbraio 1954)

Summary. — The attempt is made to explain the polarization recently observed in protons of several hundred MeV scattered by nuclei in terms of the same spin orbit coupling that is assumed in the nuclear shell model. It is found that the extrapolation to high energy of the spin orbit coupling observed at low energy is adequate to yield the correct order of magnitude of the polarization.

It has recently been observed [1] that protons of a few hundred MeV become strongly polarized when scattered by nuclei. A somewhat weaker polarization has also been observed in proton proton scattering. The polarization is observed by a double scattering experiment. The beam is polarized by a first scattering on a target usually located inside the cyclotron tank. The scattered and polarized beam is scattered a second time on a target of various materials and the polarization is shown by a difference in intensity of the scattering by the second target at equal angles to the right and to the left of the beam. According to Marshall, Marshall and De Carvalho [1] the elastically scattered protons are even more strongly polarized than those that are scattered inelastically.

In the present paper an attempt will be made to explain the polarization of the elastically scattered beam with the effect of the spin orbit coupling that is postulated in the nuclear shell model of Mayer and Jensen. The evidence of nuclear structure indicates the existence of a spin orbit interaction which

[1] C. L. C. Oxley, W. F. Cartwright, J. Rouvina, E. Baskir, D. Klein, J. Ring and W. Skillman: *Phys. Rev.*, **91**, 419 (1953); O. Chamberlain, E. Segrè, R. Tripp, C. Wiegand and T. Ypsilantis: *Phys. Rev.*, in press.; J. Marshall, L. Marshall and H. G. De Carvalho: *Phys. Rev.*, in press.

tends to depress the energy of the nucleonic orbits with spin parallel to the orbital angular momentum. This coupling is presumably present in the nucleon nucleon forces but not enough is known about them at present to substantiate this conjecture. One might expect, of course, that also in a nucleus there should be a spin orbit coupling corresponding to the so-called Thomas correction (2). This coupling, however is much weaker than the coupling that is observed empirically in nuclear levels. For example it has been estimated by HEISENBERG that the shell model of nuclear structure requires a coupling about 15 times stronger.

We will assume, therefore, that in the potential that the nucleus exerts on a nucleon there is a term 15 times larger than the Thomas correction, namely:

$$H_s = -15\,\frac{\hbar}{2M^2c^2}\,\frac{V_1'(r)}{r}\,\boldsymbol{\sigma}\cdot\boldsymbol{x}\wedge\boldsymbol{p}\,. \tag{1}$$

$V_1(r)$ is the real part of the potential to be discussed later. It is clearly a risky extrapolation to extend the spin orbit coupling (1) known to be present in bound nucleon orbits to protons of 200 or 300 MeV. It appears worthwhile, however, to discuss the consequences of this extrapolation for the polarization phenomena.

In addition to the spin orbit coupling (1) we shall assume that the nucleus exerts a central potential $V(r)$ on the nucleon. This potential will consist of a real and an imaginary part:

$$V = V_1 + iV_2\,. \tag{2}$$

The imaginary part of the potential represents in the usual way the absorption properties of the nuclear matter (3). For simplicity we will assume that both the real and the imaginary part of V have the shape of a potential well

$$V_1 + iV_2 = \begin{cases} -B - iB_a & \text{for } r < r_0 \\ 0 & \text{for } r > r_0 \end{cases} \tag{3}$$

where r_0 is the nuclear radius. We will discuss the scattering by the potentials (1) and (3) in Born approximation. This method is probably adequate to give correctly qualitative results and we hope to be able to improve on it at a later date.

(2) L. H. THOMAS: *Nature*, **117**, 514 (1926).

(3) See for example, S. FERNBACH, R. SERBER and T. B. TAYLOR: *Phys. Rev.*, **75**, 1352 (1949).

In order to compute the scattering cross-section we need the matrix elements of (1) and (3) between the final state 2 and the initial state 1. We take as initial state a plane wave of momentum p parallel to the x axis, with spin up. We are interested in the scattering in the xy plane, perpendicular to the spin direction. Our final state, therefore, will be a plane wave with momentum equal in magnitude to p, parallel to the xy plane, and forming an angle ϑ with the x axis. Observe that with this notation ϑ positive corresponds to scattering to the left and ϑ negative to scattering to the right.

In computing the matrix element of (1), V_1' will be given by

$$V_1' = B\delta(r - r_0) \tag{4}$$

in accordance with (3). The calculation of the matrix element is straightforward. One finds:

$$\langle 2 | H_s | 1 \rangle = -30\pi i(p/Mc)^2 r_0^3 B \sin\vartheta \left\{ \frac{\sin q}{q^3} - \frac{\cos q}{q^2} \right\}, \tag{5}$$

where

$$q = \frac{2pr_0}{\hbar} \sin\frac{\vartheta}{2}. \tag{6}$$

The matrix element of the potential (3) is given by

$$\langle 2 | V | 1 \rangle = -4\pi r_0^3 (B + iB_a) \left\{ \frac{\sin q}{q^3} - \frac{\cos q}{q^2} \right\}. \tag{7}$$

Both matrix elements (5) and (7) cause no change of the spin direction. The differential scattering cross-section $d\sigma/d\omega$ is proportional to the square modulus of the sum of the matrix elements (5) and (7). The proportionality coefficient is $M^2/(4\pi^2\hbar^4)$. One finds

$$\frac{d\sigma}{d\omega} = \frac{4M^2}{\hbar^4} r_0^6 B^2 \left\{ \frac{\sin q}{q^3} - \frac{\cos q}{q^2} \right\}^2 \left[1 + \left\{ \frac{B_a}{B} + \frac{15}{2}\left(\frac{p}{Mc}\right)^2 \sin\vartheta \right\} \right]. \tag{8}$$

The scattering depends on the sign of ϑ and scattering by the same angle to the right and to the left will be different.

The intensity of the polarization effects is usually described by an expression

$$e(\vartheta) = \frac{I(\text{right}) - I(\text{left})}{I(\text{right}) + I(\text{left})} \tag{9}$$

where I(right) and I(left) are the intensities of the scattering to the right and

to the left of the beam. Formula (8) gives

$$e(\vartheta) = \frac{15\left(\frac{p}{Mc}\right)^2 \frac{B_a}{B} \sin\vartheta}{1 + \left(\frac{B_a}{B}\right)^2 + \frac{225}{4}\left(\frac{p}{Mc}\right)^4 \sin^2\vartheta}. \tag{10}$$

Notice that according to this formula the polarization effects are proportional to the imaginary component of the potential. In Born approximation the matrix element (5) of the spin orbit coupling interferes only with the imaginary part of the matrix element (7) of the potential V. It may be that this feature will be in part reduced by an exact calculation. Notice also that the right left asymmetry vanishes for an infinitely strong absorptive potential.

In the numerical estimates of the right left asymmetry for 340 MeV polarized protons we have computed the absorptive potential B_a of nuclear matter assuming a proton-neutron cross-section of $32 \cdot 10^{-27}$ cm^2 and a proton-proton cross-section of $24 \cdot 10^{-27}$ cm^2. With a nuclear radius $r_0 = 1.4 \cdot 10^{-13} A^{\frac{1}{3}}$ one finds the absorption mean free path in nuclear matter $\lambda = 4.1 \cdot 10^{-13}$ cm. This corresponds to an imaginary component of the potential

$$B_a = \frac{\hbar v}{2\lambda} = 16 \text{ MeV}.$$

v is the velocity of the protons, equal to 0.68 c. The real part of the potential has been assumed $B = 27$ MeV. In Table I the calculated values of the asymmetry are listed. The first column is the scattering angle in degrees,

TABLE I.

Asymmetry in the Scattering of a 340 MeV *Polarized Proton Beam.*

Scattering angle (degrees)	Asymmetry $e(\vartheta)$	$\frac{\overline{d\sigma}}{d\omega} \cdot 10^{24}$ (for carbon)
0	0	2.7
5	0,40	2.2
10	0,51	1.2
15	0.49	0.3
20	0.42	0.02
30	0.33	0.01
40	0.27	0.03
50	0.23	0.01

the second column is the asymmetry parameter $e(\vartheta)$, the third column is the differential cross-section computed from (8) for carbon, taking the average between the values to the right and to the left.

These values of the asymmetry are in reasonably good agrement with the experimental observations. It should be noticed that at large scattering angles the elastic scattering (see column 3) becomes practically negligible compared to the inelastic scattering which is not included in the present theory, because it is due to those protons that have been eliminated by the imaginary component of the potential.

This theory leads to a definite prediction as to the sign of the polarization effect. A proton with spin up should according to it be scattered with smaller intensity to the right than to the left. No experimental information is available at present on this point.

If further research should indicate that the results of this theory are in good agreement with experiment, an interesting consequence would be that the spin orbit coupling (1) of the shell model persists with about the same intensity up to very high nucleon energies.

RIASSUNTO

Si fa l'ipotesi che la polarizzazione recentemente osservata nello scattering di protoni di alcune centinaia di MeV sia dovuta all'accoppiamento tra spin e orbita che viene postulato nel modello nucleare a shells di Mayer e Jenzen. L'esistenza di questo accoppiamento noto da fenomeni nucleari di bassa energia permette di spiegare l'ordine di grandezza dei fenomeni di polarizzazione osservati ad alte energie. L'effetto di polarizzazione è dovuto all'interferenza dell'accoppiamento tra spin e orbita con la componente immaginaria del potenziale nucleare.

LETTERE ALLA REDAZIONE

(La responsabilità scientifica degli scritti inseriti in questa rubrica è completamente lasciata dalla Direzione del periodico ai singoli autori)

Sezione d'urto per i processi (d, p) e (p, d).

E. Clementel

Istituto di Fisica dell'Università - Padova

Istituto Nazionale di Fisica Nucleare - Sezione di Padova

(ricevuto il 14 Gennaio 1954)

I processi (d, p) e (p, d) sono due esempi di urti con riordinamento (rearrangement collisions), il cui studio ha una particolare importanza per la spettroscopia nucleare, in quanto la distribuzione angolare delle particelle emesse dipende dalla parità e dallo spin dei nuclei iniziale e finale. Tali processi, e quindi in generale i processi d'urto con riordinamento, si possono discutere in modo esatto usando la teoria generale dell'urto nella formulazione di Lippmann e Schwinger (1), benchè l'autofunzione dello stato finale appartenga ad un sistema completo di autofunzioni diverso da quello relativo allo stato iniziale. Valendoci per semplicità della schematizzazione Gerjouy (2), dove il nucleo viene tratto come un centro fisso di forza, e si trascurano sia lo spin delle particelle interessate nell'urto che l'interazione coulombiana, consideriamo anzitutto il processo (d, p). L'onda piana del deutone $\Phi_a = \exp[i\boldsymbol{K}\cdot\boldsymbol{R}]w(\boldsymbol{r}, \varepsilon_d)$, dove $\boldsymbol{R} = \frac{1}{2}(\boldsymbol{r}_p + \boldsymbol{r}_n)$ ed $\boldsymbol{r} = \boldsymbol{r}_p - \boldsymbol{r}_n$, rappresenta lo stato iniziale e soddisfa l'equazione

$$H_a\Phi_a = (K + V_{np})\Phi_a = E_a\Phi_a \,. \tag{1}$$

Se con V_n e V_p indichiamo le interazioni del neutrone rispettivamente del protone col centro di forza (nucleo), la funzione di stato del nostro problema soddisfa l'equazione integrale (3)

$$\Psi_a^{(+)} = \Phi_a + \frac{1}{E_a + i\varepsilon - H_a - V_n - V_p}(V_n + V_p)\Phi_a \,. \tag{2}$$

Lo stato finale è dato da un protone diffuso e da un neutrone legato, ed è descritto pertanto dall'autofunzione $\Phi_b = \exp[i\boldsymbol{k}_p\cdot\boldsymbol{r}_p]\varphi(\boldsymbol{r}_n, \lambda_b)$, soluzione dell'equazione

$$H_b\Phi_b = (K + V_n)\Phi_b = E_b\Phi_b \,, \tag{3}$$

dove λ_b è l'energia di legame del neutrone. L'ampiezza di probabilità per lo stato finale Φ_b vale $(\Phi_b, \Psi_a^{(+)})$. Al limite per $\varepsilon \to 0$, $(\Phi_b, \Psi_a^{(+)})$ deve contenere il fattore

(1) B. A. Lippmann e J. Schwinger: *Phys. Rev.*, **79**, 469 (1950).
(2) E. Gerjouy: *Phys. Rev.*, **91**, 645 (1953).
(3) G. F. Chew e M. L. Goldberger: *Phys. Rev.*, **87**, 778 (1952).

$\delta_+(E_a - E_b)$, che caratterizza un'onda divergente [4], e conviene quindi trasformare il secondo membro della (2) in modo da far apparire l'operatore $B^{-1} = (E_a + i\varepsilon - H_b)^{-1}$. Indicando con A^{-1} l'operatore che nella (2) agisce su $(V_n + V_p)\Phi_a$, e facendo uso della relazione operatoriale [5] $A^{-1} = B^{-1} + B^{-1}(B - A)A^{-1}$, si ottiene

$$(4) \qquad (\Phi_b, \Psi_a^{(+)}) = (\Phi_b, \Phi_a) + \\ + \frac{1}{E_a + i\varepsilon - E_b}(\Phi_b, (V_n - V_{np})\Phi_a) + \left(\Phi_b, \frac{1}{E_a + i\varepsilon - H_b}(V_p + V_{np})\Psi_a^{(+)}\right).$$

Valendosi delle (1) e (3) si verifica facilmente che

$$(5) \qquad \left(\Phi_b, (V_n - V_{np})\Phi_a\right) = (E_a - E_b)(\Phi_b, \Phi_a),$$

e quindi i primi due termini a secondo membro della (4) si distruggono, e in definitiva si ha

$$(6) \qquad (\Phi_b, \Psi_a^{(+)}) = \left(\Phi_b, \frac{1}{E_a + i\varepsilon - H_b}(V_p + V_{np})\Psi_a^{(+)}\right),$$

da cui segue subito [1] l'espressione per la probabilità di transizione w_{ba} fra gli stati a e b

$$(7) \qquad W_{ba} = |(\Phi_b, \Psi_a^{(+)})|^2 = \frac{2\pi}{\hbar}\delta_+(E_a - E_b)\left|\left(\Phi_b, (V_p + V_{np})\Psi_a^{(+)}\right)\right|^2.$$

La sezione d'urto differenziale si scrive pertanto

$$(8) \qquad \frac{d\sigma_{dp}}{d\Omega} = \frac{M_d}{\hbar K}\int w_{ba}\frac{1}{(2\pi)^3}\frac{d\boldsymbol{k}_p}{d\Omega},$$

dove $v_d = \hbar K / M_d$ è la velocità del deutone incidente. Tenendo conto della relazione che esprime la conservazione dell'energia e introducendo per Φ_a e Φ_b le espressioni date, si ottiene

$$(9) \qquad \frac{d\sigma_{dp}}{d\Omega} = \frac{M_d M}{4\pi^2\hbar^4}\frac{k_p}{K}\left|\int d\boldsymbol{r}_p\, d\boldsymbol{r}_n \exp\left[-i\boldsymbol{k}_p\cdot\boldsymbol{r}_p\right]p^*(\boldsymbol{r}_n, \lambda_b)(V_p + V_{np})\Psi_a^{(+)}\right|^2.$$

Il procedimento di GERJOUY, che si basa sul calcolo dell'ampiezza dell'onda diffusa $(\varphi, \Psi_a^{(+)})$, si traduce facilmente nell'attuale formulazione. Infatti, in luogo delle (5) e (6) si hanno le

$$(10) \qquad (E_a - \lambda_b)(\varphi, \Phi_a) = (\varphi, V_n\Phi_a) - (\varphi, V_{np}\Phi_a)$$

$$(11) \qquad (\varphi, \Psi_a^{(+)}) = \left(\varphi, \frac{1}{E_a + i\varepsilon - H_b}(V_p + V_{np})\Psi_a^{(+)}\right).$$

[4] C. MØLLER: *Kgl. Danske Videnskab., Mat. Fys. Medd.*, **23**, no. 1 (1945).
[5] G. F. CHEW e G. C. WICK: *Phys. Rev.*, **85**, 636 (1952).

Poichè agli effetti del calcolo della sezione d'urto, dell'ampiezza interessa il valore asintotico per $r_p \to \infty$, si vede subito intanto che il primo membro della (17) si annulla, in quanto contiene lo stato legato del deutone, e quindi

$$(\lim r_p \to \infty) \qquad (\varphi, V_n \Phi_a) = (\varphi, V_{np} \Phi_a) \,. \tag{12}$$

Per calcolare il valore asintotico della (11), osserviamo che questa si può scrivere

$$(\varphi, \Psi_a^{(+)}) = \int d\boldsymbol{r}_n \, d\boldsymbol{r}_p' \, d\boldsymbol{r}_n' \varphi^*(\boldsymbol{r}_n, \lambda_b) \left(\boldsymbol{r}_p, \boldsymbol{r}_n \left| \frac{1}{E_a + i\varepsilon - H_b} \right| \boldsymbol{r}_p', \boldsymbol{r}_n' \right) (V_p + V_{np}) \Psi_a^{(+)}, \tag{13}$$

dove

$$\left(\boldsymbol{r}_p, \boldsymbol{r}_n \left| \frac{1}{E_a + i\varepsilon - H_b} \right| \boldsymbol{r}_p', \boldsymbol{r}_n' \right) = \tag{14}$$

$$= \frac{2M}{\hbar^2} \sum_\lambda \int \frac{d\boldsymbol{k}}{(2\pi)^3} \exp\left[i\boldsymbol{k}(\boldsymbol{r}_p - \boldsymbol{r}_p') \right] \left(\frac{1}{k_p^2 + i\eta - k^2} \right) \varphi(\boldsymbol{r}_n, \lambda) \varphi^*(\boldsymbol{r}_n', \lambda) \,,$$

avendo posto $(E_a = E) k_p^2 = (2M/\hbar^2)(E - \lambda)$, $\eta = (2M/\hbar^2)\varepsilon$. Ricordando la relazione di completezza $\sum_\lambda \varphi(\boldsymbol{r}_n, \lambda) \varphi^*(\boldsymbol{r}_n', \lambda) = \delta(\boldsymbol{r}_n - \boldsymbol{r}_n')$, (dalle (20) e (21) si ottiene

$$\lim_{r_p \to \infty} (\varphi, \Psi_a^{(+)}) = A(\boldsymbol{n}) \frac{\exp\left[i k_p r_p \right]}{r_p} \,, \tag{15}$$

dove

$$A(\boldsymbol{n}) = -\frac{1}{4\pi} \frac{2M}{\hbar^2} \int d\boldsymbol{r}_p \, d\boldsymbol{r}_n \exp\left[-i\boldsymbol{k}_p \cdot \boldsymbol{r}_p \right) \varphi^*(\boldsymbol{r}_n, \lambda_b) (V_p + V_{np}) \Psi^{(+)}, \tag{16}$$

e $\boldsymbol{k}_p = k_p \boldsymbol{n}$, essendo $\boldsymbol{n}$ un vettore unitario nella direzione di $\boldsymbol{r}_p$. La $A(\boldsymbol{n})$ non è altro che la $A_2(\boldsymbol{n})$ di Gerjouy: la $A_1(\boldsymbol{n})$ non appare in virtù della (12). Per la (15), la sezione d'urto del processo vale $(v_p/v_d) |A(\boldsymbol{n})|^2$; tenendo conto della (16) si ritrova l'espressione (9). In particolare, in approssimazione di Born $\Psi_a^{(+)}$ si può sostituire con Φ_a: segue dalla (12) che in tale approssimazione V_{np} può sostituirsi con V_n. Nell'elemento di matrice relativo al processo (d, p) ricompare così il termine iniziale (cfr. (2)) di perturbazione $V_n + V_p$, che, a differenza del termine $V_p + V_{np}$ che figura nella formulazione corretta, presenta un'immediata giustificazione intuitiva.

In modo analogo può essere trattato il processo (d, p). Si ha solo uno scambio fra stati iniziale e finale e relative equazioni d'onda, cioè $\Phi_a = \exp\left[i\boldsymbol{k}_p \cdot \boldsymbol{r}_p \right] p(\boldsymbol{r}_n, \lambda_a)$, mentre $\Phi_b = \exp\left[i\boldsymbol{K} \cdot \boldsymbol{R} \right) w(\boldsymbol{r}, \varepsilon_b)$. Il termine di interazione vale in questo caso $V_n + V_{np}$, e pertanto il vettore di stato $\Psi_a^{(+)}$ soddisfa l'equazione integrale

$$\Psi_a^{(+)} = \Phi_a + \frac{1}{E_a + i\varepsilon - H_a} (V_p + V_{np}) \Psi_a^{(+)} \,, \qquad (H_a = K + V_n) \,. \tag{17}$$

Di qui, procedendo con qualche ovvia variante come nel caso del processo (d, p),

si arriva all'espressione della sezione d'urto differenziale

$$(18) \qquad \frac{\mathrm{d}\sigma_{\mathrm{pd}}}{\mathrm{d}\Omega} = \frac{M_{\mathrm{d}} M}{4\pi^2 \hbar^4} \frac{K}{k_{\mathrm{p}}} \left| \int \mathrm{d}\boldsymbol{R}\, \mathrm{d}\boldsymbol{r} \exp\left[-i\boldsymbol{K}\cdot\boldsymbol{R}\right] w^*(\boldsymbol{r}, \varepsilon_b)(V_{\mathrm{p}} + V_{\mathrm{n}})\Psi_a^{(+)} \right| .$$

Per quanto riguarda l'uso dell'approssimazione di Born, si può tener conto che per l'urto (d, p) la corrispondente della (12) si scrive

$$(19) \qquad (\lim R \to \infty) \qquad (w, V_{\mathrm{n}}\Phi_a) = w, V_{\mathrm{np}}\Phi_a) .$$

Alla (19) si perviene calcolando il valore asintotico dell'ampiezza dell'onda diffusa $(w, \Psi_a^{(+)})$. Sia il valore di λ_b che ε_b possono essere $\lesssim 0$, a seconda che nella fase finale del processo considerato si realizza uno stato legato rispettivamente uno stato del continuo. È implicita pertanto nella sommatoria che figura nella (14) un'integrazione sugli stati del continuo. È ovvio infine che la schematizzazione del centro fisso di forza vale solo nel caso di nuclei pesanti; per nuclei leggeri M_{d} ed M vanno sostituite con le masse ridotte associate al moto relativo prima e dopo l'urto.

IL NUOVO CIMENTO Vol. XI, N. 4 1° Aprile 1954

Zum Renormierungsprogramm der Feldphysik.

W. Zimmermann

Max-Planck Institut für Physik - Göttingen

(ricevuto il 12 Febbraio 1954)

Am Beispiel der pseudoskalaren Wechselwirkung von Nukleonen mit pseudoskalaren Mesonen (einschließlich direkter Mesonenwechselwirkung) läßt sich das Renormierungsprogramm der Feldphysik in seinem gegenwärtigen Stand etwa so umreissen [1]: Als erstes werden entsprechend der Zahl der primitiv divergenten S-Matrixgraphen die Renormierungsfunktionen S'_{Fr}; Δ'_{Fr}; $\tilde{\Gamma}_{5r}$; M_r [2] eingeführt. Diese können — bei geeigneter Einrichtung der « nackten » Massen- und Kopplungskonstanten m_0, $\varkappa_0$ und g_0, λ_0 — nach Potenzen der experimentellen Kopplungskonstanten g, λ so entwickelt werden, daß in jeder Näherung ein konvergentes Endresultat erhalten wird [3].

Die Übergangselemente der S-Matrix lassen sich dann unter Vermeidung unendlicher Konstanten lediglich durch die Renormierungsfunktionen und die renormierten Wellenfunktionen der ein- und auslaufenden Teilchen ausdrücken. Die in dieser Entwicklung (nach Potenzen von g und λ) vorkommenden Integrationen über die Renormierungsfunktionen führen zu keinen neuen Divergenzen [3].

Ebenso sind die renormierten Wellenfunktionen einer bestimmten physikalischen Problemstellung (z.B. Meson-Nukleonstreuung) Gleichungen unterworfen, in denen alle Selbstenergieteile, Eckteile, M-Teile durch die Renormierungsfunktionen aufsummiert sind und keine zu neuen Divergenzen [4] führenden Integrationen mehr auftreten (siehe dazu A).

Zwischen dem Verfahren zur Berechnung der Renormierungsfunktionen einerseits und der Zurückführung der S-Matrixelemente und Wellenfunktionen auf die Renormierungsfunktionen andererseits besteht ein wesentlicher Unterschied: Wäh-

---

[1] Zur Bezeichnungsweise vgl. die im Folgenden mit A zitierte Arbeit W. Zimmermann: Blaudruck « *Renormierung von Wellenfunktionen in der Feldphysik* », *Suppl. al Nuovo Cimento*, im Erscheinen.

[2] In der Literatur gewöhnlich mit S'_{F1}; ... bezeichnet.

[3] F. J. Dyson: *Phys. Rev.*, **75**, 1736 (1949); P. T. Matthews: *Phil. Mag.*, **42**, 226 (1951); J. C. Ward: *Phys. Rev.*, **84**, 897 (1951); A. Salam: *Phys. Rev.*, **86**, 731 (1952).

[4] Gemeint sind nur Ultraviolettdivergenzen, andere Arten von Divergenzen werden hier nicht betrachtet.

rend z.B. die Bestimmung der S-Matrixelemente nach Einsetzen bereits errechneter Näherungen der Renormierungsfunktionen Divergenzen auch in den Zwischenrechnungen vermeidet, läßt es sich bei den bisher bekannten Berechnungsmethoden der Renormierungsfunktionen nicht umgehen, daß in den Zwischenrechnungen unbestimmte Ausdrücke, etwa der Form $\infty \quad \infty$, auftreten, die es unter sorgfältiger Ausnutzung der Invarianzeigenschaften der Theorie zu bestimmen gilt.

Deshalb soll im Folgenden eine Berechungsmethode der Renormierungsfunktionen angegeben werden, die divergente Zwischenresultate vollständig vermeidet.

Man geht dazu von den Definitionsgleichungen der Renormierungsfunktionen aus und zerlegt die Operatorenprodukte durch Summation über alle Zwischenzustände, beispielweise:

$$(1)\quad S'_{Fr}(x-y) = -\theta(x-y)(\Omega, \psi_r(x)\bar{\psi}_r(y)\Omega) + \theta(y-x)(\Omega, \bar{\psi}_r(y)\psi_r(x)\Omega) =$$

$$= -\theta(x-y)\sum_i (\Omega, \psi_r(x)\Phi_i)(\Phi_i, \bar{\psi}_r(y)\Omega) + \theta(y-x)\sum_i (\Omega, \bar{\psi}_r(y)\Phi_i)(\Phi_i, \psi_r(x)\Omega).$$

Die erste Summe rechts wird über alle Zustände der Nukleonenzahl $+1$, die zweite über alle Zustände der Nukleonenzahl -1 ausgeführt. Mit der naheliegenden Annahme, daß es unter den Zuständen Φ_i der Nukleonenzahl ± 1 keine *stabilen* gebundenen Zustände gibt, dürfen die renormierten Wellenfunktionen

$$(2.a)\qquad (\Omega, \psi_r(x)\Phi_i), \qquad (\Omega, \bar{\psi}_r(y)\Phi_i)$$

$$(2.b)\qquad (\Phi_i, \bar{\psi}_r(y)\Omega), \qquad (\Phi_i, \psi_r(x)\Omega)$$

nach den Wellenfunktionen der freien einlaufenden Teilchen entwickelt werden:

$$(\Omega, \psi_r(x)\Phi_i) = Z_2^{-\frac{1}{2}}(\Omega'_0, TU'(+\infty, -\infty)\psi'_0(x)\Phi'_i(-\infty)),$$

$$(\Phi_i, \bar{\psi}_r(y)\Omega) = Z_2^{-\frac{1}{2}}(\Phi'_i(-\infty), \bar{T}U'(-\infty, +\infty)\bar{\psi}'_0(y)\Omega'_0).$$

Diese Entwicklungen werden nach dem in [1] geschilderten Verfahren so umgeformt, daß die Wellenfunktionen (2.*a*,*b*) nur noch durch die wechselwirkungsfreien Wellenfunktionen [5] der einlaufenden Teilchen und die Renormierungsfunktionen S'_{Fr}, Δ'_{Fr}, $\tilde{\Gamma}_{5r}$, M_r bzw. die der antichronologischen Ordnung $\bar{T}$ entsprechenden Renormierungsfunktionen $\bar{S}'_{Fr}$, ... divergenzfrei ausgedrückt sind. Alle in den Entwicklungen der Wellenfunktionen (2.*a*) von den einlaufenden Teilchen herrührenden Wellenfunktionen können vermöge von Vollständigkeitsrelationen mit den entsprechenden Wellenfunktionen in den Entwicklungen von (2.*b*) zu S^+-, S^-- und Δ^+-Funktionen zusammengefaßt werden. So erhält man für S'_{Fr} eine Integralgleichung, die außer den Renormierungsfunktionen noch die zu den experimentellen Massen gehörenden Funktionen S^+, S^- und Δ^+ enthält:

$$(3.1)\qquad S'_{Fr} = I_1(S'_{Fr}, \Delta'_{Fr}, \tilde{\Gamma}_{5r}, M_r, S^+(m), S^-(m), \Delta^+(\varkappa), \bar{S}'_{Fr}, \bar{\Delta}'_{Fr}, \bar{\tilde{\Gamma}}_{5r}, \bar{M}_r).$$

---

(5) Diese gehören zu den experimentellen Massen.

Ganz analog führt die Aufspaltung

$$(\Omega, TA_r(y)\psi_r(x)\bar{\psi}_r(z)\Omega) = \theta(x-z)\theta(y-z)\sum_i (\Omega, TA_r(y)\psi_r(x)\Phi_i)(\Phi_i, \bar{\psi}_r(z)\Omega) +$$

$$- \theta(x-y)\theta(z-y)\sum_i (\Omega, T\psi_r(x)\bar{\psi}_r(z)\Phi_i)(\Phi_i, A_r(y)\Omega) -$$

$$- \theta(y-x)\theta(z-x)\sum_i (\Omega, TA_r(y)\bar{\psi}_r(z)\Phi_i)(\Phi_i, \psi_r(x)\Omega),$$

zusammen mit der Definitionsgleichung von $\tilde{\Gamma}_{5r}$ auf eine Gleichung (6), die $\tilde{\Gamma}_{5r}$ divergenzfrei zu den anderen Renormierungsfunktionen in Beziehung setzt:

$$(3.3) \qquad \tilde{\Gamma}_{5r} = I_3(S'_{Fr}, \Delta'_{Fr}, \tilde{\Gamma}_{5r}, M_r, S^+(m), S^-(m), \Delta^+(\varkappa), \bar{S}'_{Fr}, \bar{\Delta}'_{Fr}, \bar{\tilde{\Gamma}}_{5r}, \bar{M}_r).$$

Mit den entsprechenden Beziehungen (7) für Δ'_{Fr}, M_r, $\bar{S}'_{Fr}$, ... hat man insgesamt acht Integralgleichungen für die je vier Renormierungsfunktionen:

$$(3.1) \qquad S'_{Fr} = I_1(S'_{Fr}, \Delta'_{Fr}, \tilde{\Gamma}_{5r}, M_r, S^+(m), S^-(m), \Delta^+(\varkappa), \bar{S}'_{Fr}, \bar{\Delta}'_{Fr}, \bar{\tilde{\Gamma}}_{5r}, \bar{M}_r)$$

. . . . . .

$$(3.8) \qquad \bar{M}_r = I_8(S'_{Fr}, \Delta'_{Fr}, \tilde{\Gamma}_{5r}, M_r, S^+(m), S^-(m), \Delta^+(\varkappa), \bar{S}'_{Fr}, \bar{\Delta}'_{Fr}, \bar{\tilde{\Gamma}}_{5r}, \bar{M}_r).$$

Über die Massenkonstanten m und $\varkappa$ ist in den Gleichungen (3) bereits verfügt, denn sie treten darin in Form der Funktionen S^+, S^- und Δ^+ auf. Dagegen sind die (experimentellen) Konstanten g und λ durch die Gl. (3) *allein* nicht festgelegt (8), müssen also erst durch eine zusätzliche Bedingung eingeführt werden: Macht man mit beliebigen (endlichen) Konstanten g und λ für $\tilde{\Gamma}_{5r}$ und M_r den Ansatz

$$(4) \qquad \tilde{\Gamma}_{5r}(y\,|\,x\,|\,z) = -g\gamma_5\,\delta(x-y)\,\delta(y-z) - gA_r(y\,|\,x\,|\,z),$$

$$M_r(x_1x_2x_3x_4|\,|) = i\lambda\,\delta(x_1-x_2)\,\delta(x_2-x_3)\,\delta(x_3-x_4) + i\lambda K_r(x_1x_2r_3x_4|\,|),$$

worin A_r und K_r keine δ-Funktionen enthalten und für $g=0$, $\lambda=0$ verschwinden sollen, so werden die Integralgleichungen (3) eindeutig durch Entwicklung der acht Renormierungsfunktionen nach Potenzen von g und λ gelöst.

Als Beispiel sei die Berechnung der S'_{Fr}-Funktion bis zur g^2-Näherung ange-

(6) Man braucht hier die weitere Annahme, dass es auch zur Nukleonenzahl Null keine stabilen gebundenen Zustände gibt.

(7) Für die Funktion $\bar{M}_r$ spaltet man z.B. in der Form

$$(\Omega, \bar{T}A_r(x_1)A_r(x_2)A_r(x_3)A_r(x_4)\Omega) =$$

$$= \theta(x_2-x_1)\theta(x_3-x_1)\theta(x_4-x_1)\sum_i (\Omega, A_r(x_1)\Phi_i)(\Phi_i\,\bar{T}A_r(x_2)A_r(x_3)A_r(x_4)\Omega) + \ldots$$

auf.

(8) Natürlich wären g und λ über die Definitionsgleichungen von $\tilde{\Gamma}_{5r}$; M_r und die Differentialgleichungen der Feldoperatoren durch Vorgabe der Konstanten m_0, $\varkappa_0$, g_0, λ_0 vollkommen festgelegt. Der Rückgriff auf die Grundgleichungen der Feldphysik muss aber gerade vermieden werden, wenn die Berechnung der Renormierungsfunktionen ausschliesslich auf der Grundlage divergenzfreier Beziehungen erfolgen soll.

deutet. In nullter Näherung folgt aus (3.1):

$$S'_{Fr} = S_F$$

und in zweiter Näherung

$$(5) \qquad S'_{Fr}(x-y) = S_F(x-y) - \cdot$$

$$- \theta(x-y) g^2 \int S_F(x-x') \gamma_5 S^+(x'-y') \Delta^+(x'-y') \gamma_5 S_F(y'-y) \, \mathrm{d}x' \, \mathrm{d}y' +$$

$$+ \theta(y-x) g^2 \int S_F(x-x') \gamma_5 S^-(x'-y') \Delta^+(y'-x') \gamma_5 S_F(y'-y) \, \mathrm{d}x' \mathrm{d}y' \, ,$$

was auf die bekannte g^2-Näherung der S'_{Fr}-Funktion führt, ohne daß während der Rechnung Divergenzen irgendwelcher Art auftreten [9].

Das geschilderte Verfahren zur Berechnung der Renormierungsfunktionen ermöglicht außerdem einen neuen Beweis für die Durchführbarkeit des Renormierungsprogramms, welcher demnächst erscheinen wird.

---

[9] Ueber die Ausrechnung des Ausdrucks (5) im Einzelnen vgl. H. LEHMANN: Blaudruck *« Ueber Eigenschaften von Ausbreitungsfunktionen und Renormierungskonstanten »*, *Nuovo Cimento*, im Erscheinen.

IL NUOVO CIMENTO Vol. XI, N. 4 1° Aprile 1954

An Analysis of Two Positive τ-Mesons.

A. Debenedetti, C. M. Garelli, G. Lovera, L. Tallone and M. Vigone
Istituto Nazionale di Fisica Nucleare - Sezione di Torino

(ricevuto il 15 Marzo 1954)

In a batch of stripped plates flown at the altitude of 80000 ft during the Sardinia expedition 1953, we have observed two positive τ-mesons decaying in the emulsion.

Fig. 1.

τ_1 (Fig. 1) has been found during the scanning of the plates. It is emitted from a star of the type 15+8n, crosses 27 plates and comes to rest after 34.3 mm. The three π from the τ decay end inside the stack; two of them are π^+ which give rise to $\pi \to \mu \to e$ decay; the third one is a π^- which stops without producing a visible star.

The measured values of ranges and angles are reported in Table I.

TABLE I.

	Charge	Range (μ)	Angles	
π_1	+	20 200 ± 80	(π_1, π_2)	141° 24′ ± 6′
π_2	−	10 700 ± 140	(π_2, π_3)	193° 22′ ± 13′
π_3	+	4 500 ± 80	(π_3, π_1)	125° 15′ ± 8′

The energies of the π-mesons have been calculated:

a) Using the range-energy relation given by BRADNER *et al.* [1]

$$E = 0.251\ R^{0,58}\ M^{0,42}\ .$$

b) Using the tables and computations of VIGNERON [2].

The results, assuming for the $\pi^{\pm}$ the mass value of 273 ± 1 m_e, are given in the following table.

TABLE II.

	Energy (MeV)		Momentum (MeV/c)	
	BRADNER	VIGNERON	BRADNER	VIGNERON
π_1	35.40 ± 0.08	35.17 ± 0.08	105.5 ± 0.3	105.1 ± 0.3
π_2	24.49 ± 0.19	24.17 ± 0.19	86.2 ± 0.4	85.6 ± 0.4
π_3	14.82 ± 0.15	14.66 ± 0.15	66.0 ± 0.3	65.6 ± 0.3

The Q value is therefore:

$$Q = 74.7 \pm 0.4 \text{ MeV} \quad \text{(BRADNER)}$$

$$Q = 74.0 \pm 0.4 \text{ MeV} \quad \text{(VIGNERON)}$$

and the mass of the τ-meson is:

$$M_\tau = 965 \pm 3\ m_e \quad \text{(BRADNER)}$$

$$M_\tau = 964 \pm 3\ m_e \quad \text{(VIGNERON)}\ .$$

[1] H. BRADNER, F. M. SMITH, W. H. BARKAS and A. S. BISHOP: *Phys. Rev.*, **77**, 462 (1950).
[2] L. VIGNERON: *Journ. de Phys. et le Rad.*, **14**, 145 (1953).

The momentum values deduced from Bradner's and Vigneron's formulae respectively, give for the momentum balance ratios $p_i/\sin(\pi_h, \pi_k)$ the results

	Bradner	Vigneron
$\frac{p_1}{\sin(\pi_2, \pi_3)}$	105.7 ± 0.4	105.3 ± 0.4
$\frac{p_2}{\sin(\pi_3, \pi_1)}$	105.6 ± 0.7	104.8 ± 0.7
$\frac{\varepsilon d}{\sin(\pi_1, \pi_2)}$	105.7 ± 0.6	105.1 ± 0.6

which are equal within the experimental errors.

τ_2 (Fig. 2) has been observed following backwards a π-meson track. It is emitted from a 7+8p star and travels for 14.6 mm in the first plate and for 1.8 mm in the next one.

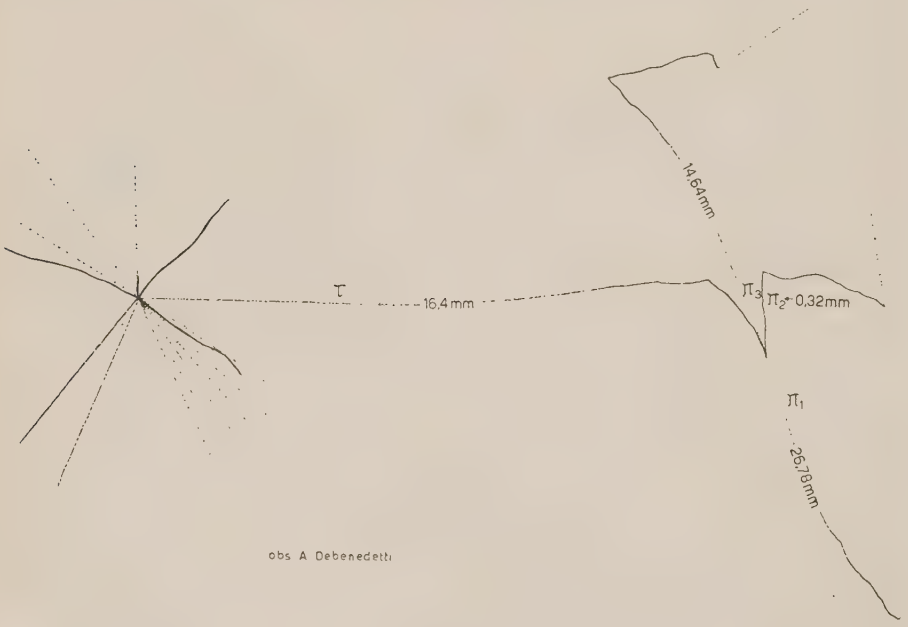

Fig. 2.

As in the τ_1 case, the three π-mesons stop inside the stack, and the negative one does not give rise to a star with visible prongs.

We made the same measurements as in the first case, and the results are summarized in the following table.

TABLE III.

	Charge	Range (μ)	Energy (MeV)		Momentum (MeV/c)	
			BRADNER	VIGNERON	BRADNER	VIGNERON
π_1	—	26780 ± 80	41.69 ± 0.08	$41.78 \pm$?	115.63 ± 0.12	$115.77 \pm$?
π_2	—	323 ± 15	3.22 ± 0.02	3.28 ± 0.02	30.13 ± 0.09	30.43 ± 0.09
π_3	+	14640 ± 40	29.37 ± 0.05	29.06 ± 0.05	95.17 ± 0.13	94.61 ± 0.09

$$(\pi_1, \pi_2) = 143^\circ\,40' \pm 1^\circ\,30'$$

$$(\pi_2, \pi_3) = 46^\circ\,40' \pm 1^\circ\,30'$$

$$(\pi_3, \pi_1) = 169^\circ\,10' \pm 30'$$

	BRADNER	VIGNERON
$\frac{p_1}{\sin(\pi_2, \pi_3)}$	160.6 ± 6	$159.7 \pm$?
$\frac{p_2}{\sin(\pi_3, \pi_1)}$	160.3 ± 8	161.9 ± 8
$\frac{p_3}{\sin(\pi_1, \pi_2)}$	159.0 ± 4	159.2 ± 4
Q	74.28 ± 0.15	$74.12 \pm$?
M_τ	964 ± 3	964 ± 3

The values of the angles are in this case affected by a sensible error, because of the large dip and scattering of π_2 track.

The π_1 energy goes outside the range of values listed in VIGNERON's work, and therefore we cannot evaluate the error in the extrapolation.

It may be worthwhile noticing some features common to the two parent stars.

In both cases the τ track appears as a grey track at a little angle with the direction of a small jet. Besides, in both stars is visible another grey track symmetrical to the τ track with respect to the jet axis. These grey tracks go out of the stack and will be studied in a next time.

We are grateful to Professors R. DEAGLIO and G. WATAGHIN for their constant interest in this work.

IL NUOVO CIMENTO Vol. XI, N. 4 1° Aprile 1954

Remarks on Recent Analyses of Cosmic Ray Jets.

C. C. Dilworth (*) and S. J. Goldsack (**)
Centre de Physique Nucleaire de l'Université Libre - Bruxelles

T. F. Hoang
Laboratoire de Physique de l'École Polytechnique - Paris

L. Scarsi
Istituto Nazionale di Fisica Nucleare - Sezione di Milano

(ricevuto il 16 Marzo 1954)

In a recent paper (1) we tried to analyse a certain number of jets which were at our disposal. The first section of our paper consisted of an analysis on the basis that jets are created in a simple nucleon-nucleon collision, an hypothesis which was formerely widely accepted. The second section was devoted to an attempt to apply the tunnel model of Roesler and McCusker (2), which seemed to us to give a very consistent picture of the way in which these jets are formed. McCusker and Roesler (3) have since advanced certain important criticisms of the application of their model to jets of median angle φ greater than that given by the upper limit $2/\varphi^2 > 500$ set by them as that corresponding to a diametrical cylindrical tunnel in a silver nucleus. Certain of their remarks are correct, others seem to be due to a misunderstanding of our arguments. We will therefore briefly recapitulate the analysis which we made and show in what points we would like to modify it in view of these criticisms and in the llght fo later information.

1. – The greater part of the material at our disposal consisted of jets of $2/\varphi^2 < 500$. The reason for this we discuss in section **2**. We attempted to analyse them on the basis of the following extrapolation of the Roesler and McCusker arguments. A primary of energy less than 16 A_{Ag} GeV which is incapable of producing a clean tunnel across the diameter of a silver nucleus can form a short cylindrical tunnel if it strikes laterally a silver or a bromine nucleus or even diametrically one of the light nuclei of the gelatine. As a control of the « cleaness » of the tunnel we eliminated all jets with more than four evaporation tracks. The criticism which McCusker and Roesler here brought (3) is that at such low energies « the tunnel will flare out » so that the number of

(*) Now at Istituto Nazionale di Fisica Nucleare, Sezione di Milano.

(**) Now at Phys. Dept. University of California, Berkeley.

(1) C. Dilworth, S. Goldsack, T. F. Hoang and L. Scarsi: *Nuovo Cimento*, **10**, 1261 (1953).

(2) F. C. Roesler and C. B. A. McCusker: *Nuovo Cimento*, **10**, 127 (1953).

(3) C. B. A. McCusker and F. C. Roesler: *Nuovo Cimento*, **2**, 98 (1954).

collisions involved will be greater than that supposed. This point is very important and led us to reconsider our analysis. As shown by HEITLER and TERRAUX (4) a cylindrical tunnel across a silver nucleus leads in general to little excitation and so to few black tracks. The shorter cylindrical tunnel formed by a primary striking the edge of the silver nucleus leads to even lower excitation. On the other hand the formation of a trumpet shaped tunnel must produce a greater evaporation than that which accompanies a cylindrical tunnel of the same length. In limiting the allowed number of black tracks to four we should have already excluded trumpet shaped tunnels formed across the diameter of the silver nucleus. We did not however exclude trumpet shaped lateral tunnels. We have now corrected this by reducing the limit of the allowed number of black tracks for the wider angle showers e.g. to 4 for $2/\varphi^2 > 300$ – to 3 for $200 < 2/\varphi^2 < 300$ – to 2 for $2/\varphi^2 < 200$.

We recalculated fig. 4 of our paper (1) using these limits and obtained Fig. 1 in which the points are less intermingled but still do not separate completely. This operation led to the recjetion of 16% of our jets.

In their paper (4) HEITLER and TERRAUX give a lower limit ($2/\varphi^2 \geqslant 100$) for the diametrical cylindrical tunnel. If we adopt this value we obtain Fig. 2 in which the demarcation between the open circles and the dots is quite clean. It is perhaps worthwhile pointing out here that if the HEITLER and TERRAUX limits are correct our elimination of jets of $2/\varphi^2 < 36$ (1) which corresponds to four collisions in this case, minimizes the contribution of very short tunnels.

This treatment seems to us reasonably sound. We take a shower and measure its opening angle. We then determine the longest cylindrical tunnel in which such a shower could have been produced. When fluctuations occur tending to increase the interaction with the nucleus, such showers are automatically rejected. The only fluctuations which cause contamination are those in which a trumpet shaped tunnel is associated with an abnormally small number of evaporation tracks. Such events must be rather rare since the excitation should increase rather rapidly after the tunnel becomes non-cylindrical.

2. – Since the primary energy spectrum falls rapidly, the greater part of the jets are of low energy. Among the miscellany of showers published by various authors, there will be a bias against low multiplicity events since events of high multiplicity are more easily seen and often of sufficient interest to merit separate publication. There is also in the group of events of DANIEL *et al.* (5) a bias against large angle showers implicit in their original definition of a jet as a « well collimated shower » accompanied by few evaporation tracks. Our group attempted a systematic search and therefore found a large proportion of wide angle showers. We must however have lost a certain number of jets of very wide angle and low evaporation which are difficult to pick up in the scanning

3. – With this reserve we give in Fig. 3 all the available evidence to date on jets in a form similar to that employed by HEITLER and TERRAUX. The points seem to fit in a band which widens with increasing energy up to about $2/\varphi^2 \sim 100$ and then remains fairly constant in width. The lower edge of this corridor is the experimental cut-off at $n_s = 4$. It is not possible to say here if this general rise in multiplicity with $2/\varphi^2$ up to 100 is due to an increasing number of col-

(4) W. HEITLER and C. TERRAUX: *Proc. Phis. Soc.*, A **66**, 929 (1953).

(5) R. R. CANIEL, J. H. DAVIES, J. H. MULVEY and D. H. PERKINS: *Phil. Mag.*, **43**, 453 (1952).

Fig. 1. – Diagram of the multiplicity factor f_n versus energy in laboratory system with Roesler and McCusker limits. The points represent the events of Fig. 4 of our former paper less those rejected in reanalysis.

● $s=1$ ○ $s=s_{max}$.

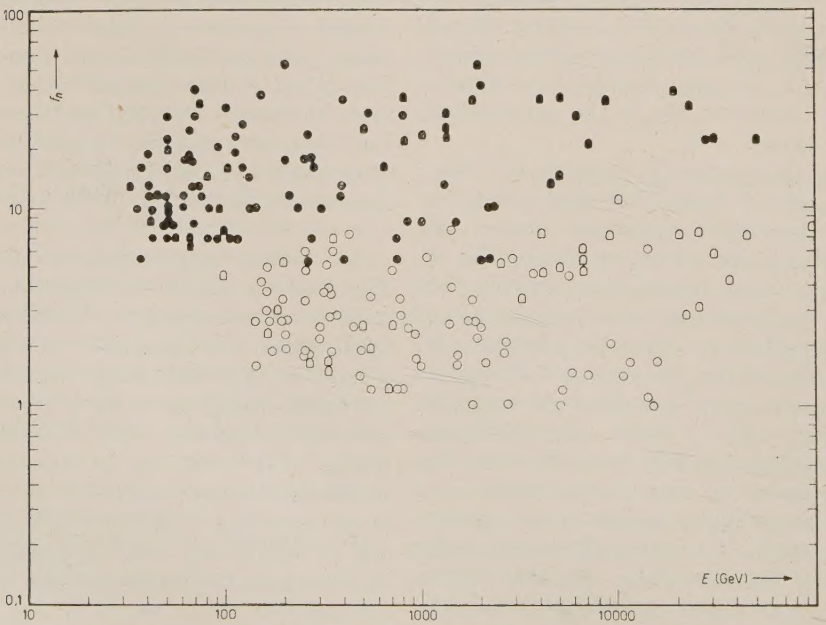

Fig. 2. – Diagram of the multiplicity factor f_n versus energy in laboratory system with Heitler-Terraux limits.

● $s=1$ ○ $s=s_{max}$. ◖ ∩ Additional points from C. CASTAGNOLI *et al.*: *Nuovo Cimento*, **10**, 1539 (1953) and KAPLON-RITSON: *Phys. Rev.*, **88**, 386 (1952).

lisions as the tunnel length increases or also to an increase in the number of mesons created in each single collision.

4. – In the objection which McCUSKER and ROESLER bring to equation (13) of our paper [1] we think there is some misunderstanding. Having said in the text that we were calculating the possible tunnel lengths in the nuclei present in the photographic emulsion, we did not think it necessary to stipulate the numerical limits to our $s_{max} = 1/2$ tg Φ. Since s is expressed in units of the nucleon diameter. s_{max} must evidently lie between 1 and 7.

a) A general criticism of our work has been that it was quite useless to study jets of median angle φ for which $2/\varphi^2$ is less than several hundred. We maintain on the contrary, that a systematic survey of these events unbiassed by selection of those with small angle or high multiplicity, is necessary to obtain a complete picture of these phenomena.

b) The error in our first analysis, pointed out by McCUSKER and ROESLER has now, we hope, been corrected, with the result that the intermingling of the dots and the circles in the ROESLER and McCUSKER type graph is reduced but not eliminated, unless we take as the limit of energy for a diametrical tunnel in Ag that given by HEITLER and TERRAUX.

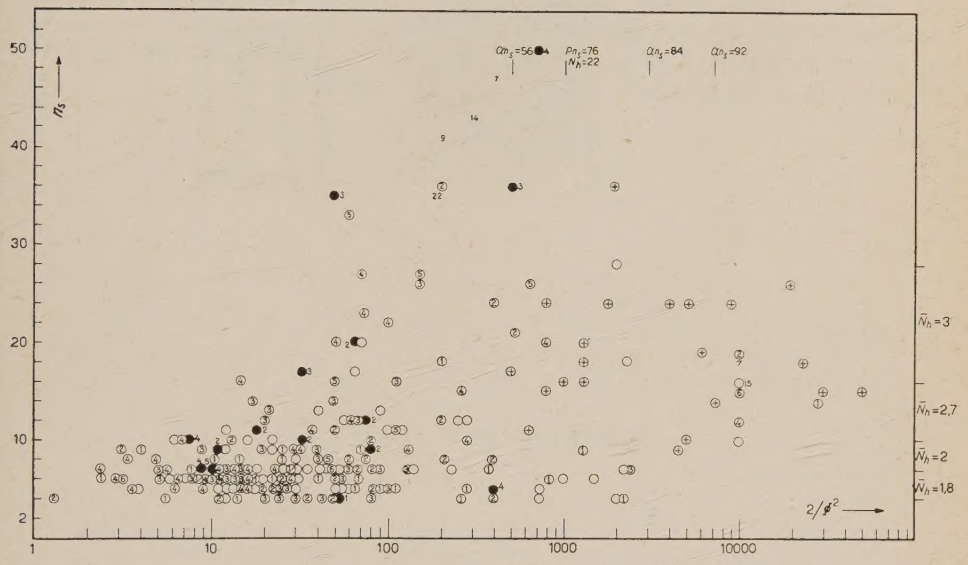

Fig. 3. – Heitler-Terraux type diagram of number of shower particles versus inverse square of the median angle of the jet.

(Nh) jets with N_h evaporation tracks. ⊕ evaporation unknown. ● α-produced jets.

c) In the type of diagram given by HEITLER and TERRAUX, which gives simply the multiplicity in terms of the inverse square of the median angle, the inclusion of wide angle jets ($2/\varphi^2 < 100$) is of interest in showing the general rise in the multiplicity with increasing energy in this region.

d) The greater part of the events are consistent with the tunnel model. The

few which are anomalous can be considered to be due to chance fluctuations or may arise from particular causes, e.g.

(i) Events with large N_h and small n_s and small φ. These may be due to the disruption of light nuclei following the formation of the tunnel.

(ii) Events with large N_h and n_s and small φ. These events have been explained by HEITLER and TERRAUX on the basis of the formation of a secondary tunnel by one of the nucleons of the jet.

An alternative explanation is that a part at least of these events might be due to primaries of charge one and mass two i.e. deuterons. If deuterons should exist in the primary stream, the bias already noted in favour of high multiplicity events would make them easier to pick up even if their number relative to that of protons should be very small. It is suggestive (Fig. 3) that α-produced jets with very small angles tend to be produced with larger N_h and n_s than most of the jets.

Direttore responsabile: G. POLVANI Tipografia Compositori - Bologna

Questo fascicolo è stato licenziato dai torchi il 24-III-1954